REMOTE SENSING TOOLS FOR LAND AND WATER MANAGEMENT IN DATA SCARCE BLUE NILE BASIN

A Dissertation

Presented to the Faculty of the Graduate School

of Cornell University

In Partial Fulfillment of the Requirements for the Degree of

Doctor of Philosophy

by

Essayas Kaba Ayana

January 2013

REMOTE SENSING TOOLS FOR LAND AND WATER MANAGEMENT IN DATA SCARCE BLUE NILE BASIN

Essayas Kaba Ayana, Ph. D.

Cornell University 2013

Ground based water resources monitoring systems are often difficult to maintain consistently in developing countries. The decline in the number of stations, data quality and changes in the data holding policy has made water resources data less reliable for use in operational purposes. The objective of this dissertation is, therefore, to evaluate the utility of existing freely available remotely sensed images to monitor water resource systems. In this dissertation Moderate Resolution Imaging Spectroradiometer (MODIS) images were evaluated on the basis of their capability to (1) measure total suspended solid (TSS) and turbidity and generate historical TSS data, (2) estimate the water storage variation of Lake Tana and (3) monitor the state of biomass in the upper Blue Nile basin . The usability of historical TSS data in hydrologic modeling is also tested. Lake water samples were collected concurrent with the satellite overpass over the lake at the entry location of Gumera River, a major tributary to the lake. Reflectance in the red and near infrared (NIR) 250 m-pixel images taken on sampling days were correlated and validated using measured TSS and turbidity. The validated correlations were applied to the ten year image archive of MODIS to generate a 10-year TSS time series for the lake. In addition, MODIS images of the years 2002 – 2003, where the lake level variation was at its minimum, were used to generate the lake near-shore bathymetric model. The new near-shore bathymetric model

reproduced water level measurements with a better accuracy than the existing bathymetric model of the lake.

The usability of the TSS data was tested by initializing a hydrologic model for the Gumera watershed using the Soil and Water Assessment Tool (SWAT). The ten year TSS data generated were used to calibrate the model. The model was capable of predicting the monthly TSS variation. The potential of MODIS images in monitoring biomass recovery was also assessed at river basin scale. The enhanced vegetation index (EVI) – land surface temperature (LST) relation is used to map the trend in the disturbance of plantations put in place as conservation measures. In this dissertation the potential of satellite imagery as a data gap filling alternative to ground based monitoring systems in data scarce regions is tested.

BIOGRAPHICAL SKETCH

Essayas Kaba Ayana was born in 1971 and grew up in Addis Ababa, Ethiopia. After he completed high school at Entoto Academic, Technical and Vocational Secondary School, he joined the then Arba Minch Water Technology Institute in 1998. During his four year stay at the institute, he became interested in GIS and remote sensing supported hydrologic modeling. He got his Bachelor of Science degree in Hydraulic Engineering in 2002. He then became a faculty member at Bahir Dar University, Engineering Faculty. After working for three years he was awarded a Dutch scholarship to study GIS and remote sensing at the International Institute for Geo – Information Science and Earth Observation (ITC) in Enschede, the Netherlands and earned a master's degree in integrated catchment and water resources management. In his MSc. research he evaluated the performance of radar altimetry data over Lake Tana, a source to the Blue Nile River. Up on return he served as chair of the Department of Water Resources Engineering at Bahir Dar University. In addition, he taught courses in the area of GIS and remote sensing. He then became a vice dean for the Engineering Faculty in 2009. Essayas joined Cornell University in fall 2009 to start his Ph.D. in the Biological and Environmental Engineering Department.

Dedicated to my wife *Heran Wolde Mariam Deginetu*; your love and kindness will always be a much appreciated constant in my life

መታሰቢያነቱ ለባለቤቴ ሔራን ወልደ ማርያም ደግነቱ፤ ፍቅርሽንና ደግነትሽን በህይወቴ ሁሉ አልረሣውም

ACKNOWLEDGEMENTS

My deepest gratitude first goes to my advisor and committee chair Tammo Steenhuis who had guided me through this research and provide all the support required during my study. I would like to thank my special committee members Wilfried Brutsaert and William Philpot for their invaluable support and guidance throughout my academic program and PhD research. I would like to thank Bahir Dar University for facilitating my study leave.

My thanks also go to Higher Education for Development (HED) for providing finance for my research and the School of Civil and Water Resources Engineering at Bahir Dar University for the provision of lab space and materials for water sample analysis. I would like to thank Teshale Tadesse and Wondimu Paulos who had relentlessly worked with me in collecting and analyzing water samples. My appreciations go to Solomon Seyoum (IWMI) who had provided the computer resource and all the requested support when running the hydrologic model. I am thankful to Steve Pacenka and Rebecca Marjerison for their support throughout my research.

I would like to thank my wife Heran Wolde Mariam for her love and encouragement. My thanks also go to my family (Damtish, Yemata, Bethy, Dany, Mikcy and Selam) for their unwavering trust, love, and encouragement. I feel indebted to Addisu Tesfaye, my country man and close friend who always opened his home and heart to host me during my stay in Ithaca. Last but not least I would like to thank my colleagues and friends Seifu Admasu, Amy S. Collick, Fasikaw Atanaw and Christian Guzman whose companionship comforted me.

TABLE OF CONTENTS

LIST OF FIGURES

LIST OF TABLES

LIST OF ABREVIATIONS

ASTER	Advanced Space borne Thermal Emission Radiometer
CoReH2O	Cold region hydrology high-resolution observatory
DEM	Digital Elevation Model
DI	Disturbance Index
EVI	Enhanced Vegetation Index
FDRE-MoWE	Federal Democratic Republic of Ethiopia – Ministry of Water and Energy
FFW	Food for Work
GPM	Global Precipitation Mission
GPS	Global Positioning System
GRACE II	Gravity Recovery and Climate Experiment mission
IGBP	International Geosphere-Biosphere Program
ISLSCP II	International Satellite Land-Surface Climatology Project, Initiative II
Landsat ETM+	Landsat Enhanced Thematic Mapper Plus
LST	Land Surface Temperature
MERET	Managing Environmental Resources to Enable Transitions to More Sustainable Livelihoods
MODIS	Moderate Resolution Imaging Spectroradiometer
MRTWeb	MODIS Re-projection Tool Web
NDWI	Normalized Difference Water Index
NDVI	Normalized Difference Vegetation Index

NGO	Non Governmental Organization
NIR	Near Infra Red
NTU	Nephelometric Turbidity Unit
RMSE	Root Mean Square Error
SMAP	Soil Moisture Active Passive mission
SSC	Suspended Sediment Concentration
SWAT	Soil and Water Assessment Tool
SWOT	Surface Water and Ocean Topography mission
TSM	Total Suspended Matter
TSS	Total Suspended Solid
USGS	United States Geological Survey
WFP	World Food Program

CHAPTER 1: INTRODUCTION

Human ability to numerically model water resource systems has progressed enormously with advances in computational power and the understanding of processes at finer scale (Silberstein, 2006). However, water resources data collection at varying scales is expensive, so that modelers often tend to conceptualize processes based on simplified views of nature (Dozier, 1992) or match the observed data even if the underlying premises are unrealistic (Kirchner, 2006). In addition, collection of water resource data, especially in developing countries, are characterized by inadequate monitoring, gaps in observations, a decline in the number of stations, chronic under funding and differences in processing and quality control (Vörösmarty et al., 2001, Harvey and Grabs, 2003). Our ability today to monitor extreme events with ground based systems is less than it was 45 years ago (Macauley and Vukovich, 2005).

Space–borne remote sensing has become a potential data source to model land and water resource systems. Remote sensing offers advantages over a single point ground measurement in that it provides an overview of the hydrologic regime and its interaction with other systems. Remote sensing has been used for many purposes: Prigent et al. (2001) used multiple satellite data sets to quantify seasonality and the extent of inundation. Site specific equations are also developed to measure turbidity (Chen et al., 2009, Shen et al., 2010), suspended sediment concentration (Jiang et al., 2009, Nechad et al., 2010), chlorophyll–a (Fiorani et al., 2006, Wang et al., 2010a), phytoplankton (Kwiatkowska and McClain, 2009), cyanobacterial blooms (Kutser et al., 2006) and other physical water quality parameters (Liu et al., 2003, Hu et al., 2004). Smith et al. (1996) and Alsdorf et al. (2000) developed a satellite based method (synthetic aperture radar) to measure water levels in the main channels of rivers, upland tributaries

and floodplain where it is impossible to install permanent gauging stations or in areas that are virtually inaccessible (Birkett, 1998). Unganai and Kogan (1998), Wang and Qu (2007), Bolten et al. (2010) and many others developed image based drought monitoring tools. Passive microwave, thermal and radar images are being used for soil moisture retrieval (Kerr et al., 2001, Verstraeten et al., 2006, Naeimi et al., 2009).

Various remote sensing platforms are available to collect water and earth science data. SPOT, Landsat, Advanced Space borne Thermal Emission and Reflection Radiometer (ASTER), ENVISAT advanced synthetic aperture radar (ASAR), Moderate Resolution Imaging Spectroradiometer (MODIS), and Advanced Very High Resolution Radiometer (AVHRR) images are the most widely used data sources in earth science applications. Using these data requires an understanding of the potentials and limitations of the data sets. Spatial and temporal resolution, data size, processing requirements, scale of application and ease of availability are factors that need to be taken into consideration in selecting the image source. In the research described in this dissertation MODIS images and data products are used. MODIS images provide the advantage of near daily availability, increased sensitivity (Hu et al., 2004) and consistent atmospheric correction. MODIS images are validated products (LPDAAC, 2010) that can be directly used in applications without further processing and hence are suitable for novice users.

A very good showcase for the possibilities that satellite images can offer in developing countries for improving the hydrologic monitoring system in the Upper Blue Nile basin, Ethiopia is the estimation of suspended sediment in lakes, estimation of water volume variation in storages and biomass monitoring at river basin scale. Current suspended sediment concentration measurements are based on rating curves that assume a unique relationship between sediment concentration and discharge. However Tilahun et al. (2012) showed that sediment concentration

tends to decrease with increased discharges in the peak of the rainfall season and as such a unique relationship does not exist. Siltation at gauging stations, bank overflow, unstable cross section or a combination of these factors (SMEC, 2008) further degrade the reliability of sediment rating curves. Models relying on these measurements are susceptible to very large error and uncertainly (Alsdorf et al., 2003). Climate change and the rapidly changing geography of water supply and use had added up to the uncertainty of measurements (Vörösmarty et al., 2000). A robust and cost effective monitoring mechanism will be an indispensible tool for water resources managers to evaluate water quality benefits of soil and water conservation works in the upland watershed, allocate water to most economically vital use (vis-à-vis hydropower, irrigation, navigation etc.) and assess state of biomass at basin or country scale.

In this dissertation the main hypothesis is that satellite imagery, and especially MODIS, is a cost effective and robust tool that can replace ground based observations and can be used operationally. Therefore the main goals of this study are to use MODIS images as the main data source for water resources system modeling in data scarce regions. In order to validate the methods used we selected a study area where relatively longer hydrologic data is available. In this dissertation we assessed the potential of MODIS images to reproduce historic sediment concentrations in water bodies, quantify storage variation in lakes and monitor the state of biomass at basin scale.

In chapter 2 of this dissertation, MODIS images are used for near–real time monitoring of total suspended solids (TSS) and turbidity in the Blue Nile basin (Ethiopia). A relationship was developed after examining which band (or possibly band combinations) provides the most accurate prediction of the concentration in the lake. Using the 10–year MODIS images archive

and the established relationship a 10 year time series of sediment concentration was generated for Lake Tana near the Gumera River mouth.

In (Chapter 3) of this thesis the modified soil and water assessment tool – a variable area source (SWAT–VAS) model implemented by Easton et al. (2008) is run for Gumera watershed in the upper Blue Nile basin in order to simulate the 10 year sediment concentration in Lake Tana determined in chapter 2. In this chapter the link between lake water quality and land cover was also assessed using the Enhanced Vegetation Index (EVI) as a proxy for land cover.

A potential application of remote sensing in water volume monitoring is also assessed (Chapter 4). The potential of MODIS images for use in lake area mapping through the use of the normalized difference vegetation index (NDVI) (Tucker, 1979) and normalized difference water index (NDWI) (Gao, 1996) is evaluated using an existing bathymetric model. The images are also used to improve the bathymetric models near lake shore. The improved bathymetric model is validated by comparing predicted lake levels with measured levels. These prototype methods can be applied to estimate the change in storage volume due to inflow of sediment from streams draining to the lake.

A relatively recent application of MODIS images is in monitoring biomass using an image based disturbance index (DI) (Mildrexler et al., 2007). The index is applied to map areas of biomass recovery in the last five years (2008 – 2012) within the upper Blue Nile basin (Chapter 5). In addition, the biomass recovery trend is evaluated at the sub basin level by comparing field observations with soil and water conservation work inventory. The results of this research provide a basis for evaluating the potential and limitations of using available remotely sensed

data for sediment monitoring in lakes, estimating lake water volume and monitoring the state of biomass at the basin or national scale.

The major shortfall of currently available images is the coarse spatial resolution. Nonetheless even with the existing limitation the images are capable of capturing anomalies in terms of lake water turbidity, lake area dynamics and biomass recovery. With new remote sensing platforms (Chapter 6) and diverse data collection missions scheduled for launch the use of remotely sensed data in water resources modeling is likely to expand. Consequently, the present shortcomings in spatial, temporal, spectral and radiometric resolutions will also improve.

References

ALSDORF, D., LETTENMAIER, D. & VÖRÖSMARTY, C. 2003. The need for global, satellite-based observations of terrestrial surface waters. *Eos, Transactions American Geophysical Union,* 84**,** 269.

ALSDORF, D. E., MELACK, J. M., DUNNE, T., MERTES, L. A. K., HESS, L. L. & SMITH, L. C. 2000. Interferometric radar measurements of water level changes on the Amazon flood plain. *Nature,* 404**,** 174-177.

BIRKETT, C. M. 1998. Contribution of the TOPEX NASA radar altimeter to the global monitoring of large rivers and wetlands. *Water Resources Research,* 34**,** 1223-1239.

BOLTEN, J. D., CROW, W. T., ZHAN, X., JACKSON, T. J. & REYNOLDS, C. A. 2010. Evaluating the utility of remotely sensed soil moisture retrievals for operational agricultural drought monitoring. *Selected Topics in Applied Earth Observations and Remote Sensing, IEEE Journal of,* 3**,** 57-66.

CHEN, S., FANG, L., ZHANG, L. & HUANG, W. 2009. Remote sensing of turbidity in seawater intrusion reaches of Pearl River Estuary-A case study in Modaomen water way, China. *Estuarine, Coastal and Shelf Science,* 82**,** 119-127.

DOZIER, J. 1992. OPPORTUN ITI ES TO IMPROVE HYDROLOGIC DATA. *Reviews of Geophysics,* 30**,** 315-331.

EASTON, Z. M., FUKA, D. R., WALTER, M. T., COWAN, D. M., SCHNEIDERMAN, E. M. & STEENHUIS, T. S. 2008. Re-conceptualizing the soil and water assessment tool (SWAT) model to predict runoff from variable source areas. *Journal of hydrology,* 348**,** 279-291.

FIORANI, L., OKLADNIKOV, I. G. & PALUCCI, A. 2006. First algorithm for chlorophyll - a retrieval from MODIS - Terra imagery of Sun - induced fluorescence in the Southern Ocean. *International Journal of Remote Sensing,* 27**,** 3615-3622.

GAO, B. C. 1996. NDWI—a normalized difference water index for remote sensing of vegetation liquid water from space. *Remote Sensing of Environment,* 58**,** 257-266.

HARVEY, K. & GRABS, W. WMO report of the GCOS. 2003. 18-20.

HU, C., CHEN, Z., CLAYTON, T. D., SWARZENSKI, P., BROCK, J. C. & MULLER–KARGER, F. E. 2004. Assessment of estuarine water-quality indicators using MODIS medium-resolution bands: Initial results from Tampa Bay, FL. *Remote Sensing of Environment,* 93**,** 423-441.

JIANG, X., TANG, J., ZHANG, M., MA, R. & DING, J. 2009. Application of MODIS data in monitoring suspended sediment of Taihu Lake, China. *Chinese Journal of Oceanology and Limnology,* 27**,** 614-620.

KERR, Y. H., WALDTEUFEL, P., WIGNERON, J. P., MARTINUZZI, J., FONT, J. & BERGER, M. 2001. Soil moisture retrieval from space: The Soil Moisture and Ocean Salinity (SMOS) mission. *Geoscience and Remote Sensing, IEEE Transactions on,* 39**,** 1729-1735.

KIRCHNER, J. W. 2006. Getting the right answers for the right reasons: Linking measurements, analyses, and models to advance the science of hydrology. *Water Resources Research,* 42**,** W03S04.

KUTSER, T., METSAMAA, L., VAHTMAE, E. & STROMBECK, N. Suitability of MODIS 250 m resolution band data for quantitative mapping of cyanobacterial blooms. 2006. 318-328.
KWIATKOWSKA, E. & MCCLAIN, C. 2009. Evaluation of SeaWiFS, MODIS Terra and MODIS Aqua coverage for studies of phytoplankton diurnal variability. *International Journal of Remote Sensing,* 30**,** 6441-6459.
LIU, Y., ISLAM, M. A. & GAO, J. 2003. Quantification of shallow water quality parameters by means of remote sensing. *Progress in Physical Geography,* 27**,** 24-43.
LPDAAC 2010. Surface Reflectance Daily L2G Global 250m.
MACAULEY, M. K. & VUKOVICH, F. M. 2005. *Earth Science Remote Sensing Data: Contributions to Natural Resources Policymaking*, Resources for the Future.
MILDREXLER, D. J., ZHAO, M., HEINSCH, F. A. & RUNNING, S. W. 2007. A new satellite-based methodology for continental-scale disturbance detection. *Ecological Applications,* 17**,** 235-250.
NAEIMI, V., SCIPAL, K., BARTALIS, Z., HASENAUER, S. & WAGNER, W. 2009. An improved soil moisture retrieval algorithm for ERS and METOP scatterometer observations. *Geoscience and Remote Sensing, IEEE Transactions on,* 47**,** 1999-2013.
NECHAD, B., RUDDICK, K. & PARK, Y. 2010. Calibration and validation of a generic multisensor algorithm for mapping of total suspended matter in turbid waters. *Remote Sensing of Environment,* 114**,** 854-866.
PRIGENT, C., MATTHEWS, E., AIRES, F. & ROSSOW, W. B. 2001. Remote sensing of global wetland dynamics with multiple satellite data sets. *Geophysical Research Letters,* 28**,** 4631-4634.
SHEN, F., SALAMA, M. H. D. S., ZHOU, Y. X., LI, J. F., SU, Z. & KUANG, D. B. 2010. Remote-sensing reflectance characteristics of highly turbid estuarine waters–a comparative experiment of the Yangtze River and the Yellow River. *International Journal of Remote Sensing,* 31**,** 2639-2654.
SILBERSTEIN, R. 2006. Hydrological models are so good, do we still need data? *Environmental Modelling & Software,* 21**,** 1340-1352.
SMEC 2008. HYDROLOGICAL STUDY OF THE TANA-BELES SUB BASINS. *SURFACE WATER INVESTIGATION REPORT.*
SMITH, L. C., ISACKS, B. L., BLOOM, A. L. & MURRAY, A. B. 1996. Estimation of discharge from three braided rivers using synthetic aperture radar satellite imagery: Potential application to ungaged basins. *Water Resources Research,* 32**,** 2021-2034.
TILAHUN, S., GUZMAN, C., ZEGEYE, A., ENGDA, T., COLLICK, A., RIMMER, A. & STEENHUIS, T. 2012. An efficient semi-distributed hillslope erosion model for the sub humid Ethiopian Highlands. *Hydrol. Earth Syst. Sci. Discuss,* 9**,** 2121-2155.
TUCKER, C. J. 1979. Red and photographic infrared linear combinations for monitoring vegetation. *Remote Sensing of Environment,* 8**,** 127-150.
UNGANAI, L. S. & KOGAN, F. N. 1998. Drought monitoring and corn yield estimation in Southern Africa from AVHRR data. *Remote Sensing of Environment,* 63**,** 219-232.
VERSTRAETEN, W. W., VEROUSTRAETE, F., VAN DER SANDE, C. J., GROOTAERS, I. & FEYEN, J. 2006. Soil moisture retrieval using thermal inertia, determined with visible and thermal spaceborne data, validated for European forests. *Remote Sensing of Environment,* 101**,** 299-314.

VÖRÖSMARTY, C., ASKEW, A., GRABS, W., BARRY, R., BIRKETT, C., DÖLL, P., GOODISON, B., HALL, A., JENNE, R. & KITAEV, L. 2001. Global water data: A newly endangered species. *Eos, Transactions American Geophysical Union,* 82**,** 54-58.

VÖRÖSMARTY, C. J., GREEN, P., SALISBURY, J. & LAMMERS, R. B. 2000. Global water resources: vulnerability from climate change and population growth. *Science,* 289**,** 284.

WANG, H., HLADIK, C., HUANG, W., MILLA, K., EDMISTON, L., HARWELL, M. & SCHALLES, J. 2010. Detecting the spatial and temporal variability of chlorophyll-a concentration and total suspended solids in Apalachicola Bay, Florida using MODIS imagery. *International Journal of Remote Sensing,* 31**,** 439-453.

WANG, L. & QU, J. J. 2007. NMDI: A normalized multi-band drought index for monitoring soil and vegetation moisture with satellite remote sensing. *Geophysical Research Letters,* 34**,** L20405.

CHAPTER 2: EVALUATING SUITABILITY OF MODIS-TERRA IMAGES FOR REPRODUCING HISTORIC SEDIMENT CONCENTRATIONS IN WATER BODIES: LAKE TANA, ETHIOPIA

Abstract

Government and NGO funded conservation programs are being implemented in developing countries with the potential benefit of reduced sediment inflow into fresh water lakes. However, the effectiveness of these programs is difficult to ascertain due to limited historical data on sediment concentration in lakes and rivers due to prohibitive costs to developing economies. Remote sensing can potentially aid in monitoring sediment concentration. With almost daily availability over the past ten years and consistent atmospheric correction applied to the images, Moderate Resolution Imaging Spectroradiometer (MODIS) 250–m images are potential resources capable of monitoring future concentrations and reconstructing historical sediment concentration records. In this paper, site-specific relationships are developed between reflectance in the near-infrared (NIR) images and three factors: total suspended solids (TSS), turbidity and Secchi depth for Lake Tana near the mouth of the Gumera River. The first two sampling campaigns on November 27, 2010 and May 13, 2011 are used for calibration. Reflectance in the NIR varies linearly with turbidity ($R^2 = 0.89$) and TSS ($R^2 = 0.95$). Secchi depth fit best to an exponential relation with R^2 of 0.74. The relationships are validated using a third sample set collected on November 7, 2011 with RMSE of 11 Nephelometric Turbidity Units (NTU) for Turbidity, 16.5 mg/l for TSS and 0.12 meters for Secchi depth. Using the relationship for TSS, a 10-year time series of sediment concentration in Lake Tana near the Gumera River was plotted. It was found that after the severe drought of 2002 and 2003 the concentration in the lake

increased significantly. The results showed that MODIS images are potential cost effective tools to monitor suspended sediment concentration and obtain a past history of concentration for evaluating the effect of best management practices.

2.1 Introduction

Reduced sediment inflow decreases sedimentation of reservoirs, ensures sunlight penetration in lake water, improves the productivity of the whole food web in the aquatic system (Vijverberg et al., 2009), increases zooplankton growth (Lind et al., 1992) and makes water supply disinfection more effective (Gadgil, 1998). In the Ethiopian highlands, conservation practices are being instituted by the government and NGO's to reduce soil erosion and thereby reduce sediment concentration in streams. Despite millions of dollars invested (Nedessa and Wickrema, 2010), very few measurements are available with which to evaluate the effectiveness of these interventions. In a few cases, soil and water conservation practices have decreased sediment concentrations (Herweg and Ludi, 1999, Nyssen et al., 2008). However, in general there is not a downward trend in sediment concentrations (Tilahun et al., 2012). Some studies suggest that 70% of reservoirs built in the last 20 years have serious siltation problems and that the useful life will end well before the dam design period (Haregeweyn et al., 2006).With the construction of new hydroelectric dams in Ethiopia it becomes more and more important to assess the effectiveness of conservation practices. One of the ways that this can be accomplished is by measuring sediment concentration in water bodies (Delmas et al., 2011).

Intensive sampling of either sediment concentration (gravimetric) or turbidity (by optical Secchi disk) on many locations is prohibitively expensive and has led to efforts to map these parameters using remotely sensed images (Forget and Ouillon, 1998, Froidefond et al., 1999, Myint and

Walker, 2002, Hu et al., 2004, Chen et al., 2007, Nechad et al., 2010, Wang et al., 2010b). Table 1 gives some of the relationships between remotely sensed reflectance and sediment concentration. All are site specific (Liu et al., 2003) due to two factors: first the combination of subjective criteria used by researchers in atmospheric correction, with empirical calibration factors for correcting the sensitivity of the sensor (Froidefond et al., 1999) and second, the infinite combinations of diverse water constituents which creates a wide variation in the spectral reflectance of shallow waters (Baban, 1993, Chami et al., 2006). In this paper a site specific relationships is developed for mapping TSS, turbidity and Secchi depth on Lake Tana. The relationship developed for TSS is used to construct a ten year sequence of suspended sediment concentrations for the Gumera River that flows to Lake Tana.

2.1.1 Remote sensing platform

The use of remotely sensed images for sediment concentration estimation has to strike a balance between ease of access and processing, sensitivity to change in water color, and temporal resolution of the remotely sensed data. In addition, the rigorous atmospheric correction required in using remotely sensed images has been a major source of uncertainty in the past because of the extreme sensitivity of most atmospheric correction algorithms to subtle changes in the visible spectrum (Werdell et al., 2010, Jolivet et al., 2007). Recent developments in remote sensing have enabled the global science community to have access to images with consistent atmospheric correction applied to them. One such achievement is the MODIS–Terra version–5 validated Stage 2 products (LPDAAC, 2010). Other advantages are that MODIS has detectors in spectral regions that provide direct estimates of atmospheric scattering and absorption (Li et al., 2003, Kaufman et al., 1998) leading to a more consistent atmospheric correction. The release of these products avoids the effort required for sensor calibration and atmospheric correction. The

accuracy of these products has been confirmed at many locations and time periods (LPDAAC, 2010). MODIS images are also available on a daily basis, and that MODIS medium–resolution images (250m) provide the advantage of increased sensitivity for suspended solid observation in that these bands are 4–5 times more sensitive than the L7–ETM+ bands (Hu et al., 2004).

Correlations between MODIS–measured reflectance and turbidity, total suspended matter (TSM), suspended sediment concentration (SSC) and/or TSS have been reported by several authors. The equations and correlations from the most recent studies using MODIS images to quantify water quality parameters are presented in Table 2-1.

Table 2-1: Correlations between different MODIS bands reflectance and water quality parameters suggest site specific regression equations

Parameter	Equation[1]	r^2	
TSS (mg/l)	$0.0052e^{(10028(R_{b1}-R_{b2}))}$ for $0.0058<(R_{b1}-R_{b2})<0.0076$	0.90	*(Hu et al., 2004)*
	$0.1915e^{(624.72R_{b1})}$ for $0.0035<R_{b1}<0.0062$	0.90	
TSM (mg/l)	$-1.91 + 1140.25 \times R_{b1}$	0.89	*(Miller and McKee, 2004)*
Turbidity (NTU)	$1203.9 \times R_{b1}^{1.087}$	0.73	*(Chen et al., 2007)*
SSC (mg/l)	$-23.03 + 60.24 \times (R_{b2} - R_{b5})$	0.73	*(Wang and Lu, 2010)*
Log(TSS) (mg/l)	$0.1497e^{\{1.859[log_{10}^{(Rb2)}/log_{10}^{(Rb1)}]\}}$	0.61	*(Wang and Lu, 2010)*
	$1.5144\left[log_{10}^{(Rb2)}/log_{10}^{(Rb1)}\right] - 0.5755$	0.72	

[1] R refers to reflectance and b followed by a number refers to band number, for example R_{b1} refers to reflectance from band one. For MODIS images band 1 represents the NIR, band 2 the red and band 5 the SWIR wavelengths.

2.2 Materials and methods

Lake Tana (Figure 2-1) is situated on the basaltic plateau of the north-western highland of Ethiopia (12°N, 37°15'E, and 1,800 m altitude) covering an area of over 3,000 km^2.

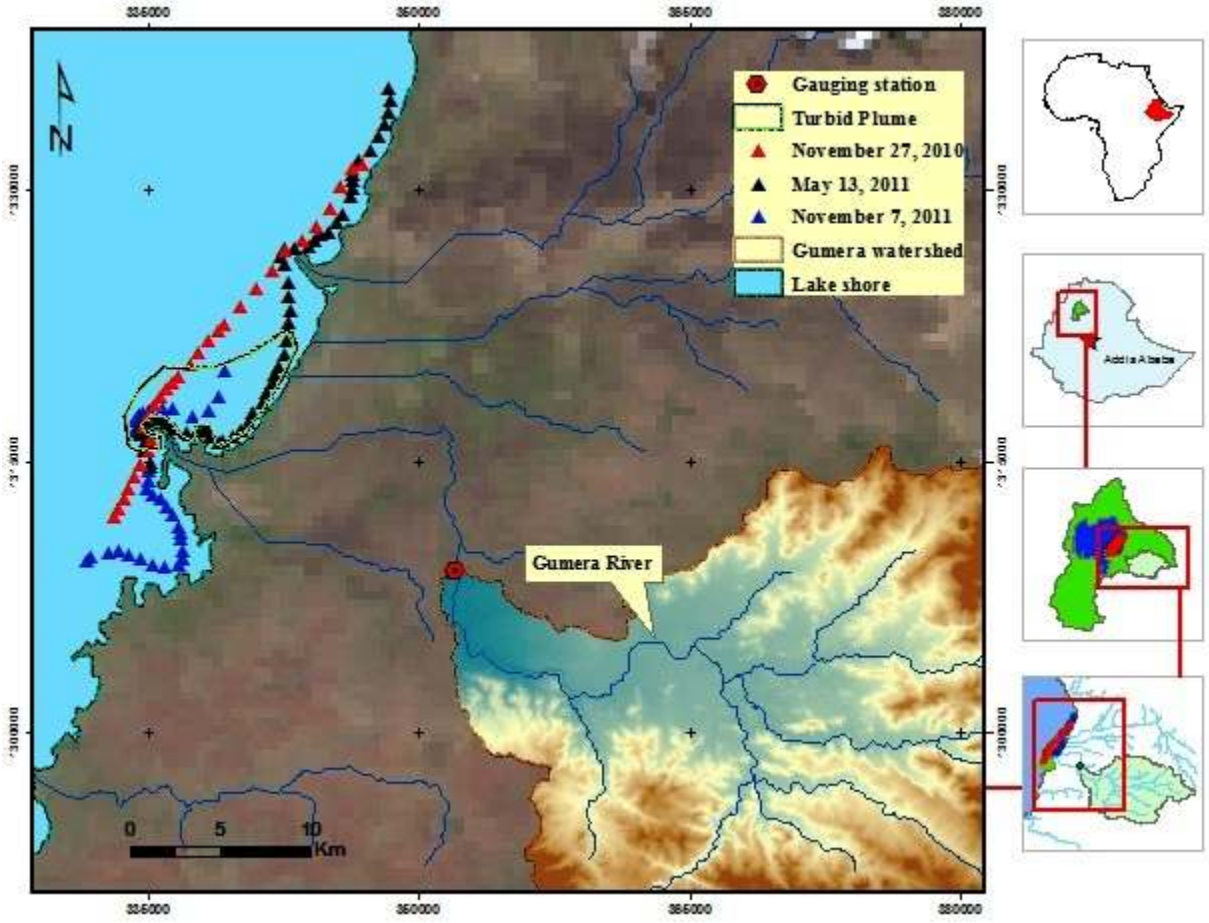

Figure 2-1: In this 13 June 2000 MODIS image, a turbid plume flows into the lake turning the shore and stream mouth locations to reddish brown and raising the water reflectance

The lake drains a catchment area of 16,000 km^2. Six permanent rivers and 40 small seasonal rivers feed the lake. The shallow lake (average depth 9 m) is Ethiopia's largest lake, containing half the country's freshwater resources, and is the third largest in the Nile Basin (Vijverberg et al., 2009). The most pronounced advantage of Lake Tana is its storage capacity, in that it accommodates a live storage which amounts to more than two times that of the five largest

reservoirs in Ethiopia[†], rendering a relatively low cost per unit of utilizable water (Gebeyehu, 2004). A bathymetric survey undertaken in 2006 showed that the lake has a maximum depth of 15 m and stretches 65 km west-east and 74 km south–north (Ayana, 2007). The main rainy monsoon season begins in June and lasts through September and temperature varies between day time extremes of 30°C to night lows of 6°C. The minimum recorded annual precipitation was 966 mm in the year 2002 and the annual maximum was 1998 mm in the year 1997(Yilma and Awulachew, 2009).

2.2.1 TSS, Turbidity and Secchi depth measurements

Three campaigns were carried out to collect water samples and measure Secchi depth within 15 minutes of the time of the satellite overpass over Lake Tana near the mouth of the Gumera River, which has a mean flow of 34 m^3/sec during the rainy season. Separate campaigns were conducted during the mornings of November 27, 2010, May 13, 2011 and November 7, 2011. Samples were collected along transects parallel to the shore during each overpass (Figure 2-2). Ground measurements were done within about ± 30 minutes of the seconds-long satellite overpass (i.e. a 1 hour period centered on 10:30 AM). Concurrent measurements are crucial as sediment concentrations during high streamflow or wind can change quickly (Petus et al., 2010). At each location along the sampling path, bulk water samples were collected from the upper 0.2 m of the water column in a 750 ml container for turbidity and TSS analysis. GPS coordinates of sampled locations were also recorded. During sampling the commonly known algal bloom areas are excluded to avoid uncertainties in the measurement.

[†]Gilgel Gibe, Koka, Finchaa, Amerti, and Melka Wakena, provide an aggregate storage capacity of about 4.4 billion m^3, compared to Lake Tana's live storage of 9 billion m^3

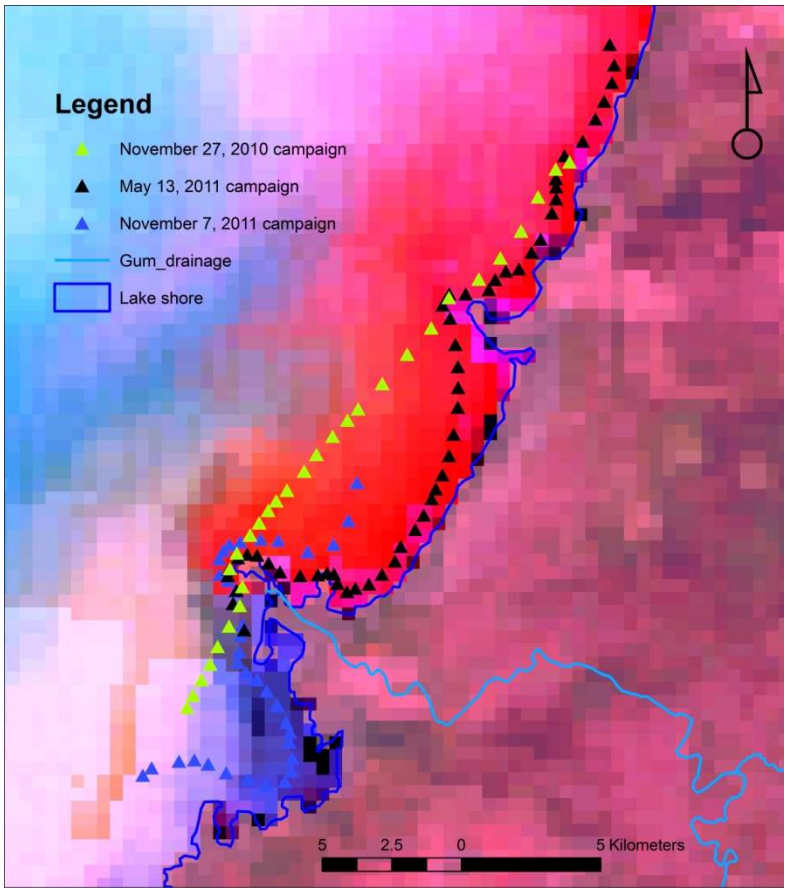

Figure 2-2: Three sampling campaigns were conducted near the outlet of Gumera River in Lake Tana: During the dry season May 13, 2011 and shortly after the end of the rainy season on November 27, 2010 and November 7, 2011

Total suspended solids measurements were made in the laboratory by drawing 10 ml aliquot from a well mixed container, centrifuging for ten minutes at 4000 rpm, pouring off supernatant, separating and drying the retained solids, and weighing (Queenan et al., 1996). Turbidity measurements were made using a Hach 2100N turbidimeter calibrated using formazin solution.

2.2.2 MODIS data

The MODIS-Terra satellite has been acquiring images of the entire globe since 2000 in 36 spectral bands with 250-m, 500-m, and 1,000-m spatial resolutions. The red (620-670 nm) and NIR (841-876 nm) bands labeled 'MOD09GQ' are available on a nearly daily basis at 250m

spatial resolution. These bands are sensitive for turbid water applications (Hu et al., 2004) . A number of previous studies have successfully used MODIS 250 m images to establish a reflectance–TSS, reflectance–turbidity and reflectance–Secchi depth relationships (Chen et al., 2007, Dall'Olmo et al., 2005, Kutser et al., 2006, Miller and McKee, 2004, Petus et al., 2010). In this study MODIS Terra data are used because our field samples were taken in the morning corresponding to Terra's imaging time. MODIS red and NIR 250 m images corresponding to the field water sampling dates (i.e. 27 November 2010, 13 May 2011 and 7 November 2011) were downloaded from the USGS site using MODIS Reprojection Tool Web Interface (MRTWeb)[†]. The following table summarizes the observations for the respective dates.

Table 2-2: Numbers of lake samples collected for the campaign days (Appendix A1)

Parameter	**Unit**	**Calibration**		**Validation**
		Nov 27, 2010 # of samples	**May 13, 2011 # of samples**	**Nov 7, 2011 # of samples**
Turbidity	NTU	54	51	30
TSS	Mg l^{-1}	54	51	34
Secchi Depth	m	54	51	30

2.2.3 MODIS reflectance relationship to TSS, turbidity and Secchi depth

In order to obtain the relationship between the MODIS reflectance and indicators of sediment concentration in the lake a multiple regression analysis was performed on various combinations of red and near infrared red (NIR) bands (Table 2-3). Following the work of Wang et al. (2010b), several combinations of bands were used (e.g. sum, the difference and ratio of reflectance of the two bands) to increase the goodness of fit of the regression equations. Normalized ratios (NIR to red), band sum and band difference are used along with single band regression. Samples from the first two campaigns of November 27, 2010 and May 13, 2011 are used to establish the relation

[†] https://mrtweb.cr.usgs.gov/

(i.e. calibration) and the third sample collected on November 7, 2011 was used to validate the relation. The goodness of fit of the models is evaluated based on the resulting coefficient of determination (R^2). Adjusted R^2 is also calculated for each regression to test if an improvement in the R^2 is due to the inclusion of a band to the regression model or a random chance. For the validation step, the accuracies of predicted TSS, turbidity and Secchi depth were assessed by root mean square error (RMSE).

2.2.4 Determining historical record of Lake sediment concentration near Gumera River

Images for a 10-year time span (2000-2009) NIR images of the area in the vicinity of the Gumera River outlet into Lake Tana were downloaded from the USGS MODIS archive via MRTWeb. Cloud contaminated images were excluded and the images were masked with the water sampling location polygon. This location is consistently more turbid during the rainy season (Figure 2-1). A mean reflectance raster image is created for each month. In each mean reflectance image the pixel with the largest reflectance is identified using the Getis–Ord Gi* statistic data mining technique (Getis and Ord, 2010). The Getis–Ord Gi* statistic is given by:

$$G_i^* = \frac{\sum_{j=1}^{n} w_{i,j}x_j - \bar{X}\sum_{j=1}^{n} w_{i,j}}{s\sqrt{\frac{\left[n\sum_{j=1}^{n} w_{i,j}^2 - \left(\sum_{j=1}^{n} w_{i,j}\right)^2\right]}{n-1}}} \qquad \text{(Equation 2-1)}$$

Where x_j is the TSS value for pixel J, $w_{i,j}$ is the spatial weight between feature i and j, n is equal to the total number of pixels, $\bar{X}$ is mean of the TSS values within the cut off distance given by $\bar{X} = \frac{\sum_{j=1}^{n} x_j}{n}$ and $s = \sqrt{\frac{\sum_{j=1}^{n} x_j^2}{n} - (\bar{X})^2}$

In this method each of the pixels within the delineated entry location will be looked within the context of its neighbouring pixels. The local sum for a pixel and its neighbours is compared proportionally to the sum of all features; when the local sum is much different than the expected local sum, and that difference is too large to be the result of random chance, a statistically significant z score results. For statistically significant positive z scores, the larger the z score is, the more intense the clustering of high values or a hot spot (Mitchell, 2005).

2.3 Results

The relationship between MODIS reflectance to TSS, turbidity and Secchi depth are given in Table 2-3. In all band combinations a linear relationship was observed between the tested NIR and red combinations of MODIS bands and either TSS, turbidity and Secchi depth. The relationship between MODIS reflectance to NIR band was consistently superior to other combinations. The calibrated regressions between TSS, turbidity, Secchi depth and the reflectance in the NIR band, ρ_{NIR} were, in order of decreasing r^2:

$$TSS = 2371.\times \rho_{NIR} - 62.8 \qquad \text{Equation 2-2}$$

where TSS is in mgl^{-1}, $n = 54$ and $p < 0.001$ and $r^2 = 0.95$

$$Turbidity = 3209 \times \rho_{NIR} - 50.1 \qquad \text{Equation 2-3}$$

where turbidity is in NTU, $n = 43$ and $p < 0.001$ and $r^2 = 0.89$

$$Secchi\ depth = 0.38\ \times e^{-12.2\times\rho_{NIR}} \qquad \text{Equation 2-4}$$

where Secchi depth is in meters, $n = 73$ and $p < 0.001$ and $r^2 = 0.74$

Applying these equations to the November 7, 2011 image resulted in a root mean square error (RMSE) of 16.5 mg l^{-1}, 15.6 NTU and 0.11 m in comparison to measured TSS, turbidity and

Secchi depth respectively. The scatter plot for observed and estimated turbidity, TSS, and Secchi depth and the residual of these estimates are shown in Figure 2-3. The residuals were distributed within ±5 mgl^{-1} for TSS, ±8 NTU for turbidity, and ±0.06 m for Secchi depth.

Table 2-3: Estimation statistics for various band combinations; bold numbers have the largest R^2

Band Combination	**R^2**	**Adjusted R^2**	**Standard error**	**Significance F**
Turbidity (N=45, mean = 100.03 NTU)				
NIR	**0.89**		16.57	0.000
NIR/Red	0.76	0.75	25.26	0.000
NIR + Red	0.08	0.06	49.4	0.063
Red - NIR	0.48	0.47	37.04	0.000
$(Red - NIR)/(Red + NIR)$	0.69	0.68	28.6	0.000
TSS (N=54, mean = 48.43 mg l^{-1})				
NIR	**0.95**		10.77	0.000
NIR/Red	0.89	0.88	16.86	0.000
NIR + Red	0.76	0.76	24.34	0.000
Red - NIR	0.86	0.85	18.96	0.000
$(Red - NIR)/(Red + NIR)$	0.88	0.88	16.92	0.000
Secchi depth (N=73, mean = 0.22m)				
NIR	**0.74**		0.02	0.000
NIR/Red	0.58	0.57	0.03	0.000
NIR + Red	0.50	0.49	0.03	0.000
Red - NIR	0.38	0.36	0.03	0.000
$(Red - NIR)/(Red + NIR)$	0.57	0.56	0.03	0.000

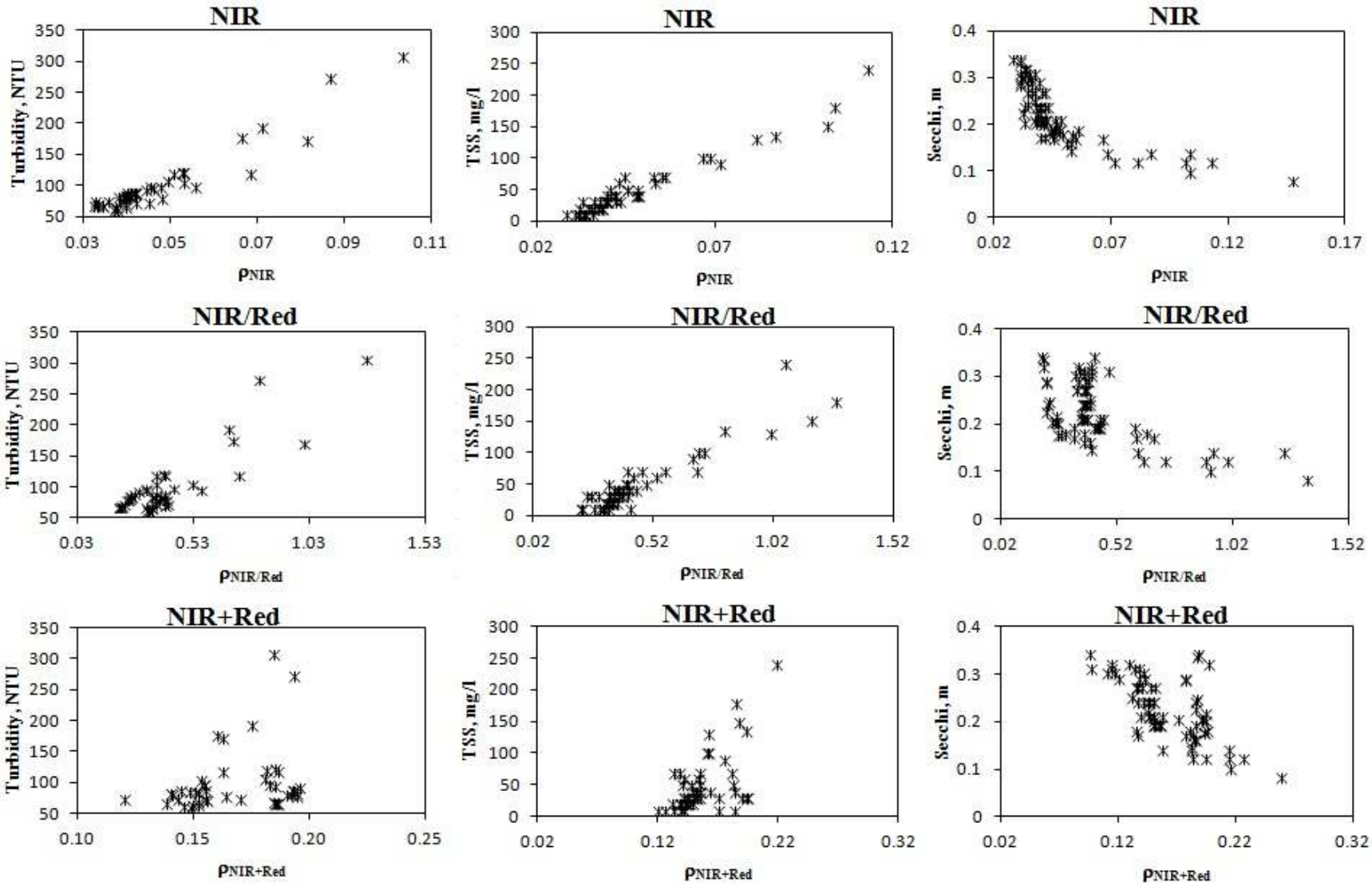
NIR
Turbidity, NTU
ρNIR
NIR
TSS, mg/l
ρNIR
NIR
Secchi, m
ρNIR
NIR/Red
Turbidity, NTU
ρNIR/Red
NIR/Red
TSS, mg/l
ρNIR/Red
NIR/Red
Secchi, m
ρNIR/Red
NIR+Red
Turbidity, NTU
ρNIR+Red
NIR+Red
TSS, mg/l
ρNIR+Red
NIR+Red
Secchi, m
ρNIR+Red

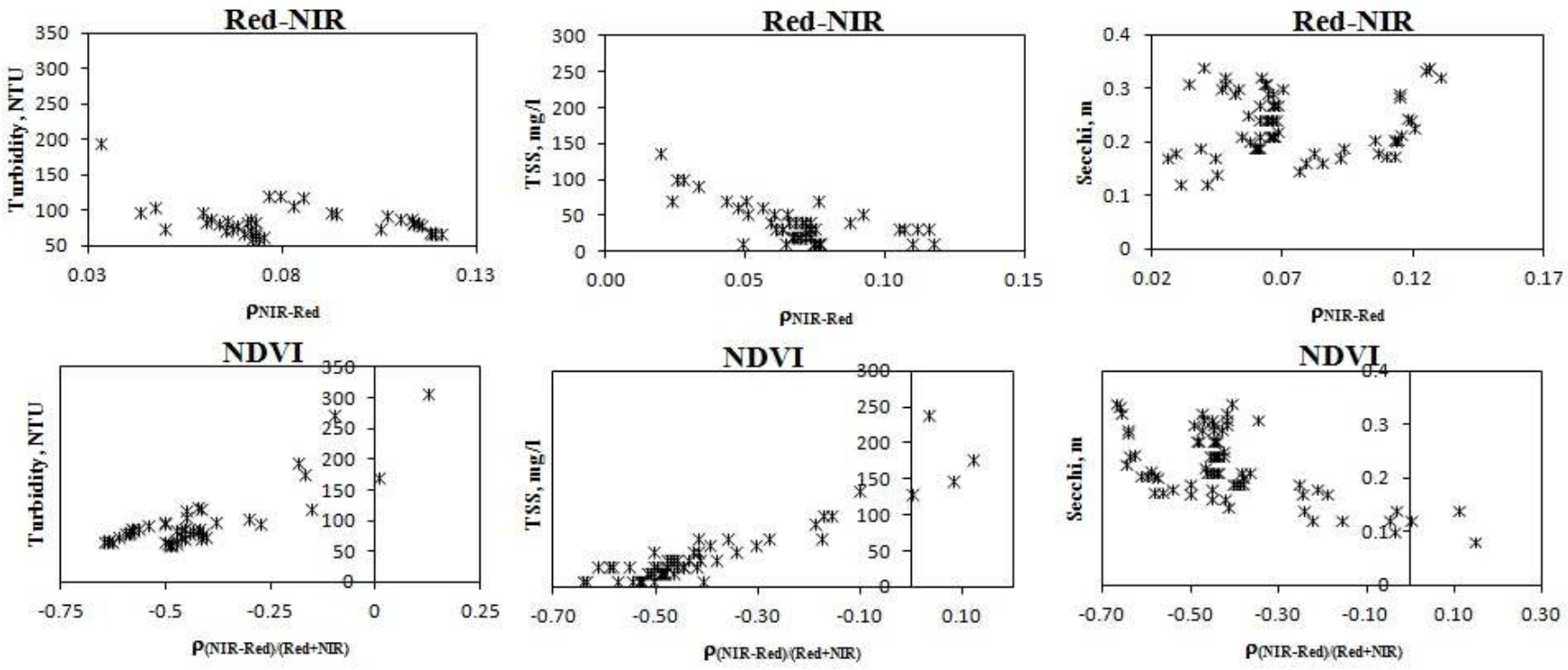

Figure 2-3: Scatter plot of water reflectance (ρ) against observed Turbidity, TSS and Secchi depth using different band combinations. The NIR band gives the best fit for all the parameters.

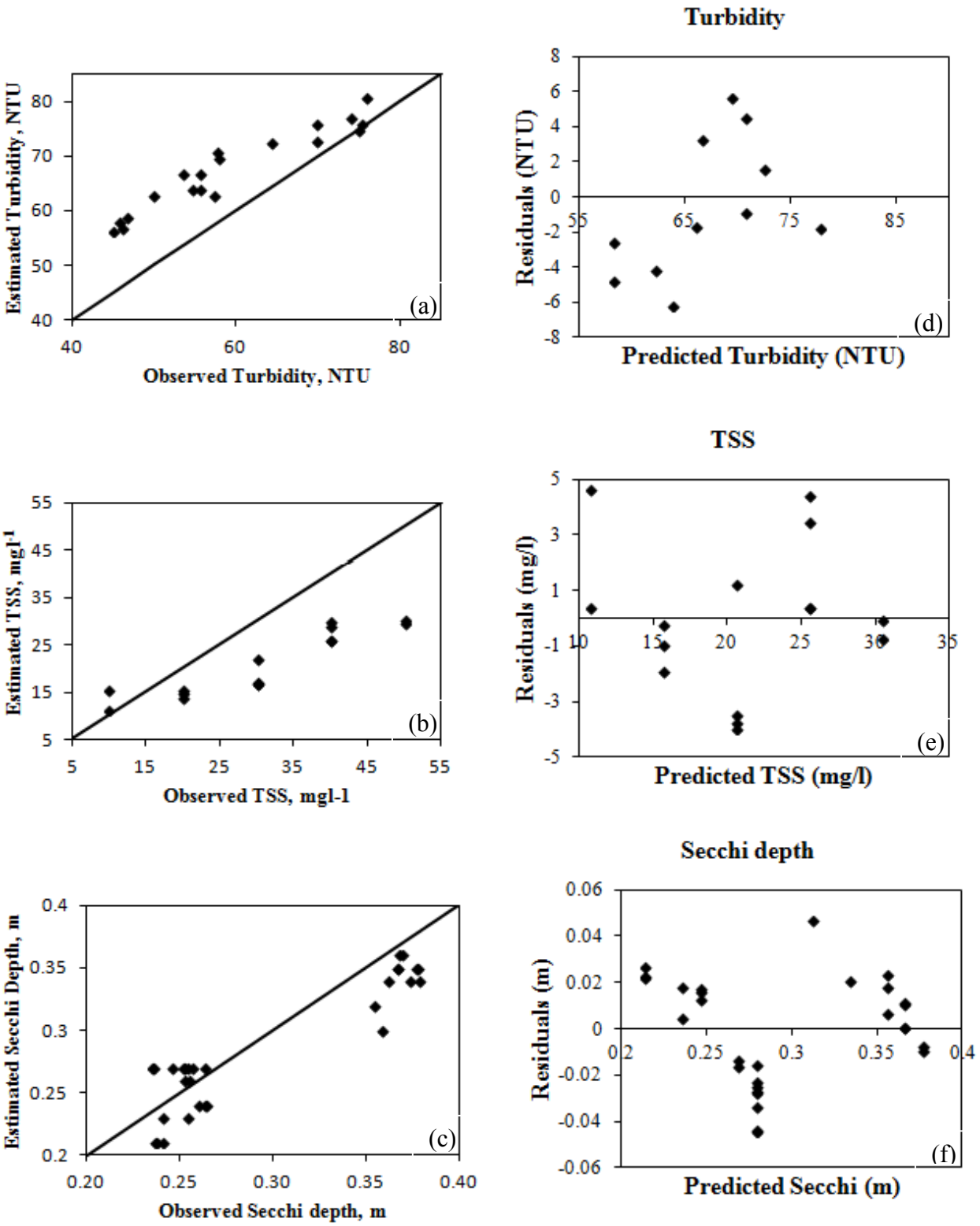

Figure 2-4: November 7, 2011 data is used to validate turbidity (a), TSS (b) and Secchi depth (c); and associated residuals (d through f)

The 10-year mean monthly time series data of maximum concentration observed at the river mouth in Lake Tana is depicted in Figure 2-5. The pixel with the highest z score for the Getis–Ord Gi* statistic is identified for the mean monthly images of the river mouth. The minimum concentration before 2004 was within the 80 – 100 mgl^{-1} range. In 2004, the minimum concentration shifted to about 200 mgl^{-1}. Greatest concentration reached the lake with the 2004 floods after which the annual peak concentration becomes approximately within the range of 450 – 600 mgl^{-1}.

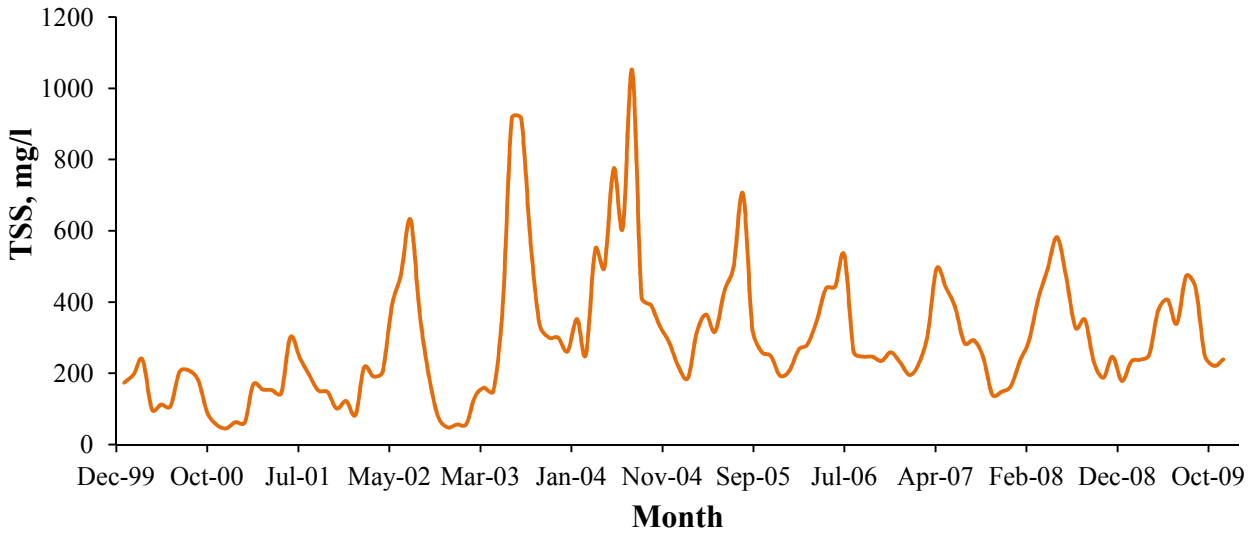

Figure 2-5: Comparison of TSS at river mouth on Lake Tana and a gauging station upstream the river mouth

2.4 Discussion

A single band regression equation performed the best in this case. The NIR band consistently yielded the highest coefficient of determination. Both TSS and turbidity exhibit a linear relationship (Equation 2-2 and 2-3) with the NIR band with a small offset (~1.5 to 2.5%). The linear relationship is in agreement with other studies (Han and Rundquist, 1994, Doxaran et al.,

2002, Ma and Dai, 2005, Wang et al., 2009). Early work (Morel and Prieur, 1977) also showed that the reflectance of an optically deep, homogeneous body of water would be proportional to a ratio of the backscattering to total attenuation (i.e. absorption + backscattering). Since most of the scattering is in the forward direction, absorption (a) is usually large relative to the backscattering (b_b) and the approximate relationship is then $= \frac{b_b}{a}$. In the infrared, where the absorption is predominantly due to water and the scattering is predominantly due to the suspended matter, it is reasonable to expect that the reflectance would be roughly linearly proportional to measures of the suspended load so long as the scattering properties are consistent over the range of observation. The small offset in the regression can be attributed to the uncertainty of the fit, at least for low concentrations. As the magnitude of TSS measured in the water samples is small, a low concentration from low reflectance values is associated with significant uncertainty. This is because a small error rapidly leads to a large relative error. Previous studies recommended the use of band combination to overcome such deficiencies (Hu et al., 2004, Wang and Lu, 2010). The red band was used in this research to exploit any advantages in improving the model. Three band combinations (band ratio, band combination and band difference) are applied but all yielded a lower R^2 in comparison to the single band regression. The band ratios including the NDVI yield better R^2 as compared to other combinations. The reason for the red band to fail to strongly correlate to TSS is likely explained by the effect of residues of aerosol that may remain in the visible bands after the atmospheric correction procedure (Wang et al., 2009). The linear relation of TSS with NIR was fairly stable over the sampling seasons and the same equation is used to generate the 10 year TSS time series (Figure 2-5).

In spite of high correlations observed between the NIR band and TSS and turbidity, it was evident that MODIS–Terra band 2 is not sensitive enough to detect turbidity variations below 60 NTU (Figure 2-6). For higher turbidity, it was found that the regression equations are fairly stable across varying seasons (two end-of rainy seasons and one dry season).

A strong linear relation (R^2=0.88, $p \leq 0.001$) is observed between TSS and turbidity (Figure 2-6). This suggests turbidity in the lake is mainly due to suspended solids and not from inflow of color causing materials. As the watershed is predominantly cultivated land (with little dispersed bush land) the inflow of color causing agents is minimal. However, the increased application of fertilizer (from none to 8.5 kg N $ha^{-1}yr^{-1}$ and 9.8 kg P $ha^{-1}yr^{-1}$ (Haileslassie et al., 2005)) and the subsequent flow of this into the lake will facilitate algal growth and hence increased biological turbidity. Nevertheless Han (2005) showed that the effect of algae on the TSS–reflectance relation was minimal at wavelengths between 700 and 900 nm. The effect of algae on TSS measurement was minimized by avoiding algal bloom areas during the sampling. The strong linear relationship is also useful in that it will enable using turbidity as a surrogate for TSS concentrations. Turbidity measurements can be automated in-situ and hence enable a nearly continuous TSS measurement.

Figure 2-7 depicts the dynamics between TSS concentration and flow (Figure 2-7(a)) and TSS concentration and water level in lake (Figure 2-7(b)). Peak concentration in the lake showed an increasing trend in the 2000 – 2004 periods with flow showing no trend for the same time period. The reduction in water level started in 2001 with the installation of five additional gates to the controlling weir which was initially operated by two gates (McCartney et al., 2010). Lake level declined at a rate of 0.5 m per year and reached historic minimum level (1784.6m) in 2003. The

minimum sediment concentration increased from 100 to 250 mg/l after 2002 due to a combination of late wet season flows and water withdrawal for hydropower generation.

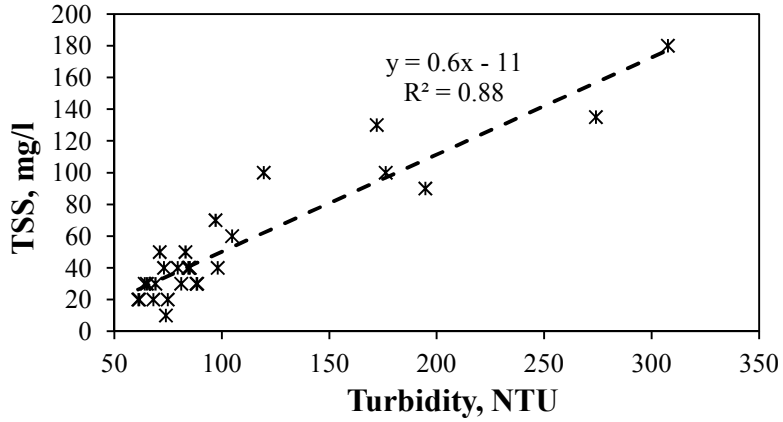

Figure 2-6: Strong correlation between TSS and turbidity indicates, turbidity below 60 NTU correlates poorly to the NIR or any of the band combination

The occurrence of TSS peak before flow peak is attributed to the loose soil condition at the start of the rainy season. The loose soil that is easily washed off cause the suspended solids concentrations peak before the rainy season gets fully underway. Concentrations in rivers in the beginning of the monsoon season are high and then decrease gradually (Steenhuis et al., 2009, Tilahun et al., 2012). In contrast, the runoff coefficient and discharge are small in the beginning of the rainy season and increase until the end of July where after the runoff coefficient becomes nearly constant (Liu et al., 2008). As the rainy season progresses, the soil becomes more cohesive and ground water begins to contribute to stream flow, further diluting the sediment concentration. TSS estimates from the regression equation are much smaller in comparison to data from a rating curve (Figure 2-5). The river gradient at entry to the lake is so small that flow velocity is low. The flood water then spreads over the river delta dropping the sediment load. Consequently, relatively less muddy water reaches the lake.

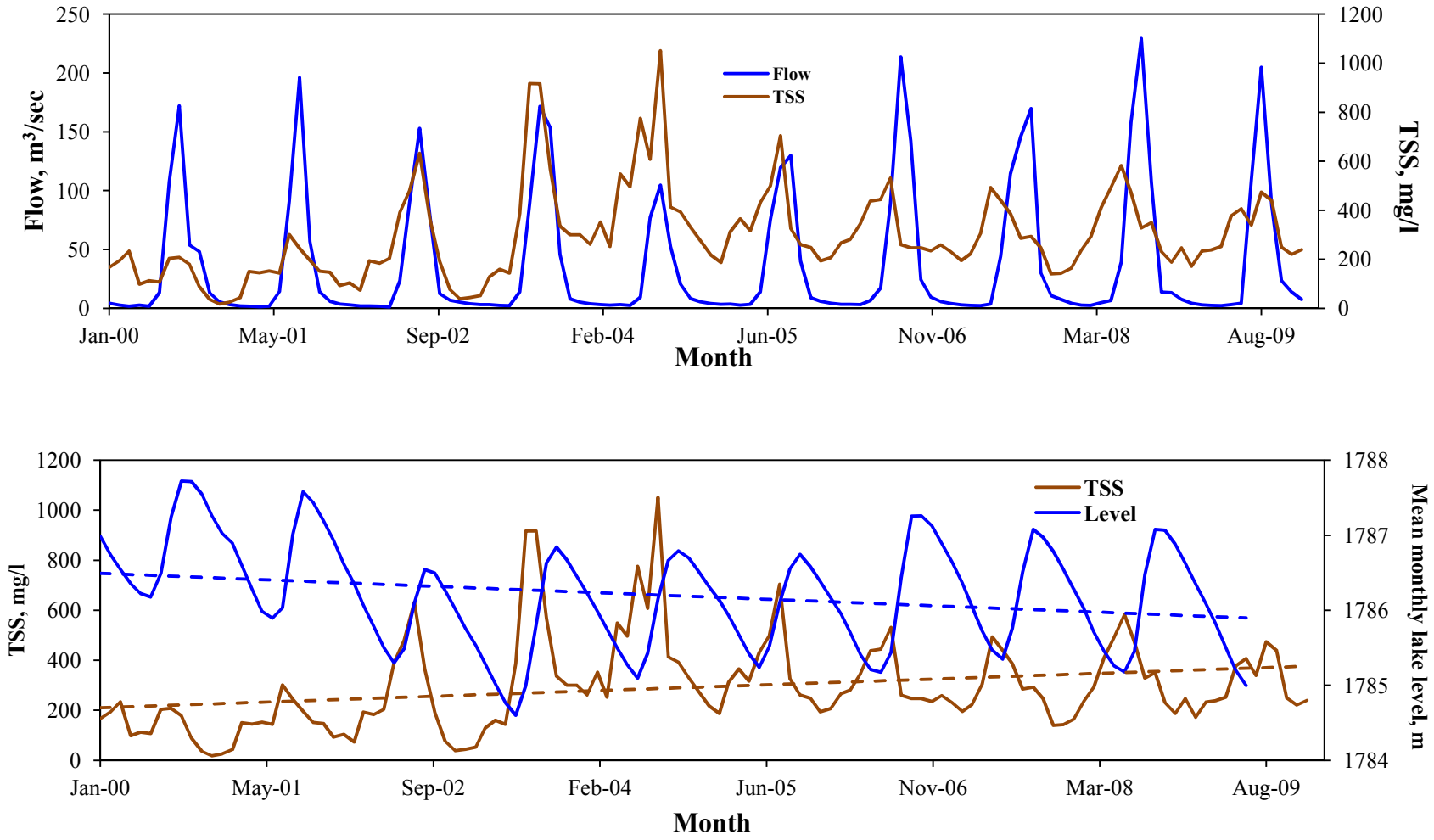

Figure 2-7: Time series plots for a) reflectance derived TSS time series for Lake Tana near mouth of Gumera River (2000–2009); a jump in the dry season TSS concentration and a spike in the peak for the years 2003 – 2004 was due to the consecutive drought years in 2002 and 2003 which brought much sediment but less water and b) comparison between lake level and TSS concentration variation, higher dry season concentration coincides with lower lake water level

The change in the dry season concentration at the end of the year in 2002 coincides with the consecutive drought years (2002 – 2003) and as a consequence the lowering of the lake by about two meters from the long term mean. In this time, the dry season TSS concentration shifted from about 100 mg/l to 250 mg/l (Figure 2-7 (a)). With a much reduced outflow during low water levels the residence time for the water, which is three years in normal seasons (Kebede et al., 2006), will increase considerably. This facilitates further mixing of the turbid plume with the lake water, rendering it a brownish color. Successive images collected right at the beginning of the rainy season show the spreading of the plume over the larger part of the lake. Thus, when the flood of the following season reaches the lake, the TSS concentration is already at a higher TSS level and hence the TSS extraction process catches this phenomenon resulting in TSS peaks for the years 2003 and 2004 (Figure 2-7 (b)). Satellite images of May through October 2002 (Figure 2-8) are used to show how the plume spreads over the lake. The mean monthly TSS map at the river mouth is overlain with TSS contour lines (Figure 2-9).

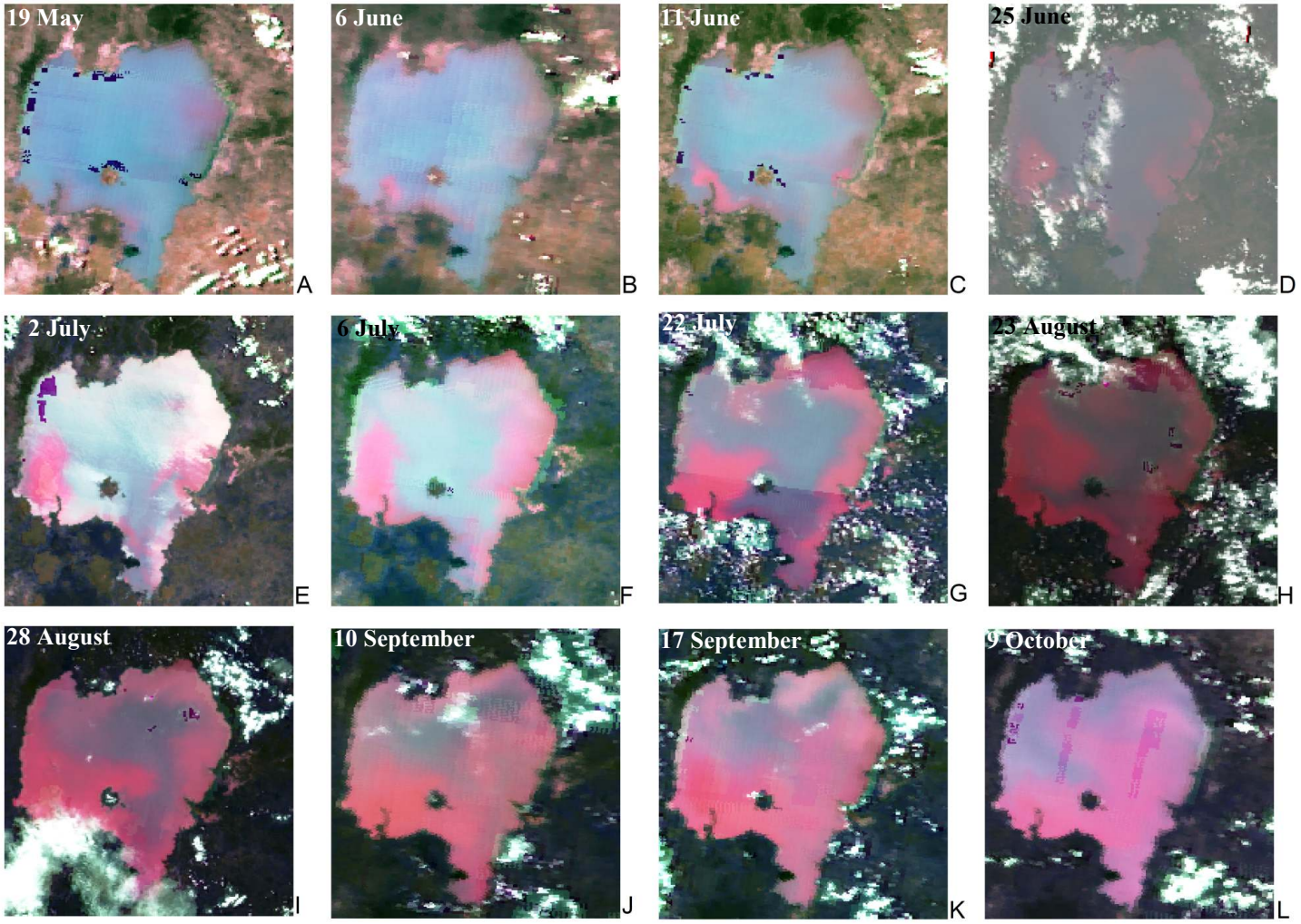

Figure 2-8: Spreading of turbid plume in the year 2002; river mouths appear relatively clean (a) just before the start of the rainy season; (b through f) as the rainy season begins, the reddish turbid plume appears at the entry location; (g through J) the plume spreads along the shore and over a wider area; (k and l) with a reduced outflow from the lake during this typically low flow season the plume spreads to cover the whole lake

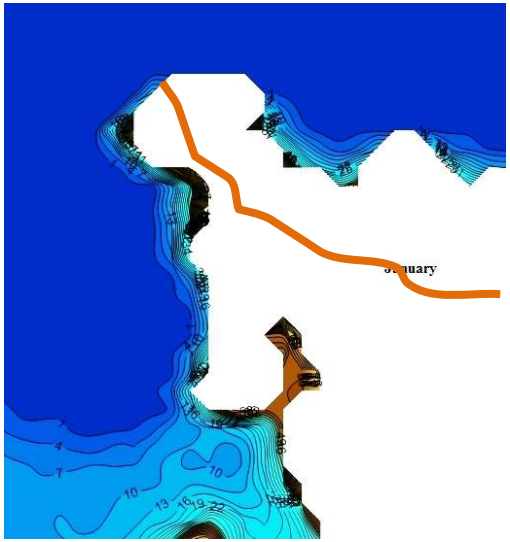

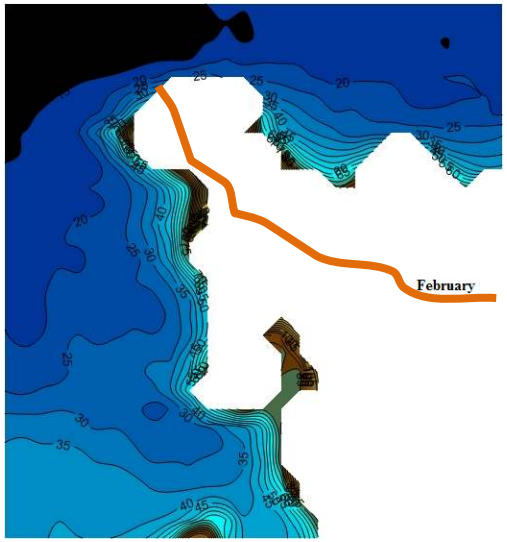
February

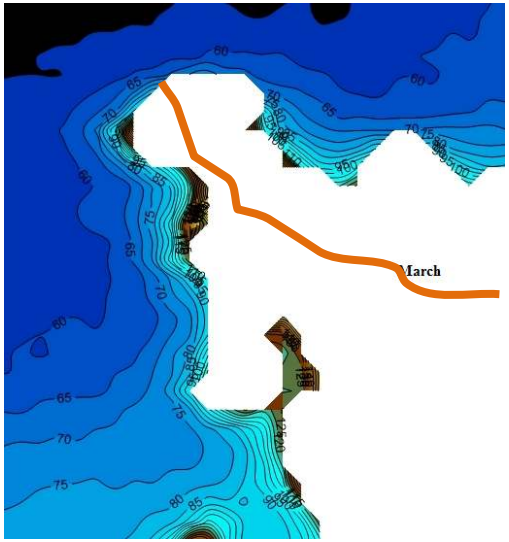
March

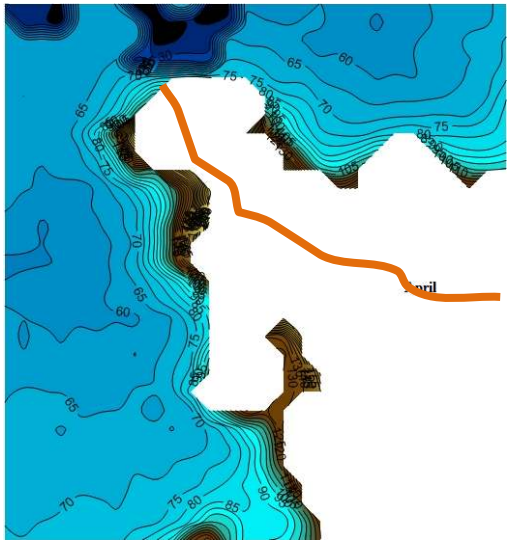

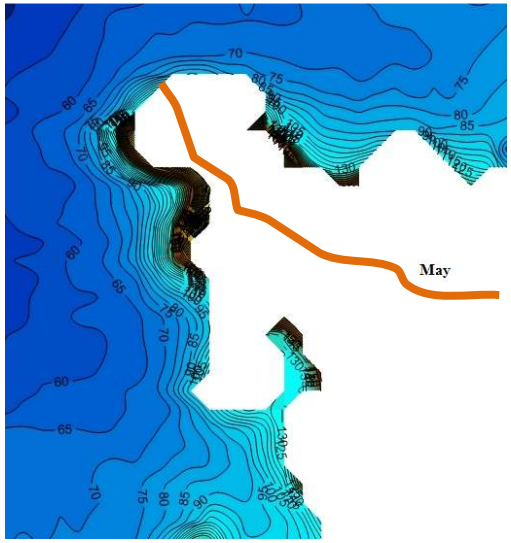
May

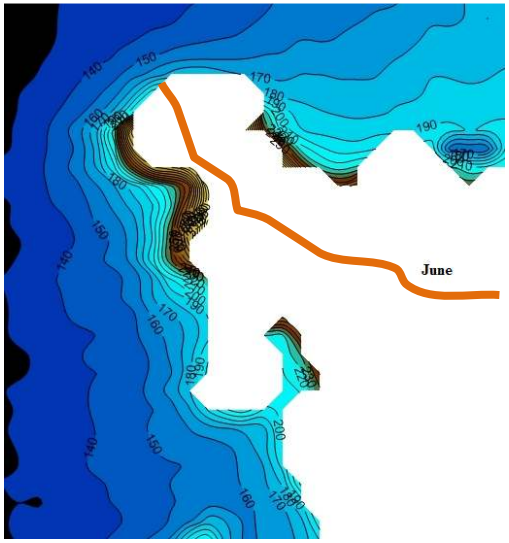
June

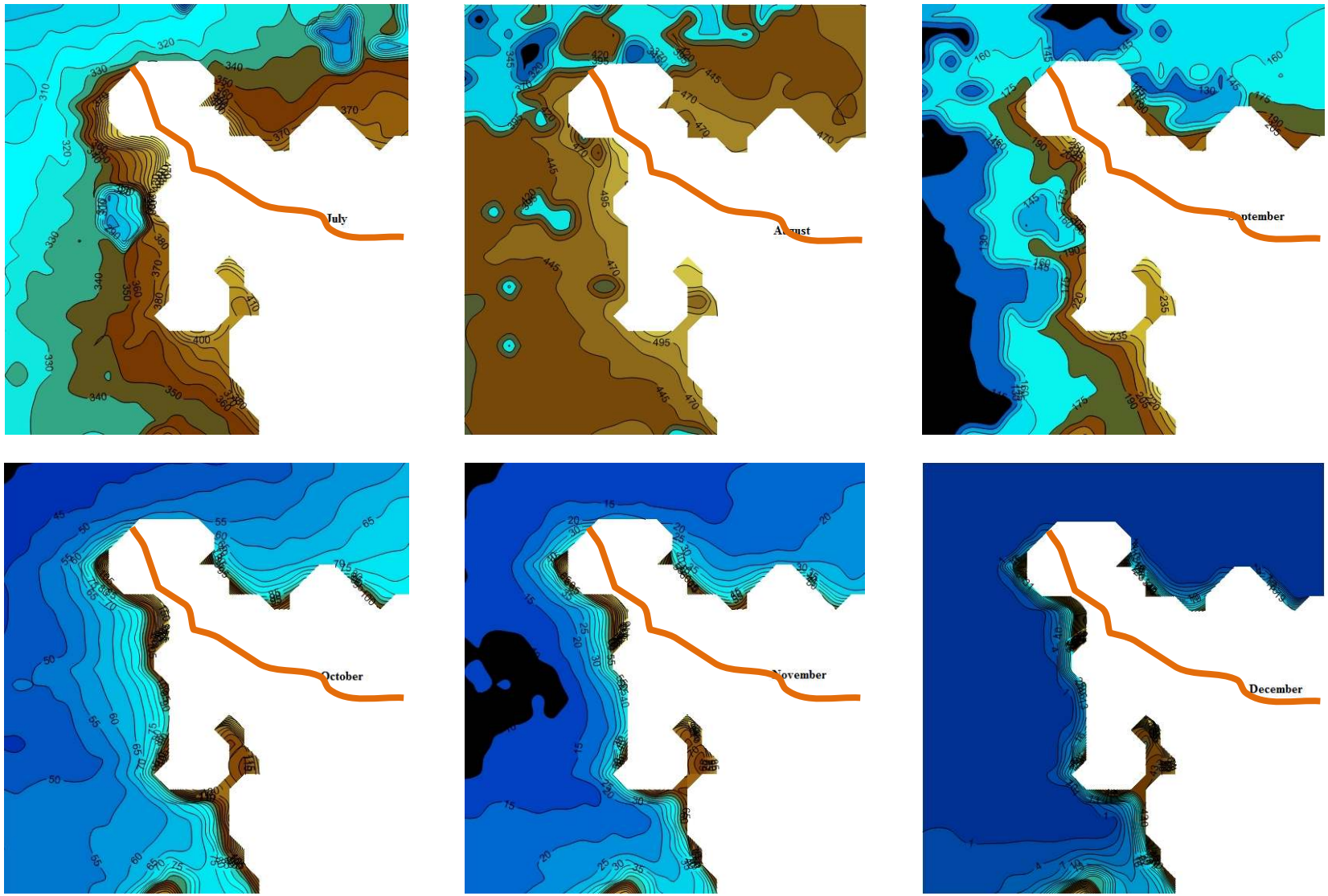

Figure 2-9: 2000-2009 mean monthly reflectance-derived TSS (mg l^{-1}) at river mouth depicting the annual cycle of alteration in the water clarity are constructed using the SURFER software

2.5 Conclusion

Unlike discharge data, which are measured generally on a daily basis, sediment concentration data often result from infrequent water quality monitoring campaigns. A robust statistical relationship was constructed between TSS, turbidity and Secchi depth and remotely sensed reflectance at the entry location of Gumera River. The established regression equations can be used to provide synoptic water quality at the river entry and hence helps to assess how soil and water conservation investments pay dividends. The availability of MODIS images on an almost daily basis provides the opportunity to monitor sediment inflow dynamics especially in the dry season and during the beginning of the rainy season, during which the peak of the sediment arrives the lake. Thus, the use of MODIS images in TSS and turbidity measurement supersedes the higher spatial resolution images in (e.g. Landsat ETM+, ASTER) due to much higher temporal resolution. MODIS images also provide the advantage of increased sensitivity (Hu et al., 2004).

The regression equations may also be applied to adjacent watersheds feeding Lake Tana that have similar soils and geological formations, as these are expected to have similar particle size characteristics and hence similar reflectance characteristics (Horsburgh et al., 2010). However the transferability of the regression equations developed here should be verified. Thus, similar regression equations have to be established for other major contributing rivers, at minimum with a validation sampling campaign and possibly including more training sampling campaigns. The work is important enough to consider extending the regression equations to cover the whole lake. Time series TSS generated from the established regression equations can then be used to calculate an annual inflow and outflow sediment budget and then estimate loss of lake storage

capacity. However the estimation of total suspended solids within the lake requires profiling vertical TSS concentrations at representative sites, or making defensible assumptions regarding the vertical distribution (Li et al., 2003). The correlation between measured TSS and total sediment, once established, can be used to determine the total inflowing sediment. The knowledge of TSS has great importance in modeling the inflow of nutrients and contaminants which has implications for eutrophication, algal blooms and degradation of aquatic habitat (Smith, 2008). A better understanding of the movement of the turbid plume can also be used in hydrodynamic modeling of the lake.

References

AYANA, E. K. 2007. Validation of radar altimetry lake level data and its application in water resource management. *International Institute for Geo-Information Science and Earth Observation), Enschede, Master's thesis, 86p*.

BABAN, S. M. J. 1993. Detecting water quality parameters in the Norfolk Broads, UK, using Landsat imagery. *International Journal of Remote Sensing,* 14**,** 1247-1267.

CHAMI, M., MARKEN, E., STAMNES, J., KHOMENKO, G. & KOROTAEV, G. 2006. Variability of the relationship between the particulate backscattering coefficient and the volume scattering function measured at fixed angles. *J. Geophys. Res,* 111**,** C05013.

CHEN, Z., HU, C. & MULLER-KARGER, F. 2007. Monitoring turbidity in Tampa Bay using MODIS/Aqua 250-m imagery. *Remote Sensing of Environment,* 109**,** 207-220.

DALL'OLMO, G., GITELSON, A. A., RUNDQUIST, D. C., LEAVITT, B., BARROW, T. & HOLZ, J. C. 2005. Assessing the potential of SeaWiFS and MODIS for estimating chlorophyll concentration in turbid productive waters using red and near-infrared bands. *Remote Sensing of Environment,* 96**,** 176-187.

DELMAS, M., CERDAN, O., CHEVIRON, B. & MOUCHEL, J. M. 2011. River basin sediment flux assessments. *Hydrological Processes,* 25**,** 1587-1596.

DOXARAN, D., FROIDEFOND, J. M., LAVENDER, S. & CASTAING, P. 2002. Spectral signature of highly turbid waters: Application with SPOT data to quantify suspended particulate matter concentrations. *Remote Sensing of Environment,* 81**,** 149-161.

FORGET, P. & OUILLON, S. 1998. Surface suspended matter off the Rhone river mouth from visible satellite imagery. *Oceanologica Acta,* 21**,** 739-750.

FROIDEFOND, J. M., CASTAING, P. & PRUD'HOMME, R. 1999. Monitoring suspended particulate matter fluxes and patterns with the AVHRR/NOAA-11 satellite: application to the Bay of Biscay. *Deep Sea Research Part II: Topical Studies in Oceanography,* 46**,** 2029-2055.

GADGIL, A. 1998. Drinking water in developing countries. *Annual review of energy and the environment,* 23**,** 253-286.

GEBEYEHU, A. 2004. The Role of Large Water Reservoirs. *Proceeding of 2nd International Conference on the Ethiopian Economy.* Addis Ababa, Ethiopia: Ethiopian Economic Association.

GETIS, A. & ORD, J. K. 2010. The analysis of spatial association by use of distance statistics. *Perspectives on Spatial Data Analysis***,** 127-145.

HAILESLASSIE, A., PRIESS, J., VELDKAMP, E., TEKETAY, D. & LESSCHEN, J. P. 2005. Assessment of soil nutrient depletion and its spatial variability on smallholders' mixed farming systems in Ethiopia using partial versus full nutrient balances. *Agriculture, ecosystems & environment,* 108**,** 1-16.

HAN, L. 2005. Estimating chlorophyll-a concentration using first-derivative spectra in coastal water. *International Journal of Remote Sensing,* 26**,** 5235-5244.

HAN, L. & RUNDQUIST, D. C. 1994. The response of both surface reflectance and the underwater light field to various levels of suspended sediments: preliminary results. *Photogrammetric Engineering and Remote Sensing,* 60**,** 1463-1471.

HAREGEWEYN, N., POESEN, J., NYSSEN, J., DE WIT, J., HAILE, M., GOVERS, G. & DECKERS, S. 2006. Reservoirs in Tigray (Northern Ethiopia): characteristics and sediment deposition problems. *Land degradation & development,* 17**,** 211-230.

HERWEG, K. & LUDI, E. 1999. The performance of selected soil and water conservation measures—case studies from Ethiopia and Eritrea. *Catena,* 36**,** 99-114.

HORSBURGH, J. S., SPACKMAN JONES, A., STEVENS, D. K., TARBOTON, D. G. & MESNER, N. O. 2010. A sensor network for high frequency estimation of water quality constituent fluxes using surrogates. *Environmental Modelling & Software,* 25**,** 1031-1044.

HU, C., CHEN, Z., CLAYTON, T. D., SWARZENSKI, P., BROCK, J. C. & MULLER–KARGER, F. E. 2004. Assessment of estuarine water-quality indicators using MODIS medium-resolution bands: Initial results from Tampa Bay, FL. *Remote Sensing of Environment,* 93**,** 423-441.

JOLIVET, D., RAMON, D., DESCHAMPS, P. Y., STEINMETZ, F., FOUGNIE, B. & HENRY, P. How the ocean color product quality is limited by atmospheric correction. 2007.

KAUFMAN, Y. J., HERRING, D. D., RANSON, K. J. & COLLATZ, G. J. 1998. Earth Observing System AM1 mission to earth. *Geoscience and Remote Sensing, IEEE Transactions on,* 36**,** 1045-1055.

KEBEDE, S., TRAVI, Y., ALEMAYEHU, T. & MARC, V. 2006. Water balance of Lake Tana and its sensitivity to fluctuations in rainfall, Blue Nile basin, Ethiopia. *Journal of Hydrology,* 316**,** 233-247.

KUTSER, T., METSAMAA, L., VAHTMAE, E. & STROMBECK, N. Suitability of MODIS 250 m resolution band data for quantitative mapping of cyanobacterial blooms. 2006. 318-328.

LI, R. R., KAUFMAN, Y. J., GAO, B. C. & DAVIS, C. O. 2003. Remote sensing of suspended sediments and shallow coastal waters. *Geoscience and Remote Sensing, IEEE Transactions on,* 41**,** 559-566.

LIND, O. T., DOYLE, R., VODOPICH, D. S., TROTTER, B. G., LIMÓN, J. G. & DAVALOS-LIND, L. 1992. Clay turbidity: regulation of phytoplankton production in a large, nutrient-rich tropical lake. *Limnology and Oceanography***,** 549-565.

LIU, B. M., COLLICK, A. S., ZELEKE, G., ADGO, E., EASTON, Z. M. & STEENHUIS, T. S. 2008. Rainfall-discharge relationships for a monsoonal climate in the Ethiopian highlands. *Hydrological Processes,* 22**,** 1059-1067.

LIU, Y., ISLAM, M. A. & GAO, J. 2003. Quantification of shallow water quality parameters by means of remote sensing. *Progress in Physical Geography,* 27**,** 24-43.

LPDAAC 2010. Surface Reflectance Daily L2G Global 250m.

MA, R. & DAI, J. 2005. Investigation of chlorophyll - a and total suspended matter concentrations using Landsat ETM and field spectral measurement in Taihu Lake, China. *International Journal of Remote Sensing,* 26**,** 2779-2795.

MCCARTNEY, M., ALEMAYEHU, T., SHIFERAW, A. & AWULACHEW, S. 2010. *Evaluation of current and future water resources development in the Lake Tana Basin, Ethiopia*, Iwmi.

MILLER, R. L. & MCKEE, B. A. 2004. Using MODIS Terra 250 m imagery to map concentrations of total suspended matter in coastal waters. *Remote Sensing of Environment,* 93**,** 259-266.

MITCHELL, A. 2005. The ESRI Guide to GIS Analysis: Spatial Measurements & Statistics. Vol. 2. *Redlands, CA: ESRI*.
MOREL, A. & PRIEUR, L. 1977. Analysis of variations in ocean color. *Limnology and Oceanography*, 709-722.
MYINT, S. & WALKER, N. 2002. Quantification of surface suspended sediments along a river dominated coast with NOAA AVHRR and SeaWiFS measurements: Louisiana, USA. *International Journal of Remote Sensing,* 23, 3229-3249.
NECHAD, B., RUDDICK, K. & PARK, Y. 2010. Calibration and validation of a generic multisensor algorithm for mapping of total suspended matter in turbid waters. *Remote Sensing of Environment,* 114, 854-866.
NEDESSA, B. & WICKREMA, S. 2010. Disaster Risk Reduction: Experience from the MERET Project in Ethiopia. Available: http://documents.wfp.org/stellent/groups/public/documents/newsroom/wfp225961.pdf.
NYSSEN, J., POESEN, J., DESCHEEMAEKER, K., HAREGEWEYN, N., HAILE, M., MOEYERSONS, J., FRANKL, A., GOVERS, G., MUNRO, N. & DECKERS, J. 2008. Effects of region-wide soil and water conservation in semi-arid areas: the case of northern Ethiopia. *Zeitschrift für Geomorphologie,* 52, 291-315.
PETUS, C., CHUST, G., GOHIN, F., DOXARAN, D., FROIDEFOND, J. M. & SAGARMINAGA, Y. 2010. Estimating turbidity and total suspended matter in the Adour River plume (South Bay of Biscay) using MODIS 250-m imagery. *Continental Shelf Research,* 30, 379-392.
QUEENAN, K., BURTON, C. & BECHIR, C. 1996. Development of a centrifuge-based procedure to analyse agricultural effluents for total and volatile suspended solids. *Bioresource technology,* 57, 259-263.
SMITH, H. G. 2008. Estimation of suspended sediment loads and delivery in an incised upland headwater catchment, south-eastern Australia. *Hydrological Processes,* 22, 3135-3148.
STEENHUIS, T. S., COLLICK, A. S., EASTON, Z. M., LEGGESSE, E. S., BAYABIL, H. K., WHITE, E. D., AWULACHEW, S. B., ADGO, E. & AHMED, A. A. 2009. Predicting discharge and sediment for the Abay (Blue Nile) with a simple model. *Hydrological Processes,* 23, 3728-3737.
TILAHUN, S., GUZMAN, C., ZEGEYE, A., ENGDA, T., COLLICK, A., RIMMER, A. & STEENHUIS, T. 2012. An efficient semi-distributed hillslope erosion model for the sub humid Ethiopian Highlands. *Hydrol. Earth Syst. Sci. Discuss,* 9, 2121-2155.
VIJVERBERG, J., SIBBING, F. A. & DEJEN, E. 2009. Lake Tana: Source of the Blue Nile. *The Nile*, 163-192.
WANG, J. J. & LU, X. 2010. Estimation of suspended sediment concentrations using Terra MODIS: An example from the Lower Yangtze River, China. *Science of the Total Environment,* 408, 1131-1138.
WANG, J. J., LU, X. X., LIEW, S. C. & ZHOU, Y. 2009. Retrieval of suspended sediment concentrations in large turbid rivers using Landsat ETM+: an example from the Yangtze River, China. *Earth Surface Processes and Landforms,* 34, 1082-1092.
WANG, J. J., LU, X. X., LIEW, S. C. & ZHOU, Y. 2010. Remote sensing of suspended sediment concentrations of large rivers using multi-temporal MODIS images: an example in the Middle and Lower Yangtze River, China. *International Journal of Remote Sensing,* 31, 1103-1111.

WERDELL, P. J., FRANZ, B. A. & BAILEY, S. W. 2010. Evaluation of shortwave infrared atmospheric correction for ocean color remote sensing of Chesapeake Bay. *Remote Sensing of Environment,* 114**,** 2238-2247.

YILMA, A. D. & AWULACHEW, S. B. 2009. Blue Nile Basin Characterization and Geospatial Atlas. *Improved Water and Land Management in the Ethiopian Highlands: Its Impact on Downstream Stakeholders Dependent on the Blue Nile***,** 6.

CHAPTER 3: MODELING TOTAL SUSPENDED SOLID EMISSION IN GUMERA WATERSHED (ETHIOPIA)

Abstract

Modeling sediment concentration in Ethiopia at intermediate to large scale is hampered by lack of historic sediment concentration data. Considerable flow and sediment concentration modeling work had been done on Gumera watershed. The models simulate sediment concentration at a gauging station upstream of Lake Tana where the river is flowing. None of these studies had modeled TSS emissions by the river to Lake Tana as there are no TSS measurements at the river mouth. In this study a 10 years TSS time series data generated from remotely sensed images generated using a regression equation established by field water sample analysis and concurrently taken MODIS/Terra 250 meter images of the near infra red (NIR) band is used to calibrate and validate a soil and water assessment tool variable source area (SWAT–VSA) model. The result showed that TSS at the river mouth can be replicated with a Nash–Sutcliffe efficiency of 0.39 for calibration and 0.32 for validation periods. Given the inaccessibility and costliness to measure TSS at river mouths to a lake the results found here are considered modest.

3.1 Introduction

Over dependency on agriculture as a source of livelihood and high population pressure in Ethiopia are inducing deforestation, expansion of agriculture to marginal lands and steep slopes, degradation of the environment (Zeleke and Hurni, 2001, Bewket and Sterk, 2005). This has increased erosion and siltation and reduced water quality in the Blue Nile basin (Awulachew et

al., 2008). Suspended sediment reduces sunlight penetration and thus modifies biological activity which will affect the whole food web in the aquatic system (Lind et al., 1992) and can result in eutrophication (Webster, 2005). Sediment reduces reservoirs storage capacity adversely affecting hydropower generation and irrigation (Ananda and Herath, 2003). FAO (1986) estimates an annual loss of over 1.9 billion tons of soil from the Ethiopian highlands of which only approximately 122 million tons reach the Ethiopia border (Ahmed and Ismail, 2008). The eroded soil creates turbid plumes in lakes such as Lake Tana in the Nile basin. These plumes can be used as an important marker of the catchment contribution to lake sedimentation. In one study Ayana et al. (in press) determined using MODIS the concentration in Lake Tana near the mouth of the Gumera River for a ten year period.

Modelling of the processes governing erosion and sedimentation can help our understanding of issues in terms of the critical factors controlling erosion and associated sediment transport. However, sediment modeling in Ethiopia has generally not been very successful because of both limited sediment data for validation. At the same time the underlying hydrology of tropical sub-humid areas is not understood very well. Initial modeling attempts used models developed in the US and Europe with a temperate to sub–humid climate, [e.g. Agricultural Non–Point Source Pollution (AGNPS) model (Haregeweyn and Yohannes, 2003, Mohamed et al., 2004), Soil and Water Assessment Tool (SWAT) (Setegn et al., 2008) and WEPP (Zeleke, 2000)]. Runoff predictions in these models are based on the SCS curve number that is not suitable with the monsoon climate condition in the Ethiopian landscape (Liu et al., 2008, Bayabil et al., 2010, Tilahun et al., 2012). More recently water balance models and modifications of SWAT taking topography into account have been more successful in predicting runoff (Easton et al., 2008, Steenhuis et al., 2009, Tilahun et al., 2012) .

Unfortunately, these improved models have been tested for a limited extent because of the general lack of time series of sediment concentrations in the various reaches of the basin. Especially there is little known about concentration in lakes. In this chapter we modeled TSS emission in to Lake Tana from Gumera watershed using SWAT–VSA model. The SWAT–VSA uses topography to determine the curve numbers to predict the saturated excess runoff and then predict the sediment concentrations. A ten years TSS time series data generated from remotely sensed images for Lake Tana at the river mouth (Ayana et al., in press) is used to calibrate and validate the model. The Gumera watershed is selected for the existing knowledge base with respect to the stream discharge modeling (Conway, 2000, Kebede et al., 2006, Tarekegn and Tadege, 2006, Setegn et al., 2008, Chebud and Melesse, 2009a, Chebud and Melesse, 2009b, Wale et al., 2009, Setegn et al., 2010, Kebede et al., 2011, Setegn et al., 2011, White et al., 2011). As there are no TSS measurements at the river mouth none of these studies had modeled TSS emissions. The objective of this study is to model TSS emissions by Gumera River into Lake Tana. The results will provide scientific basis for using TSS time series generated from MODIS reflectance measurements in lieu of sediment data from rating curves. The link between lake water turbidity and land cover is also assessed using the Enhanced Vegetation Index (EVI) as a proxy.

3.2 Material and methods

3.2.1 Study area

The Gumera catchment drains an area of about 1280 km^2, (Figure 3-1). The watershed drains into Lake Tana, a fresh water lake and source of the Blue Nile. Agriculture being a dominant activity in the area represents 96% of the watershed and only 4% is forested.

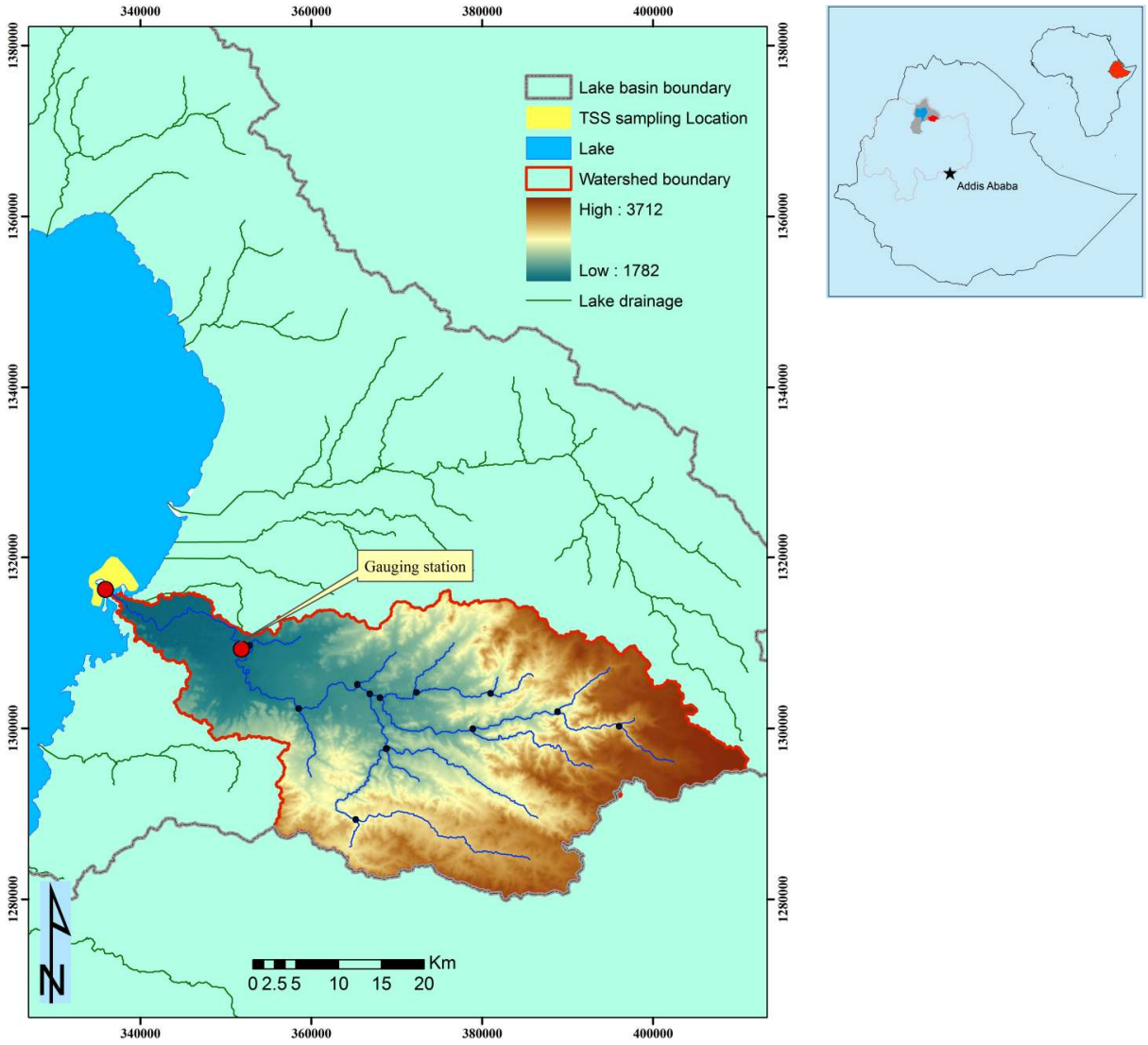

Figure 3-1: Study area

Elevation of the Gumera watershed ranges from 1792 to 3712 m. About 51% of the watershed has a slope less than 15%, with 33% within the range of 15–30% and the remaining 16% of the area is above 30%. Haplic luvisols[2] is the dominant soil covering 73% of the watershed area and 15% chromic luvisols (FAO and ISRIC, 2009). The watershed climate and vegetation are characteristic of a sub-humid zone with a high diurnal temperature variation between day time

[2] Luvisols are soils with a marked textural difference within the soil profile, with depleted clay in the surface horizon and accumulation in a subsurface horizon (http://www.isric.org accessed November, 2012)

extremes of 30°C to night lows of 6°C. Rainfall may reaches up to 2,000 mm per year falling in one rainy season from May to October with July to August the wettest (Vijverberg et al., 2009). Gumera River drains in to Lake Tana and is 75 kilometers long. The average discharge over a 33 years period is 34.4 m^3/sec. Minimum in this period was 0.04 m^3/sec and the maximum was 406 m^3/sec (FDRE–MoWE).

3.2.2 Model description

SWAT is a process–based continuous basin–scale hydrological model designed to predict the impact of land management practices on water, sediment and agricultural chemical yields. SWAT has been applied to catchments ranging few (Chanasyk *et al*., 2003) to hundreds of thousands square kilometers with varying soils, land use and management conditions (Chanasyk et al., 2003, Arnold et al., 2007). The model components include: climate, hydrology, erosion, soil temperature, plant growth, nutrients, pesticides, land management, channel and reservoir routing. SWAT divides a basin into sub–basins each connected through a stream channel. The sub–basins are further divided in to Hydrologic Response Units (HRUs). An HRU is a unique combination of soil and vegetation. SWAT simulates hydrology, vegetation growth, and management practices at the HRU level. Easton et al. (2008) re–conceptualize SWAT for mountainous areas by using the topographic wetness index in combination with land use to define the HRU. The water balance is simulated by SWAT using the following equation:

$$SW_t = SW_o + \sum_{i=1}^{n}(R_{day} - Q_{surf} - E_a - w_{seep} - Q_{gw}) \qquad \text{Equation 3-1}$$

Where,

SW_t : Soil water content at time t in mm

SW_o : Initial soil water content in mm

R_{day} : Amount of precipitation on day i in mm

Q_{surf} : Amount of surface runoff on day i in mm

E_a : Amount of evapotranspiration on day i in mm

w_{seep} : Amount of percolation on day i in mm

Q_{gw} : Amount of return flow on day i in mm

More detailed descriptions of the model can be found in Arnold et al. (1998).

3.2.3 Model Setup

The model setup involved five steps: (1) data preparation (2) sub-basin discretization and HRU definition (3) sensitivity analysis, calibration and validation

3.2.3.1 Data

The spatial data required in SWAT are the Digital Elevation Model (DEM), soil, and land use data. Point data required include weather, river discharge and TSS. These are used for prediction and calibration of streamflow and TSS.

DEM, Soil and Land Use data

A 30 m by 30 m resolution DEM (Figure 3-1) was obtained from the Ethiopian Railways Corporation (ERC). The DEM was used to delineate the watershed, analyze the drainage patterns of the land surface terrain and generate the topographic wetness index (Beven and Kirkby, 1979). Sub-basin parameters such as slope gradient, slope length of the terrain, and the stream network characteristics such as channel slope, length, and width were derived from the DEM. The soil

data is acquired from the new Harmonized World Soil Database (HWSD) which was updated by FAO-UNESCO. Important soil parameters, textural and physicochemical properties such as available water content (AWC), bulk density, hydraulic conductivity, organic carbon content and soil texture are included in the database. The land use map of the study area used by was obtained from ministry of water resources Ethiopia (BCEOM, 1999). The final land use classes are assigned as 31% agriculture - generic (AGRL), 64% agriculture – close grown (AGRC), 4% meadow brome grass (BROM), 0.5% pine (PINE) and 0.09% urban (URMD) (Appendix B, Figure B1–2).

Weather Data

Two options are available to enter meteorological data. SWAT will either read the daily meteorological data or will generate them using the weather generator model. The weather variables used in this study are daily precipitation, minimum and maximum air temperature, relative humidity and wind speed data for the 1992 – 2009 time span. These data were obtained from Ethiopian National Meteorological Agency (NMA) for stations located within and near the watershed. In order to fill gaps in some of the data the weather generator file created by White et al. (2011) was used.

Discharge and TSS

Daily river discharge for Gumera River is available since 1976. The data was obtained from FDRE – MoWE. Daily discharge data from January 2000 to December 2009 are used to calibrate and validate the model. This time span is selected for its overlap to 10 year lake sediment concentration data determined from MODIS images (chapter 2).

Enhanced Vegetation Index (EVI) data

The vegetation biomass measured using *enhanced vegetation index* (EVI). Comparison is made between EVI and TSS using ten year 1 km resolution mean monthly MODIS/Terra EVI time series data extracted for Gumera watershed.

3.2.3.2 Sub-basin discretization and HRU definition

In the standard SWAT sub-basin discretization is made based on the slope, soil and land use percentage thresholds. Sub-basins are divided into hydrologic response units (HRUs). An HRU is the smallest unit in SWAT defined on the basis of a unique combination of slope, soil type and land use. In SWAT–VSA HRUs are defined using topographic wetness index in combination with land use (Easton et al., 2008). In this way the saturation excess runoff from variable source areas which is the dominant process in Ethiopian highlands (Steenhuis et al., 2009) is incorporated into SWAT. Once Sub–basin discretization is completed parameters to represent the watershed process is selected. This will be based on the process sensitivity to these parameters (Appendix B1).

3.2.3.3 Sensitivity analysis

The sensitivity analysis tool in SWAT is used in ranking parameters based on their influence in governing flow or sediment. This is an important step in the modeling process as it helps in identifying the parameters to calibrate which otherwise will become very complex and computationally time consuming. Moreover the variation in sensitivity of parameters as the result of using two differently derived data sets will be important to understand the underlying process, like in the case of sediment deposition in the flood plain adjacent to the lake.

3.2.3.4 Calibration, validation and uncertainty analysis

SWAT calibration uncertainty programs (SWAT–CUP), linked to ArcSWAT is used to calibrate the model and perform uncertainty analysis (Figure 3-2). The SWAT–CUP program includes five calibration routines (SUFI–2, ParaSol, GLUE, MCMC and PSO). Previous detailed studies had shown sequential uncertainty fitting (SUFI–2) program performs better for Gumera watershed (Setegn et al., 2008).

In this study calibration of monthly flow and TSS was performed from 2000–2006 with the first year as a warm up period and the validation period is 2007–2009. The water balance was calibrated first and then the TSS was considered. The model parameters are checked for maintaining their physical meaning (i.e. whether they are within the specified limits). The performance of the simulation was evaluated using the *Nash–Sutcliffe coefficient of efficiency* (Nash and Sutcliffe, 1970), the *p–factor* and *r–factor* (Rouholahnejad et al., 2012). In addition percent bias (PBIAS) and ratio of the root-mean-square error (RSR) to the standard deviation of measured data are used to evaluate the model output (van Griensven et al., 2012).

The Nash–Sutcliffe coefficient of efficiency is computed as:

$$\boldsymbol{E_{NS} = 1 - \frac{\sum_{i=1}^{n}(Q_{i,s} - Q_{i,m})^2}{\sum_{i=1}^{n}(Q_{i,m} - \bar{Q}_m)^2}} \qquad \text{Equation 3-2}$$

Where, $\boldsymbol{Q_{i,s}}$ is simulated quantity (flow or TSS), $\boldsymbol{Q_{i,m}}$ is measured quantity and $\boldsymbol{\bar{Q}_m}$ is mean of the measured quantity.

For p-factor the 95 percent prediction uncertainty (95PPU) is calculated at the 2.5% and 97.5% levels of the cumulative distribution of an output variable obtained through Latin hypercube

sampling. The average distance $\bar{d}$ between the upper and the lower 95PPU is used to calculate the r–factor expressed as (Abbaspour, 2008):

$$r - factor = \frac{\bar{d}_X}{\sigma_X} \qquad \text{Equation 3-3}$$

Uncertainty is an inherent characteristic of hydrologic models. The uncertainty may be due to model simplification, under or over representation of processes, or due to processes unknown to the modeler (Abbaspour, 2008). The spatial variability of precipitation particularly in under gauged dry and mountainous areas, which is a typical characteristics of the watershed under consideration is a major source of uncertainty (Arnold et al., 2007). These uncertainties should be properly addressed and quantified for the models to be usable in decision making. In SUFI–2 a measure, p–factor is used to quantify the degree to which all uncertainties are accounted. The p–factor is the percentage of measured data bracketed by the 95% prediction uncertainty (95PPU) (Abbaspour, 2008).

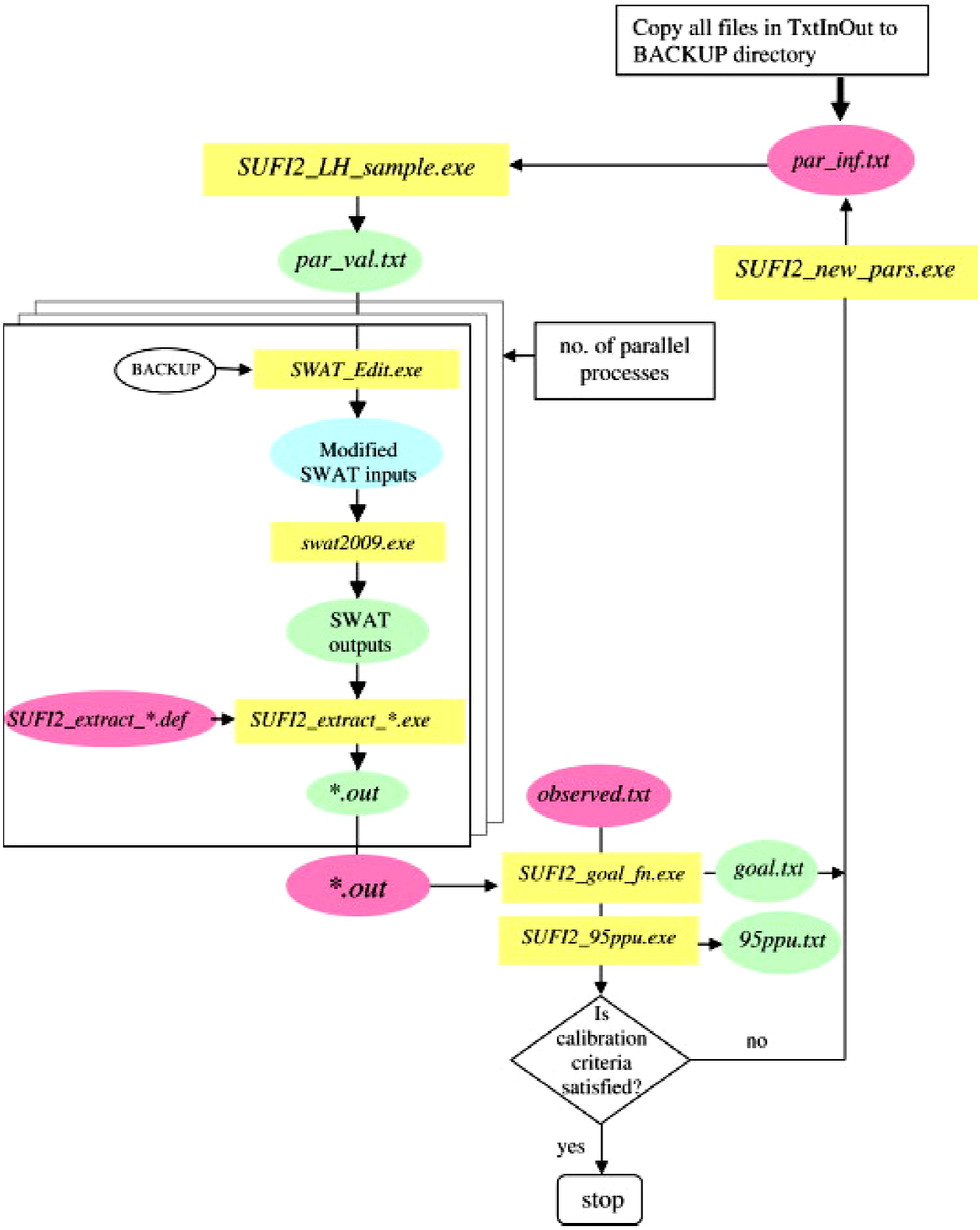

Figure 3-2: A schematic linking of SWAT and SUFI–2 (Rouholahnejad et al., 2012)

3.3 Results

Table 3-1 shows the results of the sensitivity analysis for the monthly simulation. The channel erodibility factor (CH_EROD) and the sediment transport coefficient (SPCON) were the most sensitive parameters[3] governing TSS in the lake at the river mouth.

Table 3-1: Sensitive parameters

Parameter	Fitted Value	Range
CN2	0.074	±0.25
ALPHA_BF	0.89	0-1
SURLAG	2.80	1-10
CH_EROD*	0.24	0-0.6
REVAPMN	471.75	0-500
SPCON*	0.005	0.001-0.01
CANMAX	-0.21	±0.25
ESCO	0.15	0-1
CH_K2	16.28	0-150
GW_REVAP	0.06	0-0.2
USLE_C	-0.08	±0.25

* sediment parameters

Four variables consist of p_factor, r_factor, R^2 and NS_E computed for all types of objective functions. The Nash–Sutcliffe objective function yields the best result Table 3-2. Other statistical variables were used for better judgment. The modeled values for the same are used in plotting the output (Figure 3-3 and Figure 3-4).

[3] List of parameters and explanation is given on Appendix B, Table B1–3

Table 3-2: Monthly statistical coefficients for discharge and sediment calibration and validation

Variable	Period	R^2	E_{NS}	PBIAS	RSR
Discharge	Calibration	0.79	0.75	21.4	0.50
	Validation	0.81	0.64	21.7	0.60
TSS	Calibration	0.39	0.34	-9.4	0.8
	Validation	0.32	0.21	-2.2	0.8

Table 3-3: (a) Statistical analysis on best objective function for the *calibration* period

(Discharge|TSS)

Objective function	Variables									
	p_factor		**r_factor**		**R^2**		**NS**		**BR^2**	
BR^2	0.85	1.0	0.59	16.60	0.89	0.24	0.86	-5.79	0.68	0.24
Chi^2	0.85	1.0	0.61	15.68	0.73	0.42	0.66	0.42	0.44	0.18
Mult	0.85	1.0	0.59	16.42	0.89	0.35	0.81	0.15	0.61	0.12
NS	***0.85***	***0.33***	***0.61***	***0.32***	***0.79***	***0.39***	***0.75***	***0.34***	***0.54***	***0.20***
R^2	0.74	1.0	0.41	16.65	0.86	0.46	0.39	-94.3	0.30	0.08
Sum	0.85	1.0	0.62	14.5	0.89	0.24	0.49	-0.02	0.35	0.11

(b): Statistical analysis on best objective function for the *validation* period

(Discharge|TSS)

Objective function	Variables									
	p_factor		**r_factor**		**R^2**		**NS**		**BR^2**	
BR^2	0.69	1.0	0.53	34.25	0.86	0.44	0.74	-0.91	0.55	0.43
Chi^2	0.69	1.0	0.53	34.91	0.89	0.38	0.70	-0.16	0.51	0.24
Mult	0.69	1.0	0.53	32.32	0.91	0.30	0.73	-0.45	0.53	0.24
NS	***0.69***	***0.33***	***0.55***	***36.97***	***0.81***	***0.32***	***0.64***	***0.21***	***0.44***	***0.17***
R^2	0.33	1.0	0.31	28.98	0.86	0.51	0.35	-4.88	0.29	0.12
Sum	0.69	1.0	0.53	33.98	0.82	0.42	0.67	0.18	0.47	0.32

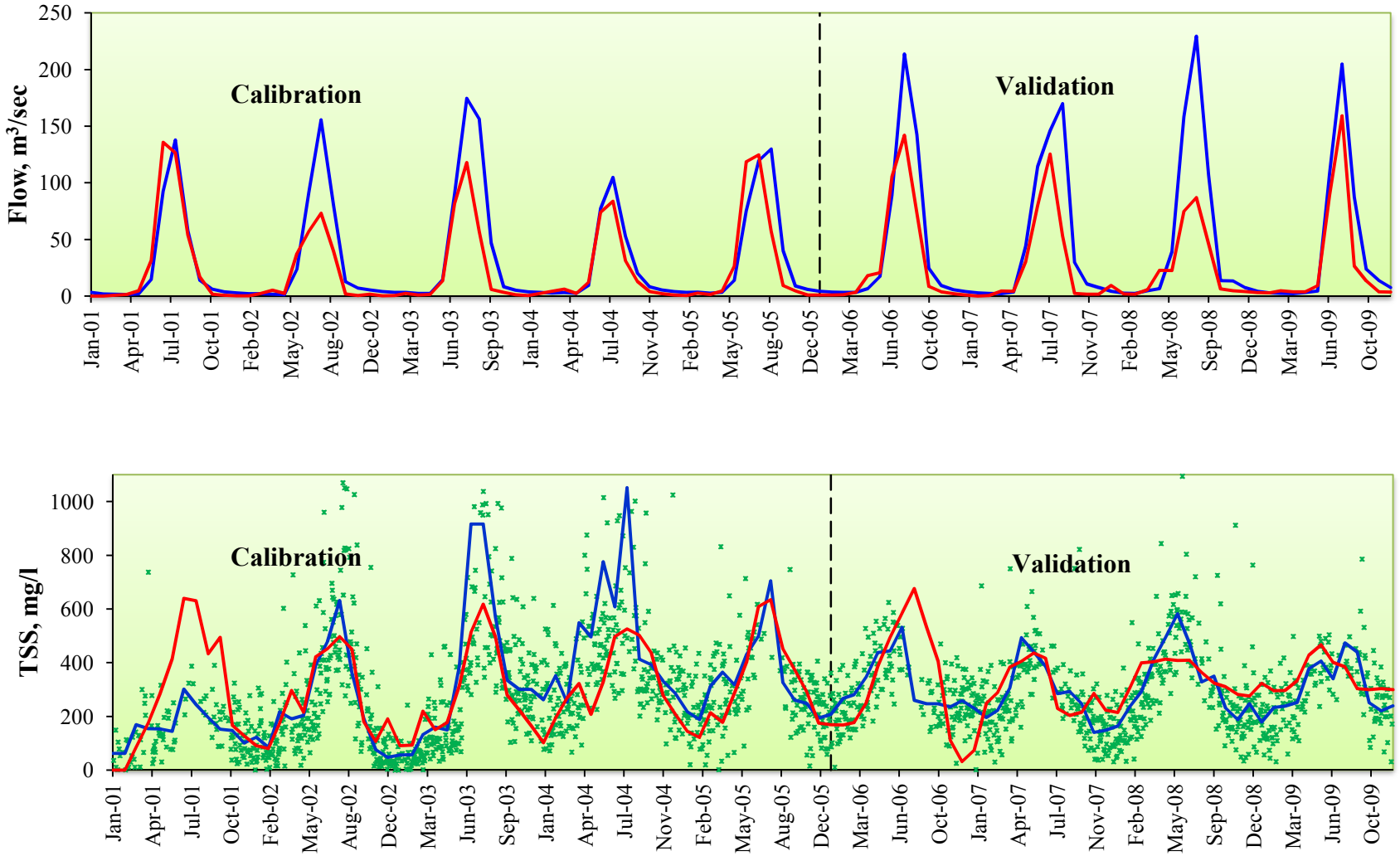

Figure 3-3: Monthly calibration and validation output for (a) monthly flow and (b) TSS; sediment data derived from MODIS images is used (measured in *blue,* modeled in *red* and points are daily TSS estimates)

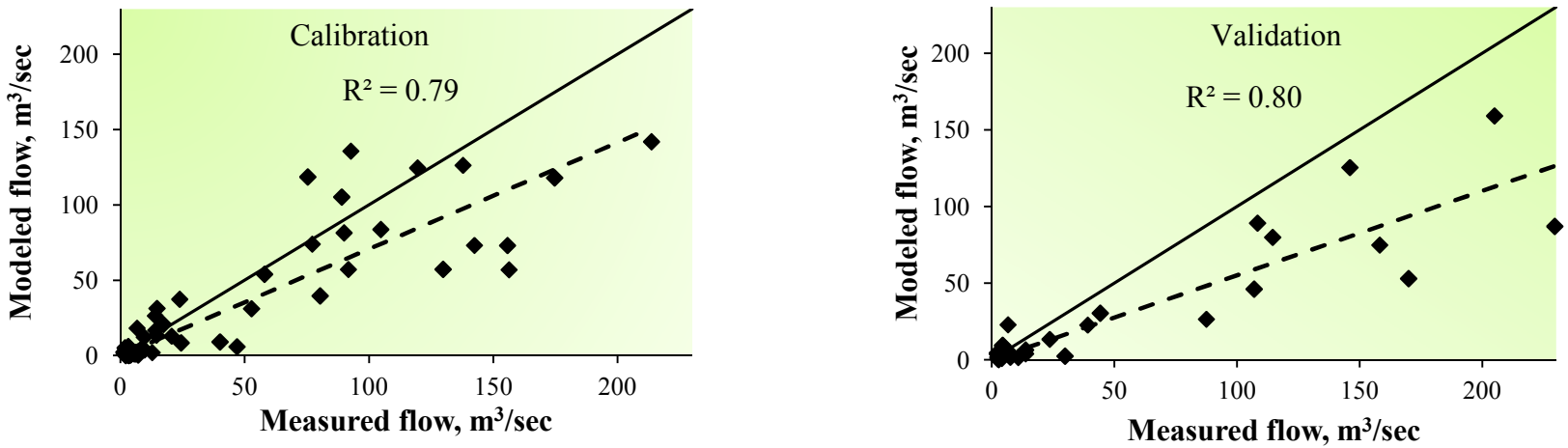

a

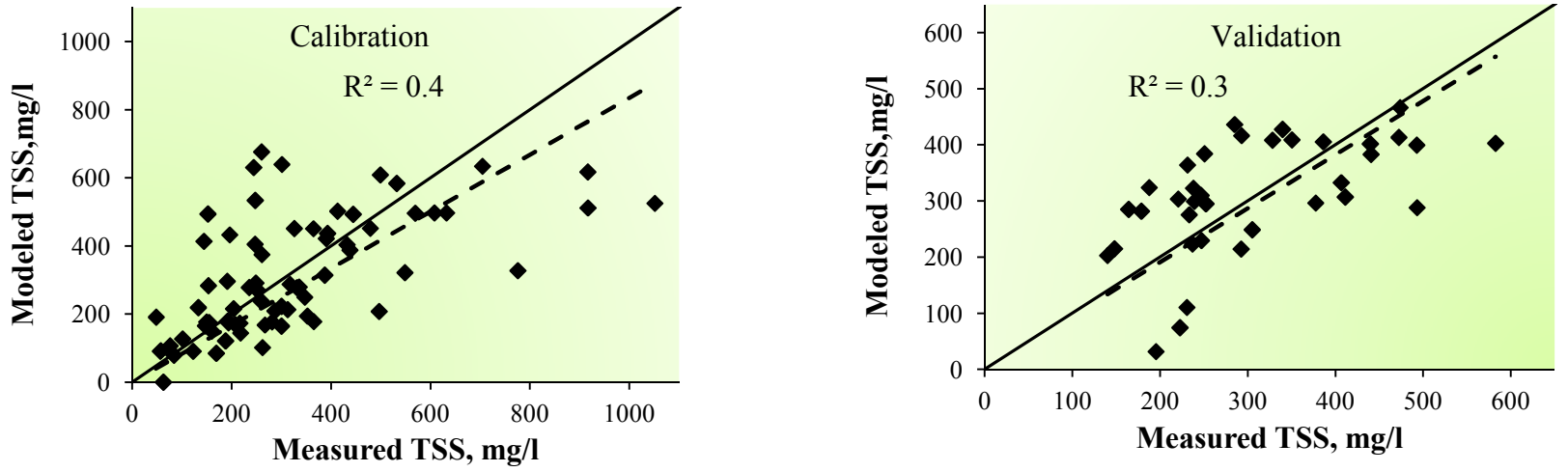

b

Figure 3-4: Comparison of measured and simulated (a) flow and (b) TSS

3.4 Discussion

Like any water quality model, SWAT must first accurately simulate the hydrologic processes before it can realistically predict pollutant transport. The predicted and observed flow resulted in Nash–Suttcliffe efficiency of 0.8 for both calibration and validation periods (Figure 3-3(a)). The results from previous modeling are provided on Table 3-4. For TSS the efficiency is 0.39 for calibration and 0.32 for validation period.

Table 3-4: Summary of model efficiencies from previous studies

Parameter	**Time scale**	**NS_E**		**Remark**
		Calibration	*Validation*	
Flow	Daily	0.62	0.60	(Setegn et al., 2008)
	Daily	0.64	0.63	(White et al., 2011)
	Daily	0.81	-	(Easton et al., 2010)

The results can be evaluated on the basis of the three criterion recommended by Van Griensven et al. (2012). These criterions are fitness to observations, fitness to reality and fitness to purpose. Fitness to observations refers to the difference between the observed and simulated values. Fitness to reality evaluates how well a model represents the physical process while maintaining parameters within their meaningful range and fitness to purpose accounts on how well certain watershed characteristics which the model output is needed to address are taken into consideration.

Based on the model fitness to observations criteria models are considered fit if NSE >0.5 and RSR≤ 0.7, and if PBIAS is ±25% and ±55% for flow and sediment respectively for a monthly time step (van Griensven et al., 2012). Moriasi et al. (2007) indicated NSE between 0 and 1 are

generally viewed as acceptable. In this perspective though the TSS simulations are acceptable it still falls short of fitness to purpose. The RSR and the PBIAS criterion are satisfied. Simulated flow satisfies the entire criterion for fitness to purpose including the dry season flow. PBIAS values tend to vary more, among different auto–calibration methods, during dry and wet years (Moriasi et al., 2007). The wet season flow is especially important as it carries the major proportion of the TSS into the lake. The PBIAS for flow indicates slight under estimation bias which will eventually degrade the TSS simulation outcome. With respect to the model fitness to reality the parameter values are checked with respect to the recommended ranges and found to be all the parameters within range (Table 1). The average sediment yield is greater than 10 metric ton per ha which is within the estimated ranges of other studies (Hurni, 1988, Hawando, 1997, Tebebu et al., 2010). The model fitness to purpose was the major criteria applied in assessing the usability of MODIS images generated TSS time series data. Despite a modest NSE for both calibration and validation (0.39 for calibration and 0.32 for validation) periods the model could bracket not more than 33% of the MODIS generated TSS data in the calibration period and 22% of it in the validation period. Two major assumptions may have played a critical role in creating the "black holes". The first assumption is that the regression equations used to generate the time series are stable over the last ten years. While the land cover and the economic activity in the watershed seems unchanged over the last ten years the factors affecting the optical characteristics of the water are far complicated than this.

In assessing the link between land cover change and lake water quality the mean monthly EVI values for the watershed are compared with the TSS estimates from MODIS images. The EVI is the most sensitive biotic component of terrestrial ecosystems to alteration (Potter et al., 2003).

These alterations follow the vegetation phenology on both the cultivated and fallow area. Agricultural activities are intense during the rainy season (June–August) and in the dry season agriculture fields are open for grazing. The plot in Figure 3-5 shows a decline in water quality (i.e. increase in TSS) with a decline in EVI.

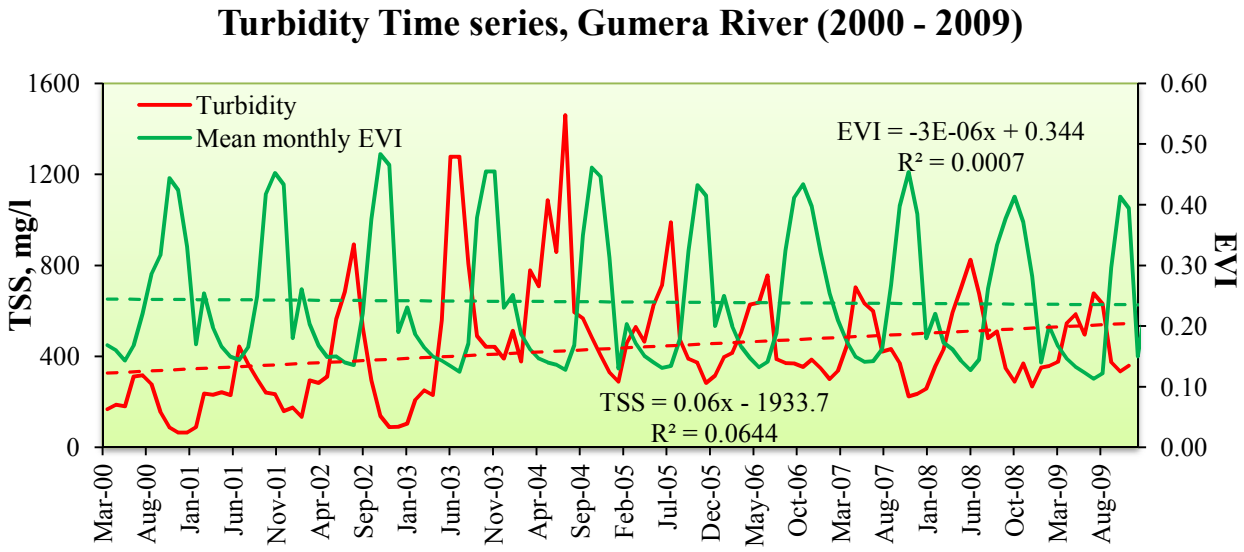

Figure 3-5: Comparison of lake water turbidity and EVI, turbidity starts to pick at the beginning of the rainy season where the EVI is at its lowest and declines with a pick in EVI

At the start of the rainy season TSS peaks as the loose soil is washed in to the streams after the first few rain events. By the time the EVI peaks the sediment concentration starts to sharply decline. It can also be seen that flow peaks often precedes EVI peaks. This is consistent with previous findings which reported sediment peaks before flow peaks (Steenhuis et al., 2009).With an increased biomass in the rainy season Long term water quality variation shows a decrease in EVI and an increase in turbidity. Trends of EVI and turbidity also support the association between the two in that while EVI is very slightly declining over the 10 years turbidity is increasing in a comparably slow but increasing trend. But this relation alone could not justify

land cover as a driver for lake water quality. The lake water quality in association with the processes in the flood plain and the lake water level should be examined and incorporated in future modeling efforts.

3.5 Conclusion

In this study the emission of TSS from the Gumera watershed into Lake Tana was modeled using the SWAT hydrological model. The model was calibrated and validated with a modest performance. The simulation over a period of 10 years (2000–2009) allowed an estimation of the annual average emissions of TSS in to Lake Tana. Given the complicated sediment transport processes that are not fully understood, the data mining techniques applied in constructing the TSS time series and the short image time series used give modest results. Harmel et al. (2006) noted that the uncertainty in using manual single point random time grab sampling could be in excess of 50% and -5.3–4.4% due to the method used in sample analysis. For a satellite overpass during transient flow conditions on ground a much higher or lower than the day's mean TSS could be reported. The inability to incorporate the major landscape element (i.e. the flood plain) to the model adds up to the reduced accuracy in the model output. Van Griensven et al. (2012) showed such landscape elements may have large impact on the hydrological and nutrient cycle. Taking all possible combinations of source of uncertainty care should be taken in using regression statistics for model evaluation.

References

ABBASPOUR, K. 2008. SWAT-CUP2: SWAT Calibration and Uncertainty Programs—A User Manual. *Department of Systems Analysis, Swiss Federal Institute of Aquatic Science and Technology, Dübendorf*.

AHMED, A. A. & ISMAIL, U. 2008. Sediment in the Nile River system. *Consultancy Study requested by UNESCO*.

ANANDA, J. & HERATH, G. 2003. Soil erosion in developing countries: a socio-economic appraisal. *Journal of environmental management,* 68**,** 343-353.

ARNOLD, J., SRINIVASAN, R., MUTTIAH, R. & WILLIAMS, J. 1998. Large area hydrologic modeling and assessment. Part I: Model development. *Water resources bulletin,* 34**,** 73-89.

ARNOLD, J. G., SRINIVASAN, R., MUTTIAH, R. S. & WILLIAMS, J. 2007. Large area hydrologic modeling and assessment part I: Model development1. *JAWRA Journal of the American Water Resources Association,* 34**,** 73-89.

AWULACHEW, S. B., MCCARTNEY, M., STEENHUIS, T. S. & AHMED, A. A. 2008. *A review of hydrology, sediment and water resource use in the Blue Nile Basin*, Iwmi.

BAYABIL, H. K., TILAHUN, S. A., COLLICK, A. S., YITAFERU, B. & STEENHUIS, T. S. 2010. Are runoff processes ecologically or topographically driven in the (sub) humid Ethiopian highlands? The case of the Maybar watershed. *Ecohydrology,* 3**,** 457-466.

BCEOM 1999. Abay River Basin integrated master plan, main report. Addis Ababa: Ministry of Water Resources.

BEVEN, K. & KIRKBY, M. 1979. A physically based, variable contributing area model of basin hydrology/Un modèle à base physique de zone d'appel variable de l'hydrologie du bassin versant. *Hydrological Sciences Journal,* 24**,** 43-69.

BEWKET, W. & STERK, G. 2005. Dynamics in land cover and its effect on stream flow in the Chemoga watershed, Blue Nile basin, Ethiopia. *Hydrological Processes,* 19**,** 445-458.

CHANASYK, D., MAPFUMO, E. & WILLMS, W. 2003. Quantification and simulation of surface runoff from fescue grassland watersheds. *Agricultural Water Management,* 59**,** 137-153.

CHEBUD, Y. A. & MELESSE, A. M. 2009a. Modelling lake stage and water balance of Lake Tana, Ethiopia. *Hydrological Processes,* 23**,** 3534-3544.

CHEBUD, Y. A. & MELESSE, A. M. 2009b. Numerical modeling of the groundwater flow system of the Gumera sub-basin in Lake Tana basin, Ethiopia. *Hydrological Processes,* 23**,** 3694-3704.

CONWAY, D. 2000. The climate and hydrology of the Upper Blue Nile River. *The Geographical Journal,* 166**,** 49-62.

EASTON, Z., FUKA, D., WHITE, E., COLLICK, A., ASHAGRE, B. B., MCCARTNEY, M., AWULACHEW, S., AHMED, A. & STEENHUIS, T. 2010. A multi basin SWAT model analysis of runoff and sedimentation in the Blue Nile, Ethiopia. *Hydrology and Earth System Sciences,* 14**,** 1827-1841.

EASTON, Z. M., FUKA, D. R., WALTER, M. T., COWAN, D. M., SCHNEIDERMAN, E. M. & STEENHUIS, T. S. 2008. Re-conceptualizing the soil and water assessment tool

(SWAT) model to predict runoff from variable source areas. *Journal of hydrology,* 348**,** 279-291.
FAO 1986. Highlands reclamation study—Ethiopia. *Final Report.* ROME: FAO.
FAO, I. & ISRIC, I. 2009. JRC Harmonized World Soil Database (version 1.1). *FAO, Rome and IIASA, Laxenburg*.
HAREGEWEYN, N. & YOHANNES, F. 2003. Testing and evaluation of the agricultural non-point source pollution model (AGNPS) on Augucho catchment, western Hararghe, Ethiopia. *Agriculture, ecosystems & environment,* 99**,** 201-212.
HARMEL, R., COOPER, R., SLADE, R., HANEY, R. & ARNOLD, J. 2006. Cumulative uncertainty in measured streamflow and water quality data for small watersheds. *TRANSACTIONS-AMERICAN SOCIETY OF AGRICULTURAL ENGINEERS,* 49**,** 689.
HAWANDO, T. 1997. Desertification in Ethiopian highlands. *Rala Report*.
HURNI, H. 1988. Degradation and conservation of the resources in the Ethiopian highlands. *Mountain Research and Development***,** 123-130.
KEBEDE, S., ADMASU, G. & TRAVI, Y. 2011. Estimating ungauged catchment flows from Lake Tana floodplains, Ethiopia: an isotope hydrological approach. *Isotopes in Environmental and Health Studies,* 47**,** 71-86.
KEBEDE, S., TRAVI, Y., ALEMAYEHU, T. & MARC, V. 2006. Water balance of Lake Tana and its sensitivity to fluctuations in rainfall, Blue Nile basin, Ethiopia. *Journal of Hydrology,* 316**,** 233-247.
LIND, O. T., DOYLE, R., VODOPICH, D. S., TROTTER, B. G., LIMÓN, J. G. & DAVALOS-LIND, L. 1992. Clay turbidity: regulation of phytoplankton production in a large, nutrient-rich tropical lake. *Limnology and Oceanography***,** 549-565.
LIU, B. M., COLLICK, A. S., ZELEKE, G., ADGO, E., EASTON, Z. M. & STEENHUIS, T. S. 2008. Rainfall-discharge relationships for a monsoonal climate in the Ethiopian highlands. *Hydrological Processes,* 22**,** 1059-1067.
MOHAMED, Y., BASTIAANSSEN, W. & SAVENIJE, H. 2004. Spatial variability of evaporation and moisture storage in the swamps of the upper Nile studied by remote sensing techniques. *Journal of hydrology,* 289**,** 145-164.
MORIASI, D., ARNOLD, J., VAN LIEW, M., BINGNER, R., HARMEL, R. & VEITH, T. 2007. Model evaluation guidelines for systematic quantification of accuracy in watershed simulations. *Transactions of the ASABE,* 50**,** 885-900.
NASH, J. E. & SUTCLIFFE, J. 1970. River flow forecasting through conceptual models part I—A discussion of principles. *Journal of hydrology,* 10**,** 282-290.
POTTER, C., TAN, P. N., STEINBACH, M., KLOOSTER, S., KUMAR, V., MYNENI, R. & GENOVESE, V. 2003. Major disturbance events in terrestrial ecosystems detected using global satellite data sets. *Global Change Biology,* 9**,** 1005-1021.
ROUHOLAHNEJAD, E., ABBASPOUR, K., VEJDANI, M., SRINIVASAN, R., SCHULIN, R. & LEHMANN, A. 2012. A parallelization framework for calibration of hydrological models. *Environmental Modelling & Software*.
SETEGN, S. G., RAYNER, D., MELESSE, A. M., DARGAHI, B. & SRINIVASAN, R. 2011. Impact of climate change on the hydroclimatology of Lake Tana Basin, Ethiopia. *Water Resources Research,* 47**,** W04511.
SETEGN, S. G., SRINIVASAN, R. & DARGAHI, B. 2008. Hydrological modelling in the Lake Tana Basin, Ethiopia using SWAT model. *The Open Hydrology Journal,* 2**,** 49-62.

SETEGN, S. G., SRINIVASAN, R., MELESSE, A. M. & DARGAHI, B. 2010. SWAT model application and prediction uncertainty analysis in the Lake Tana Basin, Ethiopia. *Hydrological Processes,* 24**,** 357-367.

STEENHUIS, T. S., COLLICK, A. S., EASTON, Z. M., LEGGESSE, E. S., BAYABIL, H. K., WHITE, E. D., AWULACHEW, S. B., ADGO, E. & AHMED, A. A. 2009. Predicting discharge and sediment for the Abay (Blue Nile) with a simple model. *Hydrological Processes,* 23**,** 3728-3737.

TAREKEGN, D. & TADEGE, A. 2006. Assessing the impact of climate change on the water resources of the Lake Tana sub-basin using the WATBAL model. *Discuss. Pap,* 30.

TEBEBU, T., ABIY, A., ZEGEYE, A., DAHLKE, H., EASTON, Z., TILAHUN, S., COLLICK, A., KIDNAU, S., MOGES, S. & DADGARI, F. 2010. Surface and subsurface flow effect on permanent gully formation and upland erosion near Lake Tana in the Northern Highlands of Ethiopia. *Hydrology and Earth System Sciences,* 14**,** 2207-2217.

TILAHUN, S., GUZMAN, C., ZEGEYE, A., ENGDA, T., COLLICK, A., RIMMER, A. & STEENHUIS, T. 2012. An efficient semi-distributed hillslope erosion model for the sub humid Ethiopian Highlands. *Hydrol. Earth Syst. Sci. Discuss,* 9**,** 2121-2155.

VAN GRIENSVEN, A., NDOMBA, P., YALEW, S. & KILONZO, F. 2012. Critical review of SWAT applications in the upper Nile basin countries. *Hydrol. Earth Syst. Sci,* 16**,** 3371-3381.

VIJVERBERG, J., SIBBING, F. A. & DEJEN, E. 2009. Lake Tana: Source of the Blue Nile. *The Nile***,** 163-192.

WALE, A., RIENTJES, T., GIESKE, A. & GETACHEW, H. 2009. Ungauged catchment contributions to Lake Tana's water balance. *Hydrological Processes,* 23**,** 3682-3693.

WEBSTER, R. M., R.P.C. 2005. Soil Erosion and Conservation, 3rd edition. *European Journal of Soil Science,* 56.

WHITE, E. D., EASTON, Z. M., FUKA, D. R., COLLICK, A. S., ADGO, E., MCCARTNEY, M., AWULACHEW, S. B., SELASSIE, Y. G. & STEENHUIS, T. S. 2011. Development and application of a physically based landscape water balance in the SWAT model. *Hydrological Processes,* 25**,** 915-925.

ZELEKE, G. 2000. Landscape dynamics and soil erosion process modeling in the north-western Ethiopian Highlands. Berne, Switzerland: Geographica Bernensia.

ZELEKE, G. & HURNI, H. 2001. Implications of land use and land cover dynamics for mountain resource degradation in the northwestern Ethiopian highlands. *Mountain Research and Development,* 21**,** 184-191.

CHAPTER 4: APPLICATION OF MODIS IMAGES FOR SHORE AREA MONITORING AND BATHYMETRIC MODEL GENERATION

Abstract

A technique to map lake area is developed using the 250-m and 500-m resolution MODIS–Terra images and is tested over Lake Tana, Ethiopia where daily observed lake level data are available. Satellite based lake area estimates were obtained from two simple image calculation procedures: Normalized Difference Vegetation Index (NDVI) and Normalized Difference Water Index (NDWI) enhanced NDVI (ENDVI). The area calculated from the images is compared with area estimates using existing bathymetry. The precision of both the ENDVI and NDVI area estimates was good but the accuracy was poor, suggesting the existing bathymetric model is not applicable for the near shore area where lake bottom depth are extrapolated. A new bathymetric model using MODIS images reproduced the water level with RMSE of 0.20 m as compared to 0.87 using the existing bathymetric model. Despite their unavailability on cloudy days, MODIS images can be a valuable tool for lake area mapping and can be used together with radar images to overcome the seasonal problems with cloud cover.

4.1 Introduction

Population increase and climatic change are putting an increasing pressure on the available water supply in the world requiring better management of our water resources (Ingram, 2008). In order to manage water, especially in times of extremes such as droughts and floods, knowledge about the quantity of water and how this quantity will be distributed in the system is needed. While in

developed countries well maintained ground based methods can measure the "water status" in developing countries these systems fail due to limited financial and institutional capacity. The goal of this paper is to evaluate to what degree remotely sensed images can replace ground based storage characteristics measurements namely lake surface area and water level.

Various remotely sensed images and image synthesis have been used to map lake area. White (1978) used Landsat–1 images to map reservoir area in New Mexico. Duane Nellis *et al*. (1998) observed temporal and spatial variation in Tuttle creek reservoir in Kansas using Landsat TM data. Liebe *et al*. (2005) used Landsat ETM+ images to measure lake surface area in Ghana. Ma *et al*. (2007) used 10 day synthesis SPOT/VEGETATION images to monitor change in Ebinur Lake area. Liebe *et al*. (2009) developed a method to monitor small reservoirs using ENVISAT ASAR[†] images along with the storage characteristics of the reservoirs. Radar images offer the advantage of image availability on cloudy days. However, these images require image processing skills and can be difficult to interpret due to partly submerged vegetation, the effect of Bragg scattering and adjacent flat smooth shorelines (Liebe et al., 2005). Temporal and spatial resolutions also affect the dependability of the images. ENVISAT ASAR, Landsat ETM+ and ASTER pass over only once every 16 days and are less suitable for flood forecasting for example. Moreover, the spatial resolution of these satellite products results in massive data volumes. Pax–Lenney and Woodcock (1997) have shown that coarse spatial resolution imagery is often a necessary trade–off in order to keep the data volumes reasonable and to allow sufficiently frequent temporal coverage. Hence, one needs a reliable method to extract accurate information from medium to low resolution image sources.

[†] Advanced Synthetic Aperture Radar

Finally, atmospheric correction applied on these images has become a major source of uncertainty. This is because different end users apply different algorithms for atmospheric correction. However, recently remotely sensed images have become available on daily bases that are uniformly corrected for atmospheric effects. One such achievement is the MODIS–Terra version–5 validated products.The MODIS–Terra version–5 images with its sweeping 2,330 km wide field of view (FOV) are designed to provide measurements in large–scale global dynamics including changes in Earth's cloud cover, radiation budget and processes occurring in the oceans, on land, and in the lower atmosphere. MODIS collects data for every point of the earth's surface every 1–2 days in 36 discrete spectral bands. The spatial resolutions of MODIS bands are 250-m (bands 1, 2), 500-m (bands 3–7) and 1000-m (bands 8–36) (LPDAAC, 2010). The release of these products has alleviated the previous drawbacks since images of smaller data size with consistent atmospheric correction are made available daily. MODIS images provide the advantage of increased sensitivity (Hu et al., 2004). In addition, retrieval of MODIS images has been made easier with a web based interactive tool available to preview, select and re–project the images. The MODIS–Terra version–5 images incorporate quality rating products that include the cloud state, which are important when selecting images during the rainy season in which frequent heavy clouds overshadow the lake. We used these images to estimate the area of Lake Tana, Ethiopia where a significant amount of lake level data is also available.

4.2 Study Area

Lake Tana (Figure 4-1) is situated on the basaltic plateau of the north–western highland of Ethiopia (12° N, 37° 15' E, and 1 800 m altitude) covering an area of over 3000 km^2. The lake

drains a catchment area of 16,000 km^2. Six permanent rivers and 40 small seasonal rivers feed the lake. The shallow lake is Ethiopia's largest lake, containing half the country's freshwater resources, and is the third largest in the Nile Basin (Vijverberg et al., 2009). A bathymetric survey undertaken in 2006 had shown that the lake has a maximum depth of 15 m and stretches 65 km west–east and 74 km south–north (Ayana, 2007).The most pronounced advantage of Lake Tana is its storage characteristics, in that it store flow of the rainy season (June to September) for use in the remaining dry season. (Vijverberg et al., 2009). The lake storage amounts to more than two times that of the five large reservoirs in Ethiopia[†], rendering a relatively low cost per unit of utilizable water (Gebeyehu, 2004).

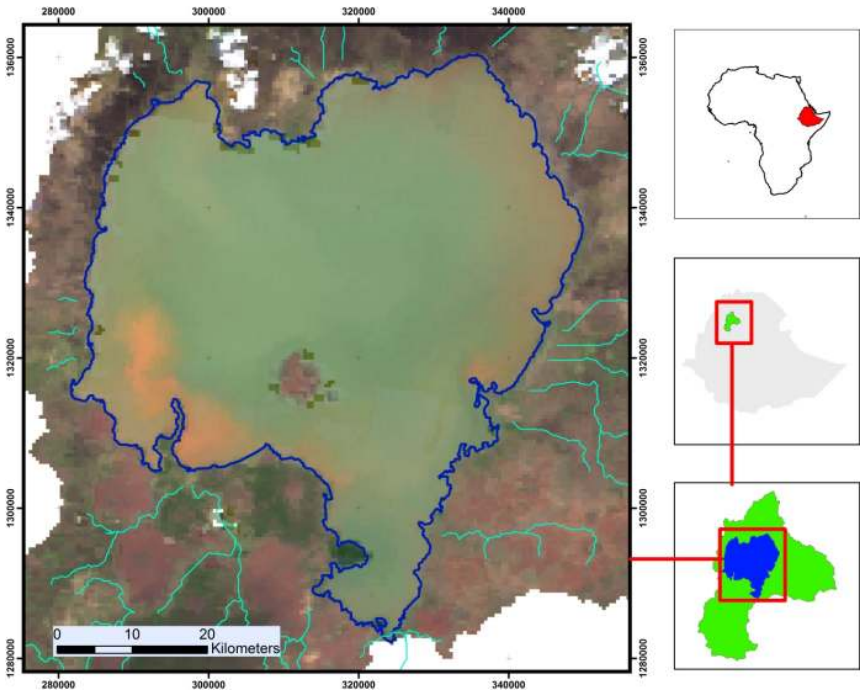

Figure 4-1: MODIS 250m true colour image of Lake Tana and its catchment (13 June 2000). At the start of the rainy season large turbid plume is flowing in to the lake turning the shore and stream entry locations to reddish brown, raising the water reflectance.

[†] Gilgel Gibe, Koka, Finchaa, Amerti, and Melka Wakena, provides an aggregate storage capacity of about 4.4 billion m^3

4.3 Materials and Methods

4.3.1 Lake bathymetry and area

A bathymetric model relates the water level to the water surface area at that water level. Ayana (2007) developed the bathymetric model for Lake Tana in 2006. The model was derived from the interpolation of 4424 depth measurements using the kriging interpolation method (Burrough et al., 1998). The interpolation fits to test points with R^2 of 0.98 and resulted in the following relationship:

$$H = 6\times10^{-6}A^3 - 8\times10^{-7}A^2 + 1.1\times10^{-3}A + 1774.1 \qquad \text{Equation 4-1}$$

where H is the water surface elevation in meters at the given lake surface area A (in square meters) (Ayana, 2007).

Depth measurements were restricted to one kilometre from the lake shore due to depth limits for instrument operation and boat access, necessitating extrapolation of the lake bottom surface for locations beyond the survey line. As the result the error variance around the lake shore was estimated to be as high as 2.50 meters (Ayana, 2007). Lake levels for the 2000–2006 times span were obtained from the Ministry of Water Resources (MoWR), Ethiopia.

4.3.2 Image data

Two distinct sets of MODIS–Terra version–5 images of 250-m and 500-m resolution were downloaded. The images incorporate quality rating products, including the cloud state, which is important when selecting images during the rainy season when frequent heavy clouds overshadow the lake (LPDAAC, 2010). To obtain a wide spread in measured areas we used a

measured lake level data plot when selecting MODIS images. The first set of eighteen images downloaded coincided with high and low lake levels during the 2000–2006 time spans. In order to improve the near lake shore bathymetry we selected a second set of 47 images between 2002 and 2003 at which time the lake level is at its lowest. In this set, two to five images were selected for each month maintaining a five to nine day interval except during months in the rainy phase of the monsoon when MODIS images were not usable due to cloud cover over the lake. For each image bands, 1, 2, and 6 were used; Band 1 is the *red* band spanning 620–670 nm, band 2 is a near infrared (*NIR)* band spanning 841–876 nm and band 6 is a short wave infrared (SWIR) band spanning 1628–1652 nm.

4.3.3 Data analysis

Two simple metrics (or indices) and a supervised classification are used to determine lake surface area at several lake level stages. The potential of the improved MODIS image data sets to map lake area is assessed using thresholds of: *Normalized Difference Vegetation Index* (NDVI), and *NDWI enhanced Normalized Difference Vegetation Index* here in after referred to as *Enhanced NDVI* (ENDVI).

Metric 1: Normalized Difference Vegetation Index (NDVI): is a measure of the degree of greenness in the vegetation cover of a land surface and can therefore effectively discriminate between clear water and land surface including papyrus (*Cyperus papurus*) (Adam and Mutanga, 2009). The NDVI is derived from reflectance measurements in the red (band 1) and

near infrared bands (band 2) centred at 645nm and 858nm, respectively. The NDVI is calculated as[†]:

$$NDVI = \frac{(\rho_{NIR} - \rho_{red})}{(\rho_{NIR} + \rho_{red})} = \frac{(\rho_{band2} - \rho_{band1})}{(\rho_{band2} + \rho_{band1})} \quad \text{Equation 4-2}$$

NDVI values range from -1 to 1, with values near zero corresponding to un-vegetated land and values approaching 1 corresponding to dense vegetation. Because water absorbs strongly in the infrared, the NDVI for water is generally negative. In this study, a pixel is designated 'water' if the NDVI is less than zero (Tucker, 1979).

The advantage of the NDVI is that it only requires two bands and is therefore simple to use. In the literature (Rees, 2001) it has been noted, however, that the reliability of the NDVI in estimating the lake surface is affected by sediment in the water. Sediment increases the reflectance in both the red and IR and can complicate the discrimination (Ma et al., 2007). This could be even more of a problem with submerged vegetation which would elevate the reflectance in the IR. Lake Tana has sediment in the water at the start of the rainy season when the lake level is at its lowest and the loose soil at the shores is washed into the lake water near the shore. Re–suspension of the sediment at the shore will also be increased by the inflowing sediment rich flood waters from the rivers.

Metric 2: Enhanced NDVI (ENDVI): In order to overcome the shortcoming of NDVI for sediment rich water, an enhancement procedure is introduced that uses bands 2 an 6 (as expressed in the Normalized Difference Water Index, NDWI) to distinguish between land and turbid water when the NDVI is positive. The NDWI is a satellite–derived index from the NIR

[†] ρ_{band} refers to reflectance of a given band, for example ρ_{Red} refers to reflectance from red band

(band 2, 858 nm) and short wave infrared (SWIR) (band 6, 1240 nm) (Gao, 1996) channels. The NDWI is calculated as:

$$NDWI = \frac{(\rho_{NIR} - \rho_{SWIR})}{(\rho_{NIR} + \rho_{SWIR})} = \frac{(\rho_{band2} - \rho_{band6})}{(\rho_{band2} + \rho_{band6})} \quad \text{Equation 4-3}$$

According to the *ENDVI* metric a pixel is assigned to 'water' if the NDVI is less than zero and the NDWI is greater than zero. Thus,

ENDVI = if (NDVI<0, "*water*" else if NDWI>0, "*water*" else "*land*") Equation 4-4

The work flow diagram (Figure 4-2) summarizes the processes applied in the method.

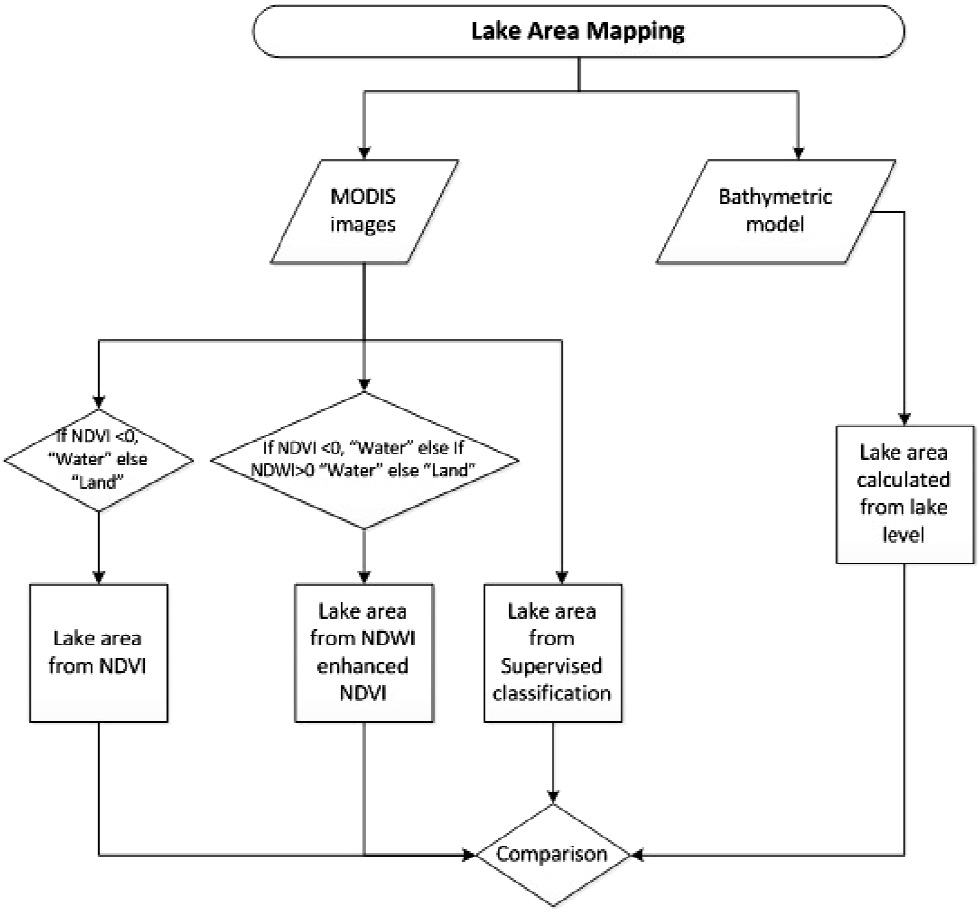

Figure 4-2: Work flow for area estimation

Supervised classification consists of two processes, training and classification. Supervised classification uses information about the known distribution of classes to initiate the process (Rees, 2001). In this work, two classes are defined "Water" and "Land" based on the characteristics of user-supplied samples of water and land in each image. In this study, the maximum likelihood classification algorithm within ENVI, an image processing tool, is used in the classification process. The maximum likelihood classification assumes that spectral values of training pixels are normally distributed according to a multivariate normal (Gaussian) probability density function. Each pixel is assigned to the class to which it is most likely to belong based on the probability distribution of the training data. Two dimensional scatter plots of the red (band 1) and near infrared bands (band 2) are used in ENVI to identify the training pixels for the supervised classification.

4.3.4 Comparison of satellite based methods

The NDVI, ENDVI and supervised classification had resulted in six maps for each selected image in 250 m and 500 m resolutions. The areas derived using these images were compared to the areas obtained from the bathymetric model (Equation 4-1) using the lake level data for the image date. The residual variance (RMSE) and coefficient of determination (R^2) between the area from the bathymetric model and from the metrics (NDVI and ENDVI) were used to evaluate the accuracy of the methods.

4.4 Results and discussion

Lake surface areas extracted from MODIS images and the corresponding lake areas obtained from the bathymetric model (Equation 4-1) are shown on Table 4-1. The lake level (column 2) is

the measured gauge level at the selected date for which the images are analyzed. In the next columns (columns 4–9) the areas mapped using *NDVI* (Equation 4-2), *ENDVI* (Equation 4-3) and *supervised classification* are shown for both the 250m and 500m resolution images.

Table 4-1: Comparison of image–mapped lake surface area and the area determined from the storage characteristic curve

Image Date	Lake water level at image date, m	Area, bathymetric model km^2 (Equation 4-1)	Area from MODIS image					
			NDVI		NDWI enhanced NDVI		Supervised Classification	
			250m	500m	250m	500m	250m	500m
10-Sep-00	1787.52	3087	3024	3005	3025	3004	3054	3014
16-Sep-00	1787.58	3091	3032	3015	3037	3016	3025	2971
17-Sep-01	1787.46	3082	3034	3026	3027	3024	3053	3026
20-Sep-01	1787.46	3082	3013	2985	3005	2983	3073	2980
21-Sep-01	1787.50	3085	3010	2992	3010	2986	3098	3017
22-Sep-01	1787.47	3083	3032	3012	3032	3010	3069	3032
22-Sep-02	1786.41	3001	3010	2981	3010	2978	3004	2943
24-Sep-02	1786.42	3002	2962	2935	2962	2931	3003	2880
10-Jun-03	1784.32	2822	2944	2943	2946	2940	2849	2797
12-Jun-03	1784.40	2830	2942	2943	2944	2940	2862	2817
26-Sep-03	1786.62	3017	2983	2947	2982	2980	3027	2759
28-Sep-03	1786.64	3019	3003	2984	3003	2980	3010	2993
9-Jun-04	1784.89	2873	2960	2958	2962	2956	2945	2971
4-Oct-05	1786.50	3011	3003	2986	3003	2980	3012	2926
7-Oct-05	1786.54	3012	3011	2989	3011	2986	2536	3041
10-Oct-05	1786.53	3010	2988	2971	2990	2966	2146	2517
15-Jun-06	1784.88	2873	2916	2901	2921	2897	1921	2222
16-Jun-06	1784.87	2872	2945	2933	2950	2928	2291	2725

Table 4-2: Correlation between lake area derived from MODIS images and the storage characteristics curve

Method	NDVI		ENDVI		Supervised Classification	
Image Resolution	250m	500m	250m	500m	250m	500m
RMSE, km^2						
High lake level	47	66	48	66	286	177
Low lake level	84	80	86	79	457	277
Overall accuracy						
RMSE, km^2	67	130	66	76	352	215
R^2	0.81	0.61	0.83	0.64	0.23	0.27

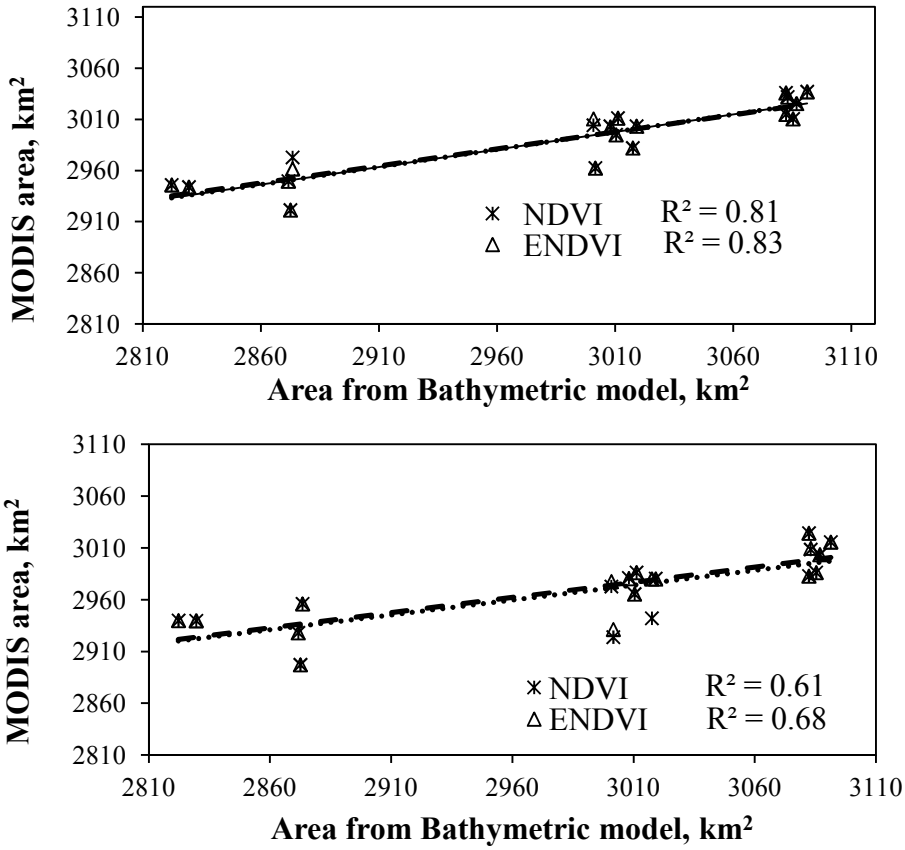

Figure 4-3:Correlation between bathymetric model and image mapped lake surface area (a) 250m images and (b) 500m images

Areas mapped from *NDVI* and *ENDVI* are compared with surface areas determined from the bathymetric model of the lake. The image–based reservoir area using *ENDVI* correlates slightly

better with the bathymetry–based reservoir area ($R^2 = 0.83$) (Figure 4-3(*a*)) than the NDVI ($R^2 = 0.81$) (Figure 4-3(*b*)).

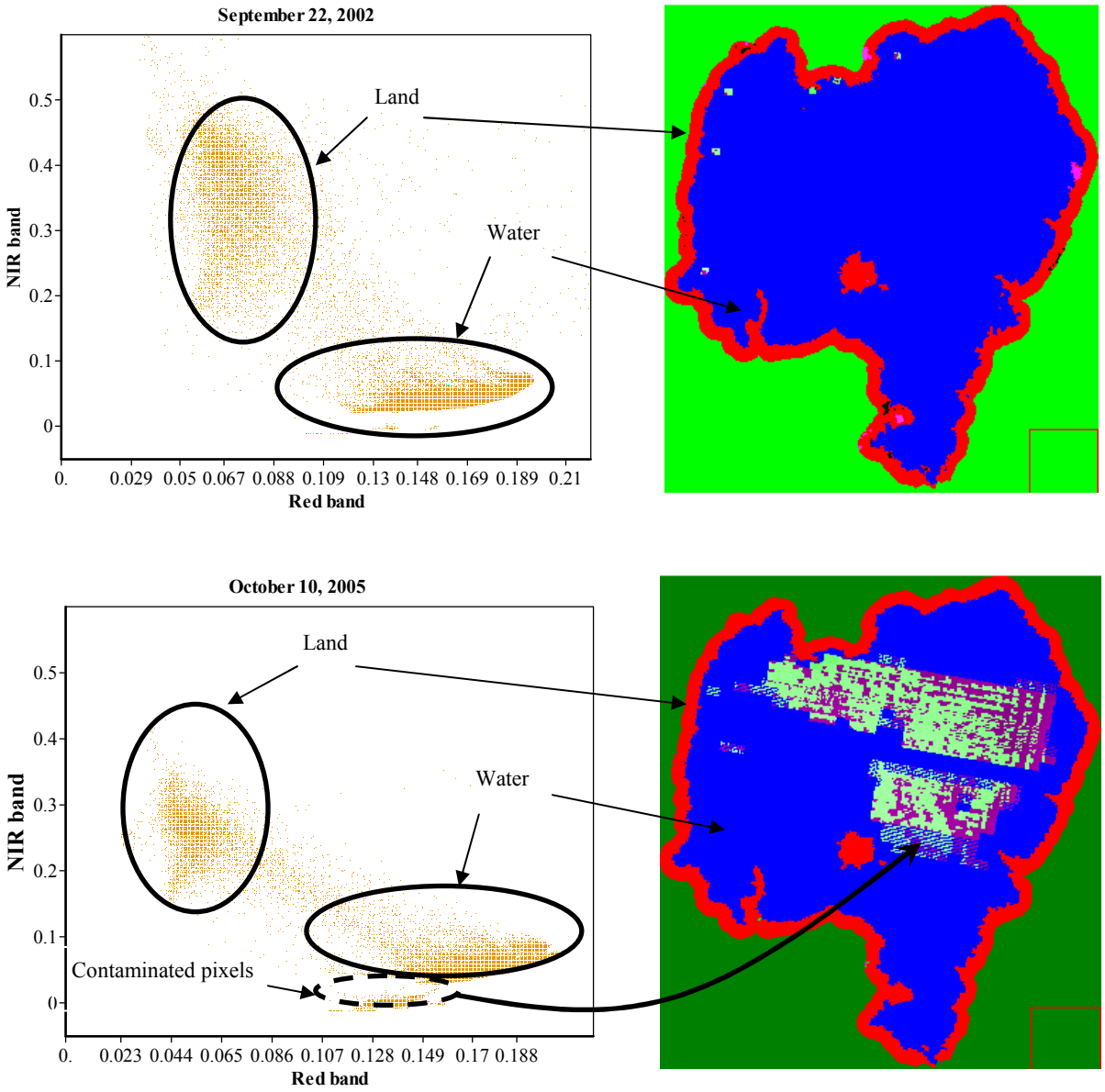

Figure 4-4:A scatter plot of the NIR versus red bands, ordinary image classification methods (e.g. supervised classification used here) often fail to overcome shortcomings in image quality due to contamination. In the September 22, 2002 image the classification more accurate due to the clean image where as in the October 10, 2005 image defective pixels are classified as two classes (seen in cyan and turquoise colours)

Supervised classification did not perform well (Figure 4-4). Using all the 18 images, the supervised classification resulted in an R^2 value of 0.23 for the 250m and 0.27 with the 500m resolution. The poor correlation was due primarily to contaminated pixels (Figure 4-4). The supervised classification outperforms the metrics when applied to *clean images* (e.g. 10 Sept. 2000; 17 Sept. 2001; 22 Sept. 2002; 10 June 2002; 12 June 2003; 28 Sept. 2003; and 4 Oct. 2004) with an R^2 of 0.92 and 0.87 for 250m and 500m resolution respectively.

The metrics also performed differently at higher (≥1786.5m) and lower (< 1786.5m) water levels and also at different image resolutions (Table 4-2). At higher lake levels both metrics resulted in comparable results while at lower water levels both methods are found to be less sensitive to image resolution. The overall accuracy of the metrics is only marginally improved after enhancement using the ENDVI, although the enhancement of the NDVI maps using NDWI renders them less sensitive to change in image resolution. Generally the ENDVI metric is less sensitive to image resolution in that with increased resolution (from 500 to 250m) the resulting improvement in RMSE is only 13% while for the NDVI metric 49% is obtained (Table 4-2). It is important to note here that the improvement in accuracy resulted in a fourfold increase in data volume and hence one should make a compromise between acceptable level of accuracy and costs associated with data storage issues.

Despite the good agreement as measured by R^2 between the bathymetric model and the satellite derived products, estimates of Lake area differed significantly (Table 4-1). MODIS *NDVI* and *ENDVI* area estimates for lake levels below an elevation of 1786m[4] were less than levels from the bathymetric model estimated area with Equation 4-1. Area estimates from MODIS are consistently larger than estimates using Equation 4-1 for lake water levels above 1786m. Thus

[4] All elevations in meters above mean sea level

the precision of the measurements between the NDVI and ENDVI methods with the bathymetric survey derived data was good but the accuracy was poor. In this section we will examine why the area estimates do not agree. To do this we selected 47 images in the period from January 2002 to December 2003 where the lake level decreased by over 2.50m. The 2002 images were used to derive the bathymetric model and the 2003 images are used to validate the accuracy of the model by calculating back the lake level. A new bathymetric model is generated using the ENDVI metric mapped lake surface area and the measured lake level of the image date.

Table 4-3: Calibration (2002) and validation (2003) of MODIS derived near shore bathymetric model

Date	Measured level	Estimated level using existing bathymetric model	Area Estimate from MODIS	Estimated level using MODIS modified bathymetric model	Error[5]	
					Δ_1	Δ_2
(1)	**(2)**	**(3)**	**(4)**	**(5)**	**(6)**	**(7)**
23-Jan-02	1786.53	1786.83	3034.20	1786.50	-0.30	0.03
30-Jan-02	1786.52	1786.82	3033.29	1786.48	-0.30	0.04
4-Feb-02	1786.45	1786.69	3023.20	1786.28	-0.24	0.17
10-Feb-02	1786.38	1786.68	3022.07	1786.25	-0.30	0.13
15-Feb-02	1786.33	1786.74	3027.06	1786.35	-0.41	-0.02
20-Feb-02	1786.32	1786.64	3018.69	1786.18	-0.32	0.14
24-Feb-02	1786.3	1786.75	3027.87	1786.37	-0.45	-0.07
7-Mar-02	1786.16	1786.59	3014.93	1786.11	-0.43	0.05
16-Mar-02	1786.08	1786.50	3007.64	1785.96	-0.42	0.12
8-Apr-02	1785.87	1786.50	3007.69	1785.96	-0.63	-0.09
22-Apr-02	1785.74	1786.52	3009.62	1786.00	-0.78	-0.26
29-Apr-02	1785.66	1786.57	3013.22	1786.07	-0.91	-0.41
8-May-02	1785.66	1786.46	3004.74	1785.90	-0.80	-0.24
14-May-02	1785.45	1786.15	2980.11	1785.39	-0.70	0.06
21-May-02	1785.4	1786.24	2987.08	1785.54	-0.84	-0.14
11-Jun-02	1785.24	1786.32	2993.79	1785.67	-1.08	-0.43
5-Jun-02	1785.32	1786.42	3001.52	1785.83	-1.10	-0.51
26-May-02	1785.42	1786.37	2997.39	1785.75	-0.95	-0.33
2-Jul-02	1785.38	1786.21	2984.61	1785.48	-0.83	-0.10
16-Jul-02	1785.44	1786.03	2969.86	1785.18	-0.59	0.26

[5] Δ_1 and Δ_2 refers to lake level estimate error using the existing and modified bathymetric model respectively

7-Nov-02	1786.32	1786.67	3021.54	1786.24	-0.35	0.08
30-Nov-02	1786.15	1786.63	3017.99	1786.17	-0.48	-0.02
25-Nov-02	1786.19	1786.58	3014.45	1786.10	-0.39	0.09
5-Dec-02	1786.08	1786.46	3004.68	1785.90	-0.38	0.18
11-Dec-02	1786.06	1786.53	3010.10	1786.01	-0.47	0.05
16-Dec-02	1786.02	1786.58	3014.61	1786.10	-0.56	-0.08
21-Dec-02	1785.98	1786.39	2999.59	1785.79	-0.41	0.19
30-Dec-02	1785.88	1786.49	3007.21	1785.95	-0.61	-0.07
17-Jan-03	1785.76	1786.49	3007.15	1785.95	-0.73	-0.19
26-Jan-03	1785.67	1786.49	3006.83	1785.94	-0.82	-0.27
2-Feb-03	1785.64	1786.46	3004.42	1785.89	-0.82	-0.25
9-Feb-03	1785.56	1786.44	3003.56	1785.87	-0.88	-0.31
3-Mar-03	1785.42	1786.21	2984.45	1785.48	-0.79	-0.06
25-Feb-03	1785.43	1786.41	3000.66	1785.81	-0.98	-0.38
16-Feb-03	1785.52	1786.41	3000.61	1785.81	-0.89	-0.29
26-Mar-03	1785.18	1786.15	2980.21	1785.39	-0.97	-0.21
18-Mar-03	1785.24	1786.21	2984.78	1785.49	-0.97	-0.25
10-Mar-03	1785.32	1786.22	2985.79	1785.51	-0.90	-0.19
2-Apr-03	1785.08	1786.12	2977.05	1785.33	-1.04	-0.25
13-Apr-03	1785.07	1785.79	2949.95	1784.77	-0.72	0.30
20-Apr-03	1784.98	1785.91	2959.93	1784.98	-0.93	0.00
20-May-03	1784.74	1785.79	2949.89	1784.77	-1.05	-0.03
11-May-03	1784.8	1785.70	2942.81	1784.63	-0.90	0.17
29-Apr-03	1784.91	1785.83	2953.81	1784.85	-0.92	0.06
29-May-03	1784.66	1785.75	2947.10	1784.72	-1.09	-0.06
8-Jun-03	1784.64	1785.84	2954.56	1784.87	-1.20	-0.23
21-Jun-03	1784.59	1785.64	2938.03	1784.53	-1.05	0.06

The modified equation for the shore area is given by:

$$H = 0.0205A + 1724.3 \qquad \text{Equation 4-5}$$

The new bathymetric model suggested a linear surface around the lake shore in contrast to the cubic polynomial fitted by the initial model (Figure 4-5). The accuracy of the new bathymetric model is validated by estimating the lake water level (Table 4-3) using lake area from 2003 images. The RMSE for such water level estimate using the new MODIS derived bathymetric model is reduced to 0.20 from 0.87 using the initial bathymetric model. The area estimate by the bathymetric survey is much smoother as one would expect when the points are extrapolated from

smooth lake bottom. The measurements of the bathymetric survey (that were taken to approximately 1km off the shoreline) do not overlap with the satellite derived images.

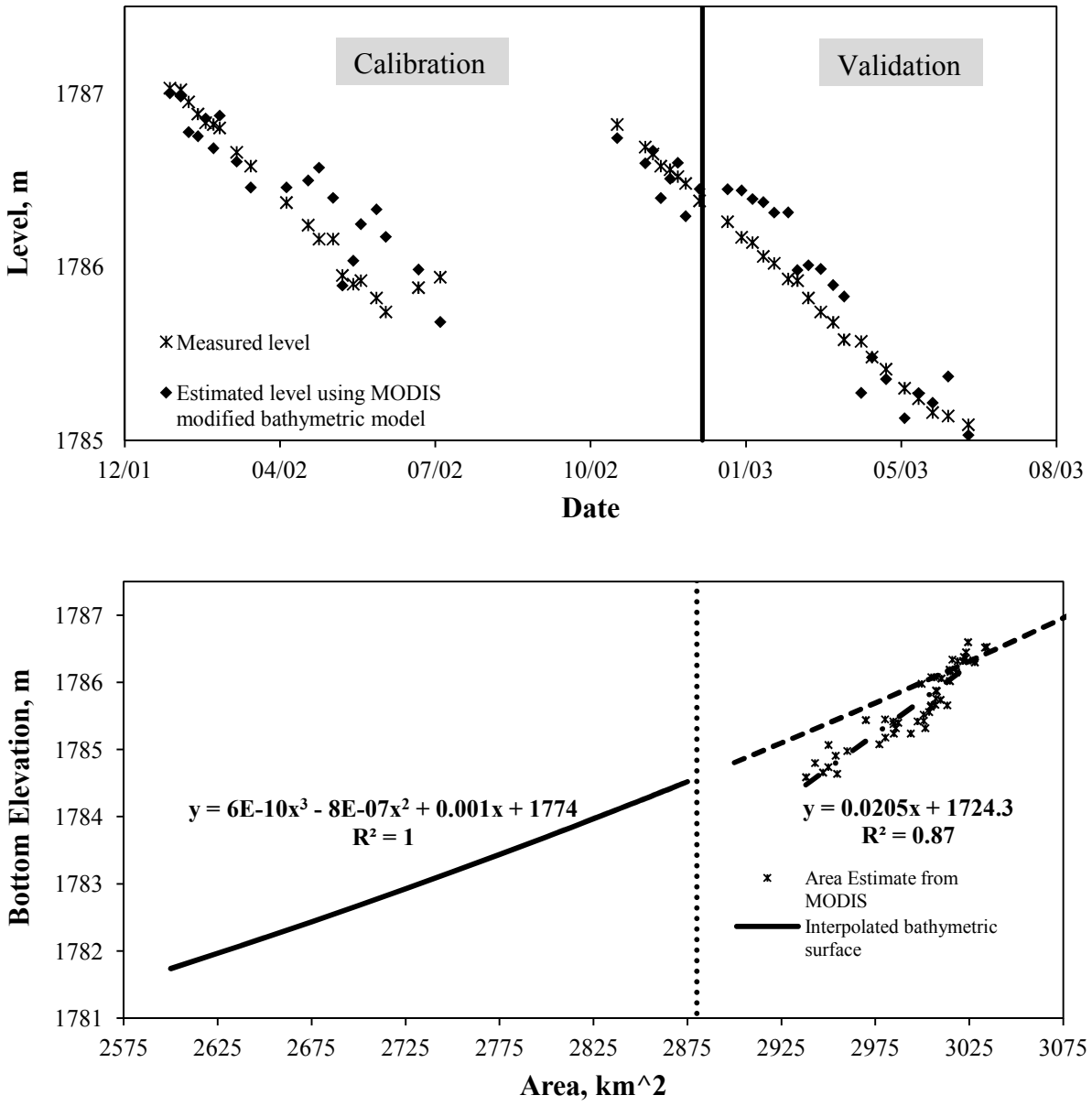

Figure 4-5:a) Comparison of measured and estimated lake levels using January 2002 to December 2003 MODIS images b) Near shore bathymetry generated from MODIS images was capable of capturing lake water level more accurately than existing bathymetric model

In Figure 4-5(*b*) the area estimated from MODIS images and by the bathymetric survey is plotted as a function of the lake level. The new bathymetry (Figure 4-5) suggested a steep bank just offshore from approximately 1784.5m to 1786.5m elevation and then a shelf that has a slight slope. During the wet season, as the velocity of the incoming water breaks abruptly at entry to the lake, the sand settles at the shore. The remaining silt load remains in suspension and spreads slowly into the lake. With the longer water residence time (Kebede et al., 2006) part of the silt load then settles over a larger area forming a relatively flatter bottom.

4.5 Conclusion

The use of MODIS–Terra version–5 images as a tool for lake area mapping offers the advantages of higher temporal resolution and reduced data size. The higher temporal resolution enables an analysis of short term, yet significant changes in lake area and monitoring of coastal areas. Further investigations must be carried out to assess to what lake size the MODIS images are capable to map area. At the beginning of the rainy season where the lake level is at its lowest, the effect of exposed lake shore vegetation compounds with the sediment plume and degrades the accuracy of the methods. Combined with the easy retrieval tools available and the simple mapping techniques that we tried to demonstrate in this research, the potential of MODIS–Terra version–5 images to monitor lake area is high. There is a high correlation between lake areas predicted by MODIS and from the bathymetric survey indication that the MODIS area estimates are consistent in time. The bathymetric survey of Ayana (2007) did not measure the depth of the lake within 1 km from the shore because of inaccessibility of the shore and therefore the satellite derived water level lake area relation is likely more accurate than the bathymetric survey.

A major drawback with MODIS images is cloud contamination. However the metrics (i.e., NDVI and ENDVI) used are found to be foolproof for images slightly contaminated by cloud as compared to the commonly applied classification algorithms (e.g. supervised classification). Monitoring is more critical during the rainy season as the lake area varies abruptly due to high inflow from streams draining to the lake. But this may be difficult due to high cloud cover over the lake. Therefore, radar images will be an ideal substitute during such gaps. Methods developed using ENVISAT ASAR images have resulted in a coefficient of correlation as high as 0.95 (Liebe et al., 2009). However, MODIS images have proved to be increasingly important resources in resource mapping because these data are robust, inexpensive, simple to use, and provide frequent synoptic coverage.

References

ADAM, E. & MUTANGA, O. 2009. Spectral discrimination of papyrus vegetation (Cyperus papyrus L.) in swamp wetlands using field spectrometry. *ISPRS Journal of Photogrammetry and Remote Sensing,* 64**,** 612-620.

AYANA, E. K. 2007. Validation of radar altimetry lake level data and its application in water resource management. *International Institute for Geo-Information Science and Earth Observation), Enschede, Master's thesis, 86p*.

BURROUGH, P. A., MCDONNELL, R. A. & MCDONNELL, R. 1998. *Principles of geographical information systems*, Oxford university press Oxford.

DUANE NELLIS, M., HARRINGTON, J. A. & WU, J. 1998. Remote sensing of temporal and spatial variations in pool size, suspended sediment, turbidity, and Secchi depth in Tuttle Creek Reservoir, Kansas: 1993. *Geomorphology,* 21**,** 281-293.

GAO, B. C. 1996. NDWI—a normalized difference water index for remote sensing of vegetation liquid water from space. *Remote Sensing of Environment,* 58**,** 257-266.

GEBEYEHU, A. 2004. The Role of Large Water Reservoirs. *Proceeding of 2nd International Conference on the Ethiopian Economy.* Addis Ababa, Ethiopia: Ethiopian Economic Association.

HU, C., CHEN, Z., CLAYTON, T. D., SWARZENSKI, P., BROCK, J. C. & MULLER–KARGER, F. E. 2004. Assessment of estuarine water-quality indicators using MODIS medium-resolution bands: Initial results from Tampa Bay, FL. *Remote Sensing of Environment,* 93**,** 423-441.

INGRAM, H. M. 2008. *Decision support experiments and evaluations using seasonal-to-interannual forecasts and observation data: a focus on water resources: synthesis and assessment product 5.3 report*, US Climate Change Science Program.

KEBEDE, S., TRAVI, Y., ALEMAYEHU, T. & MARC, V. 2006. Water balance of Lake Tana and its sensitivity to fluctuations in rainfall, Blue Nile basin, Ethiopia. *Journal of Hydrology,* 316**,** 233-247.

LIEBE, J., VAN DE GIESEN, N. & ANDREINI, M. 2005. Estimation of small reservoir storage capacities in a semi-arid environment:: A case study in the Upper East Region of Ghana. *Physics and Chemistry of the Earth, Parts A/B/C,* 30**,** 448-454.

LIEBE, J. R., VAN DE GIESEN, N., ANDREINI, M. S., STEENHUIS, T. S. & WALTER, M. T. 2009. Suitability and limitations of ENVISAT ASAR for monitoring small reservoirs in a semiarid area. *Geoscience and Remote Sensing, IEEE Transactions on,* 47**,** 1536-1547.

LPDAAC 2010. Surface Reflectance Daily L2G Global 250m.

MA, M., WANG, X., VEROUSTRAETE, F. & DONG, L. 2007. Change in area of Ebinur Lake during the 1998–2005 period. *International Journal of Remote Sensing,* 28**,** 5523-5533.

PAX-LENNEY, M. & WOODCOCK, C. E. 1997. The effect of spatial resolution on the ability to monitor the status of agricultural lands. *Remote Sensing of Environment,* 61**,** 210-220.

REES, G. 2001. *Physical principles of remote sensing*, Cambridge Univ Pr.

TUCKER, C. J. 1979. Red and photographic infrared linear combinations for monitoring vegetation. *Remote Sensing of Environment,* 8**,** 127-150.

VIJVERBERG, J., SIBBING, F. A. & DEJEN, E. 2009. Lake Tana: Source of the Blue Nile. *The Nile***,** 163-192.

WHITE, M. E. 1978. Reservoir surface area from Landsat imagery. *Photogrametric engineering and remote sensing,* 44**,** 1421-1426.

CHAPTER 5: MONITORING STATE OF BIOMASS RECOVERY IN THE BLUE NILE BASIN USING IMAGE BASED DISTURBANCE INDEX

Abstract

The heavy dependence of the Ethiopian rural population on natural resources, particularly land, to maintain their livelihood is an underlying cause for the degradation of land and other natural resources. The Ethiopian highlands, which are the center of major agricultural and economic activities, have been eroding for many years. Various actors have undertaken reforestation programs with an aim to mitigate the land degradation problem; however, the status of these plantations has never been evaluated at a basin scale. The image based disturbance index (DI) measure the status of the ecosystem on the basis of the ratio of long-term enhanced vegetation index (EVI) and the land surface temperature (LST). This study applied the DI to assess the current state of biomass in the upper Blue Nile basin with a focus on areas where degradation mitigation measures are implemented through reforestation campaigns. The DI maps are validated through field visits on 19 selected sites and inventory data obtained from WFP over five sites. The results showed that the largest expansion of plantations has taken place in five sub basins and is between 6 to 8.5% of the sub basin area with expansion in the remaining eleven sub basins ranging from 3 to 5%. Despite the very low annual rate of expansion it can be concluded that the mitigation measures implemented through reforestation campaigns contribute to the total recovered forest area.

5.1 Introduction

Land degradation is a major problem in Ethiopia. It takes place in the form of soil erosion, gully formation, soil fertility loss and severe soil moisture stress, which is partly the result of loss in soil depth and organic matter (Hagos et al., 1999). The excessive dependence of the Ethiopian rural population on natural resources, particularly land, as a means of livelihood is an underlying cause for land and other natural resources degradation (Bekele, 2008). Agriculture accounts for 45 percent of the gross domestic product (GDP), 85 percent of export revenue and 80 percent of employment (EPA, 1997). The demand for farm land, timber, fuel wood and grazing lands drives the overexploitation of forest resources (Gebremedhin et al., 2003) in the Ethiopian highlands where the bulk of the population lives. As a consequence the Ethiopian highlands have experienced accelerated soil erosion for many years.

The annual soil erosion in Ethiopia ranges from 16 tons/ha/yr to 300 tons/ha/yr depending mainly on the slope, land cover, and rainfall intensities (Hawando, 1997, Tebebu et al., 2010). A reclamation study by the Food and Agriculture Organization (FAO) estimated the degraded area on the highlands at 27 million ha of which 14 million hectares is very seriously eroded with 2 million hectares of this having reached a point of no return (Constable and Belshaw, 1986). High population growth and the need for further agricultural expansion into marginal areas of fragile soils or critical habitats for biodiversity will lead to significant environmental degradation and deterioration of resilience for future environmental shocks unless intervention measures are introduced (Jagger and Pender, 2003).

With an aim to mitigate land degradation problems in Ethiopia, the federal and local governments and various NGO's have undertaken soil and water conservation measures. World

Food Program (WFP) "Project 2488", Managing Environmental Resources to Enable Transitions to More Sustainable Livelihoods (MERET) project, the Millennium "one man two tree" campaign, and other similar initiatives are part of the ambitious soil and water conservation efforts that have been made by the Ethiopian government (Nedessa and Wickrema, 2010). Some studies show that by the mid 1980s, nearly 180,000 hectares had been afforested and 460,000 hectares had been treated through soil conservation practices (Admassie, 1998), together amounting to 5% of the area in the highlands requiring conservation (Shiferaw and Holden, 1999).

5.2 Review of the Disturbance theory

The capacity of the landscape to sustain biomass longer is an important marker of its state of degradation. Such capacity can be improved by measures such as increasing organic matter, deeper plow depth (in agricultural fields), conservation of water on the landscapes and better drainage infrastructure (in waterlogged areas). In this research context, biomass longevity refers to the landscape's ability to support the growth of vegetation that has been put in place through past reforestation campaigns. Such plantings are sustainable only when there is enough water available for photosynthesis and human interference is controlled. These plantations avoid further degradation by reducing rainfall impact and interrupting surface runoff. Because of the cooling effect of vegetation on the ground, soil evaporation is reduced, and infiltration is facilitated, making more water available for the increased biomass.

The evaluation of the state of biomass can be made by quantifying biomass disturbance trajectories using vegetation indices (Michener and Houhoulis, 1997, Ruiz and Garbin, 2004, Jin and Sader, 2005, Van Leeuwen, 2008, Ferreira et al., 2010, Spruce et al., 2010). Here, the image

based DI tool suggested by Mildrexler et al. (2007) is used to assess the trend in the area expansion of these plantations. The method is used to assess the status of the biomass on the basis of the ratio of long-term enhanced vegetation index (EVI) and the land surface temperature (LST) as measured by Moderate Resolution Imaging Spectroradiometer (MODIS).

Vegetation indices and land surface temperature are the most vulnerable biotic and abiotic components, respectively, of a terrestrial ecosystem to detectable alteration during disturbance events (Mildrexler et al., 2007). The EVI, which is sensitive to vegetation changes, is calculated from red, near infrared, and blue bands (Huete et al., 2002).

$$EVI = G \times \frac{(NIR - Red)}{(NIR + C1 \times Red - C2 \times Blue + L)} \qquad \text{Equation 5- 1}$$

where *NIR, Red* and *Blue* are surface reflectance at the respective bands, *L* is the canopy background adjustment factor, *C*1, *C*2 are the coefficients of the aerosol resistance term, *L*=1, *C*1=6, *C*2=7.5 are coefficients in the EVI algorithm and *G* (gain factor)=2.5 (Huete et al., 1994, Huete et al., 1997).

Vegetated areas generally yield high EVI values as they reflect more in NIR but low in the visible band. More importantly LST is strongly related to vegetation density due to the cooling effect of the vegetation through latent heat transfer (Coops et al., 2009). Thus higher vegetation density results in lower land surface temperature. Capitalizing on these phenomena, long term measurements in the form of remotely sensed images can be used to see the temporal change in the biomass in the larger spatial extent of the river basin. Causes for disturbance should however be properly identified.

There are various causes for changes in biomass that result in positive or negative disturbances. Drought and wildfire are major stressors that affect forest ecosystem functioning and processes (Van Leeuwen, 2008). A number of studies have mapped fire disturbance using the EVI (Coops et al., 2009, Forzieri et al., 2010). Disease, geological incidences (land slide, volcano etc), infrastructure expansion, resettlement and clear cutting also cause positive disturbance. Vegetation recovery due to reforestation and irrigation result in negative disturbance values.

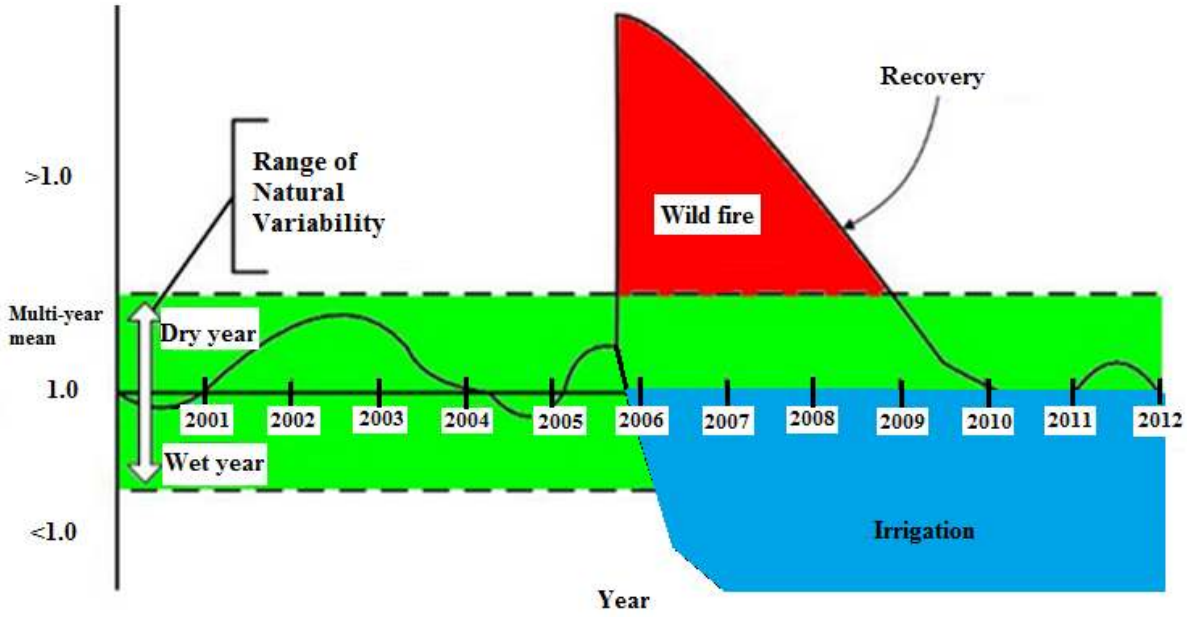

Figure 5-1: The disturbance index plot (Mildrexler et al., 2007) explains the undergoing process; instantaneous events (e.g. wild fire) causes a sharp decline of biomass and a recovery taking place over extended time

Disturbances may also be short lived or prolonged (Figure 5-1). The usual cycle of cropping and harvesting cause increased EVI and reduced LST at peak vegetation season followed by reduced EVI and increased LST at harvest. On the other hand drought, disease and urbanization result in prolonged reduction in the EVI and thereby an increase in LST for longer duration. Thus the length of prevalence of the disturbance index tells the type of phenomena causing the disturbance

(positive or negative). Seasonal increases or decreases in DI that occur, mainly due to vegetation phenology, fall within an explainable range of variability.

Various image sources are available for use in the DI calculation. Although high spatial resolution satellite images may offer a more detailed view of land surfaces, their limited area coverage and temporal sampling have restricted their use to local research rather than large scale monitoring (Ruiz and Garbin, 2004). To be used for regional scale studies, the high spatial resolution images require significant image processing skills. For example using Landsat TM/ETM images for vegetation monitoring in the upper Blue Nile basin requires the mosaicking of 17 image tiles, applying geometric correction, radiometric normalization and transformation, cloud screening, and atmospheric correction. The fact that the images are not taken on the same dates further complicates the atmospheric correction making these images challenging for use by professionals with limited remote sensing data processing skills. On a regional scale and in heterogeneous environments, such as the Blue Nile region, moderate resolution images are preferred over finer resolution images for their reduced data volume, processing requirement and increased temporal coverage. Ruiz and Garbin (2004) used AVHRR 8 km images to estimating the burn area for tropical Africa. Coops et al. (2009) and Mildrexler et al. (2009) applied Moderate Resolution Imaging Spectrophotometer (MODIS) images to monitor a large swath of area in Northern America. In this study archives of satellite data from MODIS are used. Despite their relatively coarse resolution these images have been successfully used to study vegetation cover change at regional to global scales (Hill et al., 2008). MODIS images provide the advantages of high temporal resolution, smaller data volume and require minimum technical skill for analysis. More importantly, in using MODIS images, much of the uncertainty associated with atmospheric corrections can be avoided.

The objective of this research is to evaluate the state of the conservation measures in the upper Blue Nile basin which are put in place through reforestation campaigns using the DI computed with MODIS images. The resulting DI maps are validated through field visits to areas flagged by the analysis and independent inventory data from WFP. The expected outcome of this study is a measure of the total recovered area, spatial distribution of the recovered areas within the basin and the recovery trend. As equivalent tools are currently nonexistent, the results of this research will help decision makers to apply similar methods to monitor the recovery trend of biomass in conserved areas for the future. It will also help to identify location of areas in which reforestation has been successful so as to recommend those practices for scaling up at a river basin scale.

5.3 Method and materials

5.3.1 Study area

The Blue Nile is located between 16° 2' N and 7° 40' N latitude, and 32° 30' E and 39° 49' E longitude (Figure 5-2). It has an estimated area of 311,437 sq. km (Yilma and Awulachew, 2009). The Blue Nile Basin (Abbay), with a total area of about 200,000 square kilometers (20% of Ethiopia's land mass), and accommodating 25% of the population, is one of the most important river basins in Ethiopia. About 40% of agricultural products and 45% of the surface water of the country are contributed by this basin (Erkossa et al., 2009). The Blue Nile represents about 8% of the total Nile catchment area but contributes about 60% of the flow of Nile at Aswan, Egypt. A highland plateau, steep slopes adjoining the plateau that tilt to the west and the western low lands with gentler topography characterizes the Basin. The steep slopes and the plateaus extend from 1700m (Bahir Dar) to 4000 m (North east highlands) above sea level. Geologically the basin is comprised of 32% exposed crystalline basement, 11% sedimentary

formations and 52% volcanic formations. The dominant soil texture is Vertisol, covering about 15% of the Basin (Gebrehiwot et al., 2011). The Blue Nile basin has a short rainy season that that extends from March to May, a main rainy season that extends from June to September and a dry season extending from October to February. The rainfall within the basin shows high seasonality with the peaks in July. The annual rainfall in the Blue Nile ranged from 880 to 2200 mm (Taye and Willems, 2012).

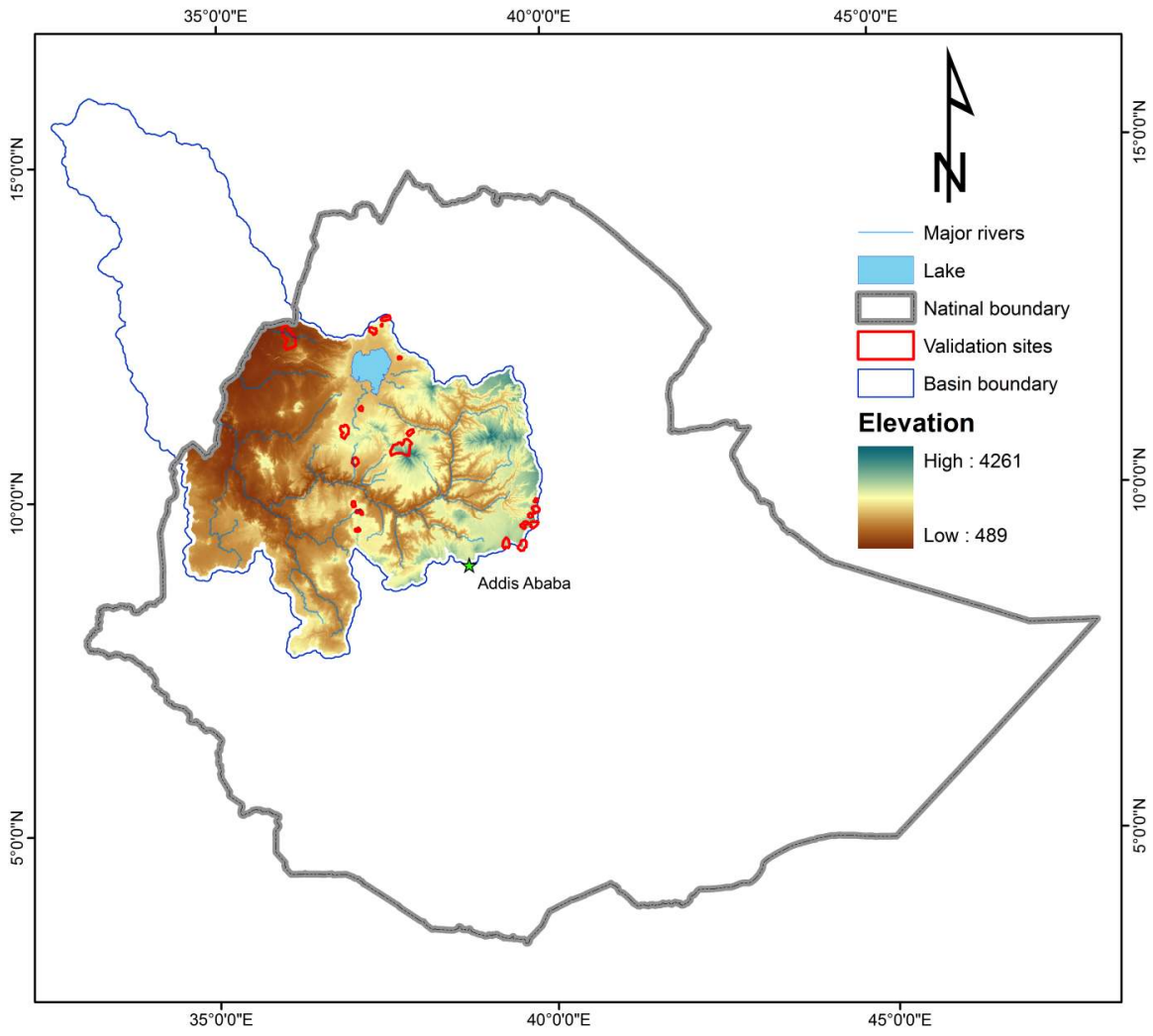

Figure 5-2: Upper Blue Nile basin (also called Abbay Basin) and selected ground validation sites

5.3.2 Methodology

5.3.2.1 DI map development

The DI map is developed by computing the ratio of annual maximum composite LST and EVI on a pixel by pixel basis, such that:

$$DI_i = \frac{LST_{imax}/EVI_{imax}}{\sum_{i-1}(LST_{max}/EVI_{max})} \qquad \text{Equation 5- 2}$$

where DI_i is the Disturbance Index (DI) value for year i, LST_{imax} is the annual maximum eight-day composite LST for year i, EVI_{imax} is the annual maximum 16-day EVI for year i, LST_{max} is the multiyear mean of LST_{max} up to but not including the analysis year ($i-1$) and EVI_{max} is the multiyear mean of EVI_{max} up to but not including the analysis year ($i-1$). The DI is a dimensionless value that, in the absence of disturbance, approaches unity.

The annual LST_{max} and EVI_{max} values are computed for each of the 10 years (2003-2012) and the LST_{max} for each year is then divided by the corresponding EVI_{max} value on a pixel-by-pixel basis, resulting in a ratio of LST_{max} to EVI_{max} from 2003 to 2012. These annual DI layers are then divided by the long-term average of the index for that pixel, averaged over all previous years. For example the DI for the year 2005 is calculated as the ratio of LST_{max} to EVI_{max} of 2005 divided by the multiyear mean for the years previous to 2005 (i.e. mean of 2003 and 2004). Any DI values within the range of natural variability will be considered as having undergone no change; whereas, pixels outside of this central range are flagged as subject to disturbance.

The biophysical relationship outlined by Nemani and Running (1997) is also tested for validity. For each land cover type the annual maximum LST and EVI raster are produced and the mean of the raster values recorded as mean-maximum LST and mean-maximum EVI.

5.3.2.2 Identifying disturbed areas

Coops et al. (2009) recommends values within ±1 standard deviation of the long term mean be considered as within the natural variability range. Both instantaneous (fire, disease and the like) and prolonged (drought, urbanization and the like) phenomena extend out of this natural range of variability. Therefore a departure higher than ±1 standard deviation will be flagged as potential disturbance areas. The ability of the calculated DI to capture these phenomena should be verified by a field survey in strategically selected flagged areas. In addition the validation work involves the compilation and thorough review of ancillary data collected from organizations implementing reforestation campaigns.

5.3.3 Data

5.3.3.1 Image and vector data

MODIS images of eight day maximum LST (MOD11A2) and 16-day EVI (MOD13A2) products from 2002 to 2010 are downloaded. The ISLSCP II MODIS IGBP[6] Land Cover (Friedl et al., 2010) data is used to stratify mean-maximum LST and EVI over the study area. The data consists of 18 land cover types with water, forest Shrub land, savanna, cropland, built-up, snow and barren land as main categories. Vector data layers are used extract the DI values to analyze biomass recovery patterns at sub basins level. The disturbed area (Positive or negative) for the 16

[6] **I**nternational **S**atellite **L**and – **S**urface **C**limatology **P**roject, **I**nitiative II MODIS **I**nternational **G**eosphere – **B**iosphere **P**rogram

sub basins is extracted and the total area calculated for each sub basin on a year by year basis. Boundaries for validation sites are manually digitized and imported into a handheld GIS.

5.3.3.2 Field data

Based on the DI map generated, nineteen sites were selected and field campaigns were carried out to compare the DI map results with actual ground conditions, to verify the type and extent of the disturbance and peasants' perception of the different conservation measures. Semi-structured interviews with key informants were conducted at several households. Focus group discussions were held to facilitate information exchange on the environmental impact of the disturbance areas and the overall participation of the community in initiating, undertaking and sustaining the gains.

5.3.3.3 Ancillary data for validation

Ancillary data includes details on watershed conservation and micro irrigation projects within the basin. As irrigated areas certainly add to the negatively disturbed area (which may wrongly be considered as recovered areas) the field validation campaigns helps in identifying irrigated areas and exclude them from the area calculation of recovered areas.

The data on conservation work with in the basin is obtained from agricultural bureaus of Amhara region and WFP MERET project (Figure 5-3). The ancillary data includes list of location, areas and time of implementation of plantations (Appendix D, Table D1–5). The land covers where the SWC works concentrate are assumed to be those where no existing agricultural activity takes place. Thus water bodies, grasslands, permanent wetlands, croplands and urban/built-up areas are masked out. On the remaining land cover types, the areas showing biomass recovery trends are

taken to be pixels with DI values less than one standard deviation from the long-term mean. The total recovering area is then calculated for the 16 sub basins in the 2004 – 2012 time span. The proportion of the recovering area to the sub basin area is used to standardize the results and for ease of comparison.

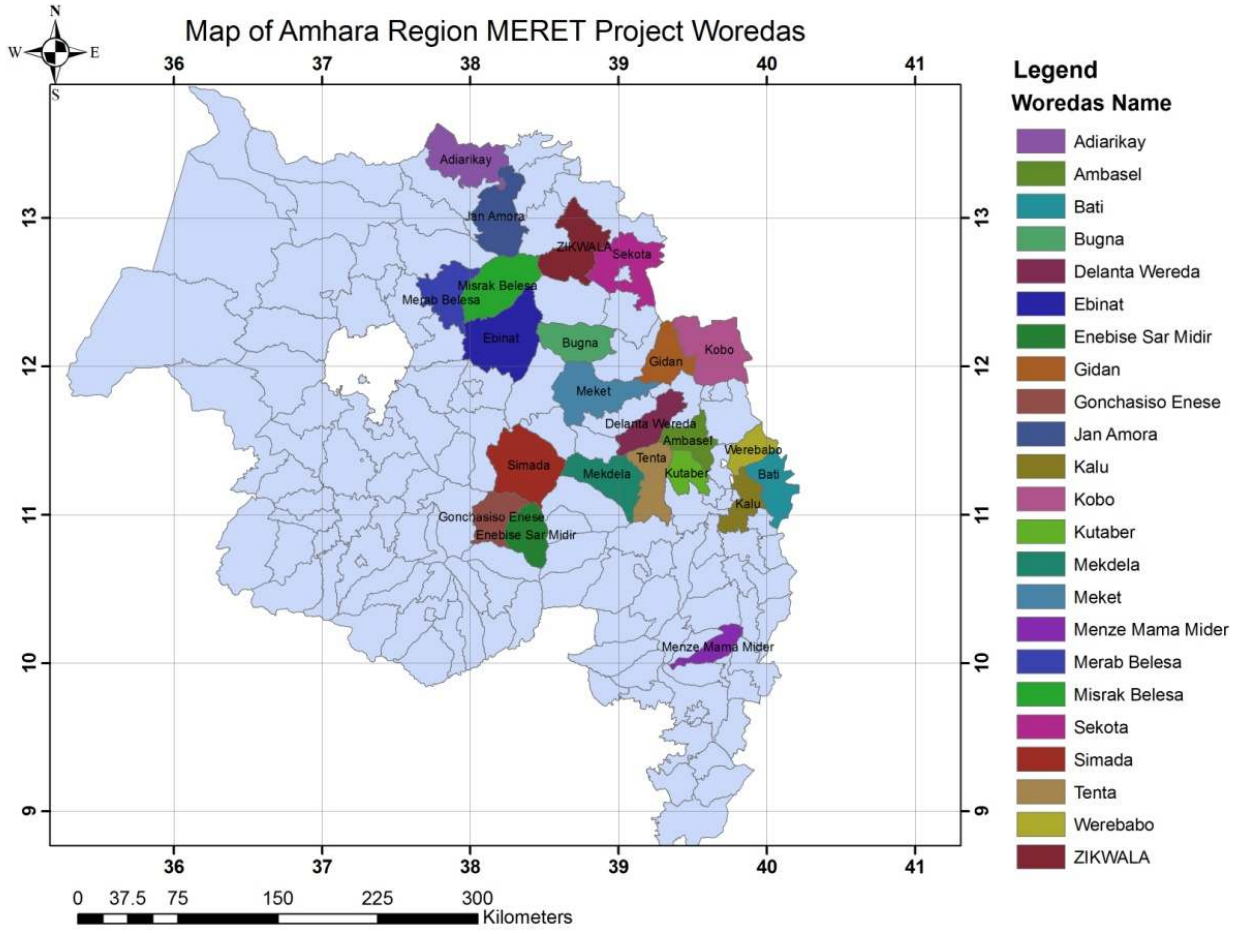

Figure 5-3: Districts of community managed watershed projects in Amhara region, five of the districts are used to validate the DI maps, Source: MERET project, https://sites.google.com/site/meretproject04/ (visited November 2012)

5.4 Result and discussion

5.4.1 Validity of disturbance trajectory

Figure 5-4 shows the biophysical relationship between mean-maximum LST and mean-maximum EVI for the 2003-2012 dataset. The figure depicts the disturbance trajectory for the different ISLSCP II MODIS IGBP land cover types (Appendix D, Tables D1–2 and D1–3).

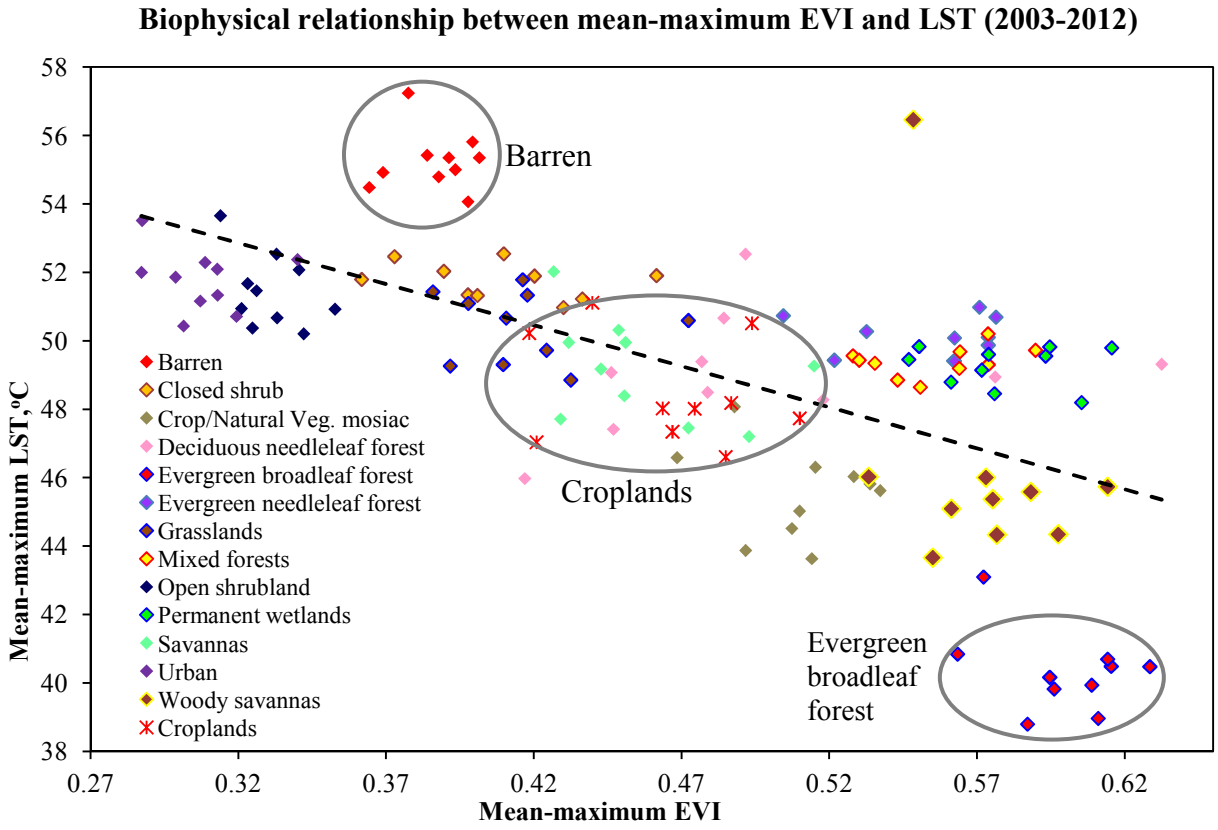

Figure 5-4: Biophysical relationship between mean-maximum EVI and LST (2003-2012), higher land surface temperature is associated with low biomass due to lower latent heat transfer. Land surface temperature on barren, open shrub, savanna and woody savanna peaked in 2011 with reduced EVI

The mean-maximum LST and mean-maximum EVI are strongly negatively correlated with higher LST associated to low biomass due to lower latent heat transfer. This validates the hypothesis that the energy balance relationship for the land cover grouping is related to the

disturbance trajectory. High mean-maximum LST values are not anomalies, instead are effect of fire seasonally set to clear agricultural fields and stimulate growth. As the fire removes all biomass the evaporative cooling potential diminishes and albedo increases due to a blackened surface (Running, 2008).

5.4.2 Biomass recovery trend

The long term (i.e. ten years) average DI for the selected land cover classes was 1.47 and for the whole basin was 1.53 with standard deviations 0.64 and 0.69, respectively. The threshold value for one standard deviation below long term mean is thus 0.83 (i.e. 1.47 – 0.64). Field visits helped to identify that the majority of the areas identified as spots of biomass recovery are plantations initiated by the previous government after the 1984 drought. Eucalyptus tree dominate plantations with considerable mix of coniferous tree and some indigenous trees in the central and south east of the basin. This is in agreement with the national statistics in that out of the reported 161,000 ha that the state planted up to the year 1989 Eucalyptus accounts for more than 55% (EFAP, 1994).

Table 1 shows the area of recovered biomass for the years 2008 – 2012, reclassified based on the threshold given as proportion of the sub basin area. Taking Lake Tana sub basin as an example the results for 2008 and 2012 can be interpreted. In 2008 1.3 percent of the sub basin area had LST to EVI (i.e. DI) ratio, which is less than one standard deviation to the long term DI, whereas in 2012 the area expanded to 3.5 percent of the sub basin area. The results of the DI analysis showed a negative biomass recovery trend for 12 out of the 16 sub basins. North Gojjam, Dabus, Rehad and Tana basins showed a positive biomass recovery trend.

Table 5-1: Biomass recovery trend (2008 – 2012) as percentage of area ((ha/ha)×100) recovered at sub basin level (Appendix D, Figure D1–1)

NAME	08	09	10	11	12
	Area proportion with DI below 1 standard deviation of the long term mean				
Anger	1.4	1.2	2.5	2.2	0.7
Beles	1.3	0.3	1.9	0.5	0.9
Beshelo	4	8.5	2.7	2.1	2.3
Dabus	1.3	0.7	2	1.7	2
Didessa	1.1	4	4	1.4	0.9
Dinder	1.7	0.3	2	0.4	0.5
Fincha	3.7	3.5	5.6	2.5	1.8
Guder	1.5	1.3	8.4	1.1	1.2
Jemma	4.4	3.8	6	5.2	2.7
Muger	3.3	1.5	6.9	4.4	1.5
North Gojjam	1.1	2.1	5.2	1.8	4.4
Rahad	0.6	0.2	1.4	0.8	0.4
South Gojjam	2.6	1.7	3.5	2.8	1.6
Tana	1.3	2.7	2	2.2	3.5
Welaka	5.8	2.8	3.9	2.6	2.3
Wenbera	1.4	0.7	0.8	1.5	0.8

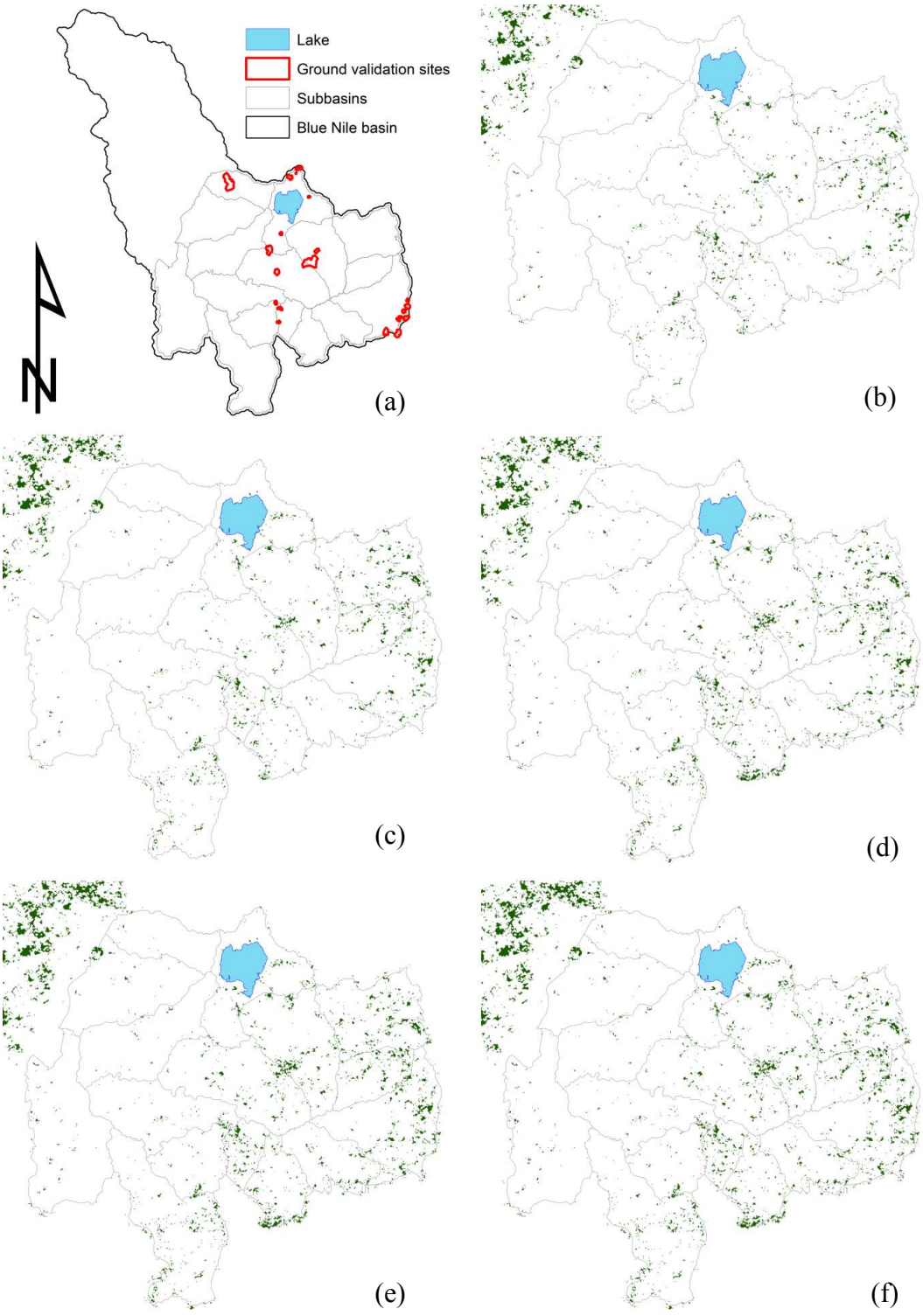

Figure 5-5: a) Sub basins (b – e) DI maps for 2008 – 2012, green areas are recovering areas; irrigated land adjacent to the Blue Nile River (Sudan) appears as a recovering area due to the year round high biomass availability due to adequate water supply and energy availability for photosynthesis

The five sub basins with largest biomass recovery are Muger, Dabus, Weleka, Dinder and Beles. The recovered areas represent 6 to 7% of the sub basins. Fincha, Wenbera, Tana, South Gojjam and Anger sub basins are least recovering with recovered areas of 3 to 4%. The total basin level biomass recovery is 2% as of 2012. The annual recovered area is in a declining trend in all the sub basins except Tana and North Gojjam sub basins. The positive trend in these two sub basins may be explained by the steady increase in irrigated land at Koga irrigation (Tana sub basin) scheme which expands to 6,000 ha towards the end of 2011 (Eguavoen and Tesfai, 2012). In North Gojjam sub basin a considerable expansion of commercial eucalyptus plantations have been observed during the field visit.

5.4.3 Comparison with ancillary data

Plantations initiated after the 1984 famine have become the dominant features of the Ethiopian highland landscapes. With a relatively longer protection the plantations survive deforestation except in the case of those plantations planned for fuel wood consumption. The plantation campaigns are aimed at dislodging farmers from steep slope areas and cover the land with plantation. In 80% of the field validation sites visited farmers responded that planning was not participatory. In all of these plantations community participated against their will and often times land for plantation is acquired by evicting farmers plowing the steep slopes. Bewket and Sterk (2002) reported similar observations. Recent SWC works had implemented a different approach in that the activities are undertaken as a community managed SWC projects. Even though the outcome of these conservation works cannot be seen on the DI analysis output as in the case of the large plantations undertaken by the previous government comparison of reported recovered area is found to be consistently identical with over all biomass recovery trend of the sub basins in which these projects are situated Figure 5-6.

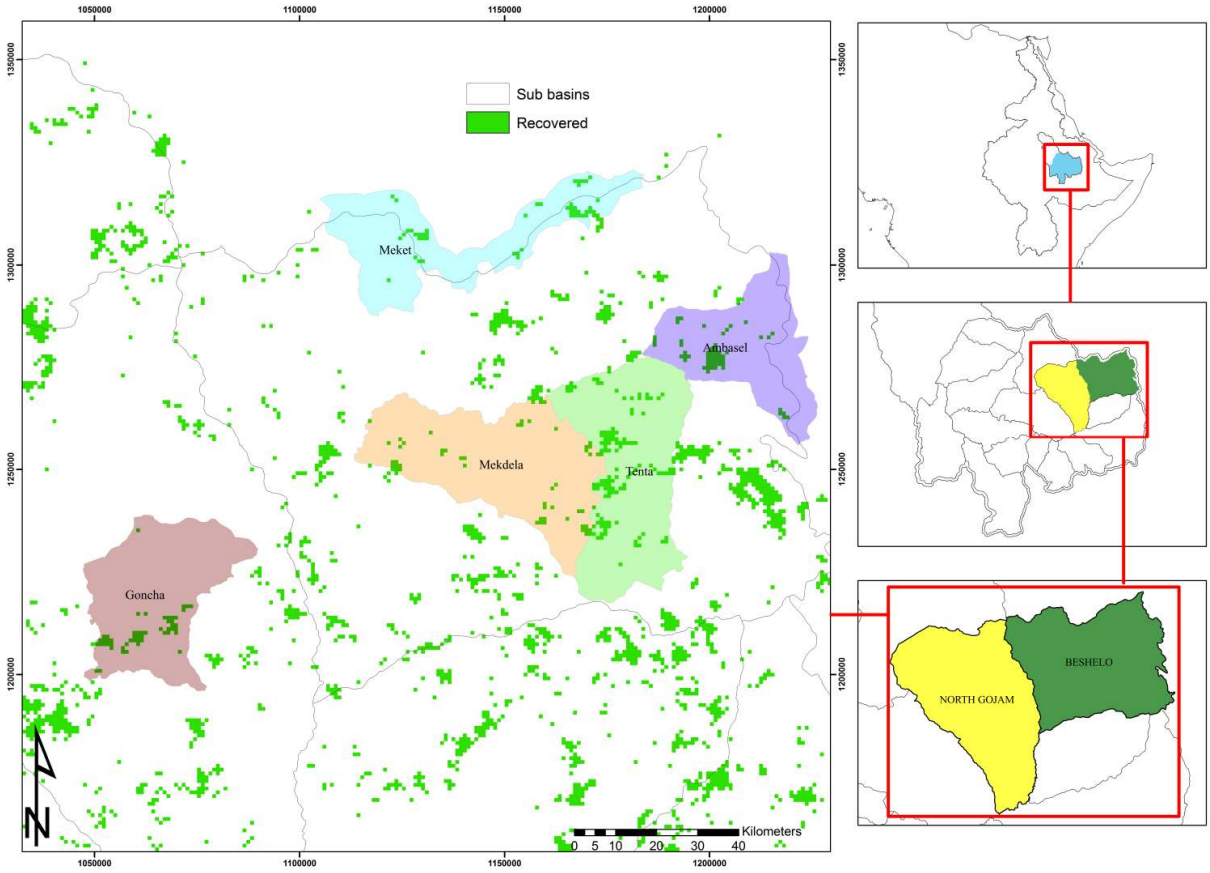

Figure 5-6: Biomass recovery trend in five community managed watersheds supported by MERET project since 2003 are compared with the biomass recovery trend in their respective sub basin with similar biomass recovery trajectories observed at both scales.

Recovered area statistics of five watersheds in two sub basins as recorded by WFP are compared with the DI maps for the sub basins where these watersheds are located. Four watersheds are in Meket, Tenta, Ambassel, and Mekdela provinces located within Beshelo sub basin and one watershed in Goncha province which is located in the North Gojjam sub basin (Figure 5-6). The total recovered area in these watersheds showed similar trend (Figure 5-7) to their respective sub basin. The low level of total recovered area in 2008 in the sub basins is identical to the total recovered area in the provinces.

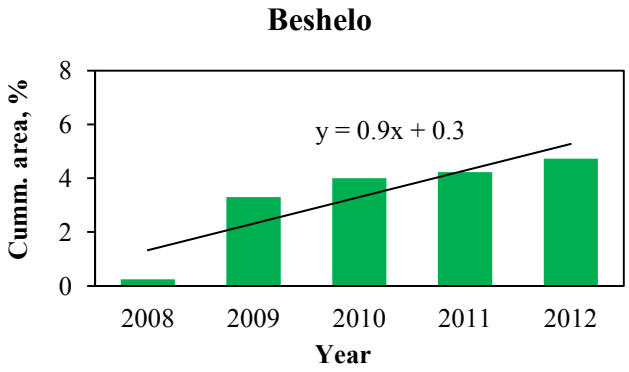
Beshelo
Cumm. area, %
y = 0.9x + 0.3
0
2
4
6
8
2008
2009
2010
2011
2012
Year

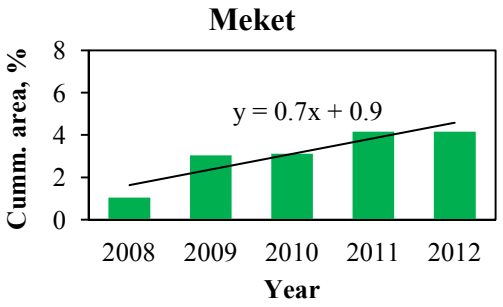
Meket
Cumm. area, %
y = 0.7x + 0.9
0
2
4
6
8
2008
2009
2010
2011
2012
Year

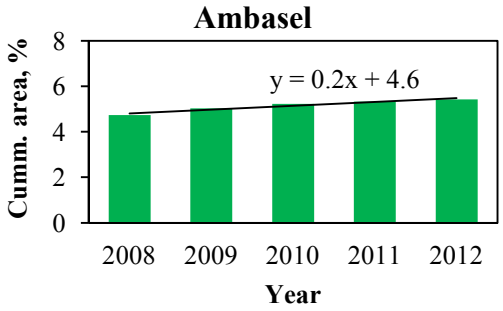
Ambasel
Cumm. area, %
y = 0.2x + 4.6
0
2
4
6
8
2008
2009
2010
2011
2012
Year

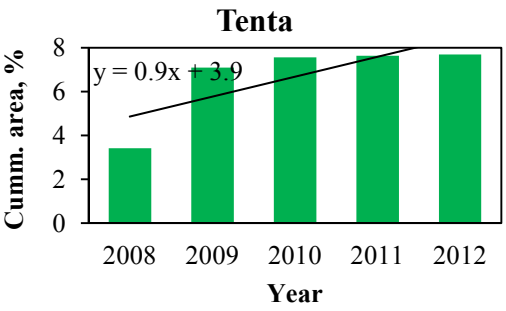
Tenta
Cumm. area, %
y = 0.9x + 3.9
0
2
4
6
8
2008
2009
2010
2011
2012
Year

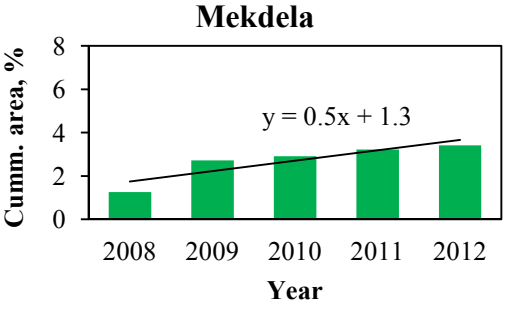
Mekdela
Cumm. area, %
y = 0.5x + 1.3
0
2
4
6
8
2008
2009
2010
2011
2012
Year

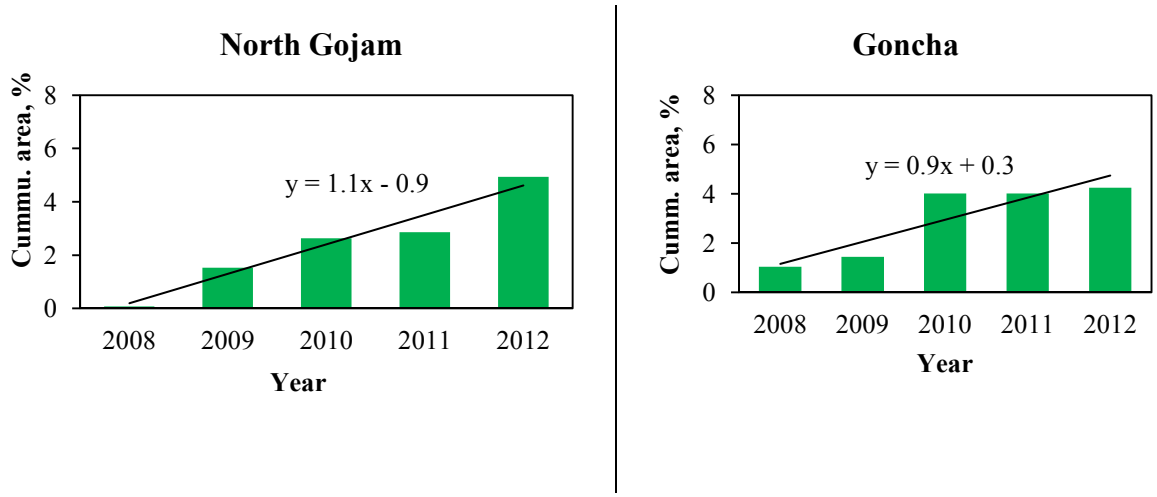

Figure 5-7: The trend in total recovered area of Beshelo and North Gojjam sub basins determined from the DI analysis was identical to the biomass recovery trend reported by community managed SWC trend in five community managed watersheds supported by MERET project since 2003 are compared with the biomass recovery trend in their respective sub basin with similar biomass recovery trajectories observed at both scales. The cumulative area is expressed as the percentage of the sub basin area.

5.5 Conclusion

Tracking state of biomass recovery trend is necessary step in evaluating the effectiveness of SWC measures. The DI tool was previously tested on continental US using two years of MODIS EVI and LST products (2003 – 2004). It was difficult to represent the range of natural variability using two years data. In this research ten years (2003 – 2012) data was used in applying the tool to monitor state of biomass in the Blue Nile River basin. As the result disturbance detection of ecosystems with high inter annual variability is improved and false disturbance detection are minimized. The DI maps can be also be easily updated with additional year of data. Nonetheless precaution should be made in interpreting the maps. With number of irrigation projects under implementation it is also important to note that inflated biomass recovery figures may result. The interpretation on the index should thus be further rectified by masking out irrigation land. The major limitation of the method is its shortfall in detecting small scale and

fragmented SWC works. This shortfall is attributed to the coarser resolution EVI and LST data availability. Such SWC works are typical in community managed watersheds and should be quantified in some way. Additional steps are required to apply the method for use in small scale SWC using finer resolution images.

The implementation strategy of the plantations determines their sustainability. The top-down approach in the past did not bring about significant results. Plantations are often associated with subsidence of the ground water level mainly manifested by drying up of local springs. The current community managed SWC approach is instrumental in uprooting past oversight and instate a participatory approach. The investment returns of the new approach are yet to be seen in the future. The cost – benefit analysis of investment on SWC should incorporate the change in soil composition, water availability, production of woody biomass, and crop and horticultural productivity. In this regard the DI can be applied as a typical tool to measure the production of woody biomass.

References

ADMASSIE, Y. 1998. *Twenty Years to Nowhere: Property Rights, Land Management & Conservation in Ethiopia*, Red Sea Press.

BEKELE, M. Ethiopia's environmental policies, strategies and program. 2008. 337-370.

BEWKET, W. & STERK, G. 2002. Farmers' participation in soil and water conservation activities in the Chemoga watershed, Blue Nile basin, Ethiopia. *Land Degradation & Development,* 13**,** 189-200.

CONSTABLE, M. & BELSHAW, D. The Ethiopian highlands reclamation study: Major findings and recommendations. 1986. 8-12.

COOPS, N. C., WULDER, M. A. & IWANICKA, D. 2009. Large area monitoring with a MODIS-based Disturbance Index (DI) sensitive to annual and seasonal variations. *Remote Sensing of Environment,* 113**,** 1250-1261.

EFAP 1994. Ethiopian forestry action program. Vol. II. The challenges for development. Addis Ababa: EFAP Secretariat.

EGUAVOEN, I. & TESFAI, W. 2012. Social impact and impoverishment risks of the Koga irrigation scheme, Blue Nile basin, Ethiopia. *Afrika Focus,* 25**,** 39-60.

EPA 1997. Environmental Policy. Addis Ababa: Environmental Protection Authority of FDRE.

ERKOSSA, T., AWULACHEW, S. B., HAILESLASSIE, A. & DENEKEW, A. 2009. Impacts of improving water management of smallholder agriculture in the Upper Blue Nile Basin. *Improved Water and Land Management in the Ethiopian Highlands: Its Impact on Downstream Stakeholders Dependent on the Blue Nile***,** 7.

FERREIRA, N., FERREIRA, L. & HUETE, A. 2010. Assessing the response of the MODIS vegetation indices to landscape disturbance in the forested areas of the legal Brazilian Amazon. *International Journal of Remote Sensing,* 31**,** 745-759.

FORZIERI, G., CASTELLI, F. & VIVONI, E. R. 2010. A Predictive Multidimensional Model for Vegetation Anomalies Derived From Remote-Sensing Observations. *Geoscience and Remote Sensing, IEEE Transactions on,* 48**,** 1729-1741.

FRIEDL, M., STRAHLER, A. & HODGES, J. 2010. ISLSCP II MODIS (Collection 4) IGBP Land Cover, 2000-2001. *ISLSCP Initiative II Collection. Data set. Available on-line [http://daac.ornl.gov/] from Oak Ridge National Laboratory Distributed Active Archive Center, Oak Ridge, Tennessee, USA doi,* 10.

GEBREHIWOT, S. G., ILSTEDT, U., GÄRDENÄS, A. & BISHOP, K. 2011. Hydrological characterization of watersheds in the Blue Nile Basin, Ethiopia.

GEBREMEDHIN, B., PENDER, J. & TESFAY, G. 2003. Community natural resource management: the case of woodlots in northern Ethiopia. *Environment and Development Economics,* 8**,** 129-148.

HAGOS, F., PENDER, J. & GEBRESELASSIE, N. 1999. *Land degradation in the highlands of Tigray and strategies for sustainable land management*, Livestock Policy Analysis Project, International Livestock Research Institute.

HAWANDO, T. 1997. Desertification in Ethiopian highlands. *Rala Report*.

HILL, J., STELLMES, M., UDELHOVEN, T., RÖDER, A. & SOMMER, S. 2008. Mediterranean desertification and land degradation: mapping related land use change syndromes based on satellite observations. *Global and Planetary Change,* 64**,** 146-157.

HUETE, A., DIDAN, K., MIURA, T., RODRIGUEZ, E. P., GAO, X. & FERREIRA, L. G. 2002. Overview of the radiometric and biophysical performance of the MODIS vegetation indices. *Remote Sensing of Environment,* 83**,** 195-213.

HUETE, A., JUSTICE, C. & LIU, H. 1994. Development of vegetation and soil indices for MODIS-EOS. *Remote Sensing of Environment,* 49**,** 224-234.

HUETE, A., LIU, H., BATCHILY, K. & VAN LEEUWEN, W. 1997. A comparison of vegetation indices over a global set of TM images for EOS-MODIS. *Remote Sensing of Environment,* 59**,** 440-451.

JAGGER, P. & PENDER, J. 2003. The role of trees for sustainable management of less-favored lands: the case of eucalyptus in Ethiopia. *Forest Policy and Economics,* 5**,** 83-95.

JIN, S. & SADER, S. A. 2005. MODIS time-series imagery for forest disturbance detection and quantification of patch size effects. *Remote Sensing of Environment,* 99**,** 462-470.

MICHENER, W. K. & HOUHOULIS, P. F. 1997. Detection of vegetation changes associated with extensive flooding in a forested ecosystem. *Photogrammetric engineering and remote sensing,* 63**,** 1363-1374.

MILDREXLER, D. J., ZHAO, M., HEINSCH, F. A. & RUNNING, S. W. 2007. A new satellite-based methodology for continental-scale disturbance detection. *Ecological Applications,* 17**,** 235-250.

MILDREXLER, D. J., ZHAO, M. & RUNNING, S. W. 2009. Testing a MODIS global disturbance index across North America. *Remote Sensing of Environment,* 113**,** 2103-2117.

NEDESSA, B. & WICKREMA, S. 2010. Disaster Risk Reduction: Experience from the MERET Project in Ethiopia. Available: http://documents.wfp.org/stellent/groups/public/documents/newsroom/wfp225961.pdf.

NEMANI, R. & RUNNING, S. 1997. Land cover characterization using multitemporal red, near-IR, and thermal-IR data from NOAA/AVHRR. *Ecological Applications,* 7**,** 79-90.

RUIZ, J. A. M. & GARBIN, M. C. 2004. Estimating burned area for Tropical Africa for the year 1990 with the NOAA-NASA Pathfinder AVHRR 8 km land dataset. *International Journal of Remote Sensing,* 25**,** 3389-3440.

RUNNING, S. W. 2008. Ecosystem disturbance, carbon, and climate. *Science,* 321**,** 652-653.

SHIFERAW, B. & HOLDEN, S. 1999. Soil erosion and smallholders' conservation decisions in the highlands of Ethiopia. *World Development,* 27**,** 739-752.

SPRUCE, J. P., SADER, S., RYAN, R. E., SMOOT, J., KUPER, P., ROSS, K., PRADOS, D., RUSSELL, J., GASSER, G. & MCKELLIP, R. 2010. Assessment of MODIS NDVI time series data products for detecting forest defoliation by gypsy moth outbreaks. *Remote Sensing of Environment*.

TAYE, M. T. & WILLEMS, P. 2012. Temporal variability of hydroclimatic extremes in the Blue Nile basin. *Water Resources Research,* 48**,** W03513.

TEBEBU, T., ABIY, A., ZEGEYE, A., DAHLKE, H., EASTON, Z., TILAHUN, S., COLLICK, A., KIDNAU, S., MOGES, S. & DADGARI, F. 2010. Surface and subsurface flow effect on permanent gully formation and upland erosion near Lake Tana in the Northern Highlands of Ethiopia. *Hydrology and Earth System Sciences,* 14**,** 2207-2217.

VAN LEEUWEN, W. J. D. 2008. Monitoring the effects of forest restoration treatments on post-fire vegetation recovery with MODIS multitemporal data. *Sensors,* 8**,** 2017-2042.

YILMA, A. D. & AWULACHEW, S. B. 2009. Blue Nile Basin Characterization and Geospatial Atlas. *Improved Water and Land Management in the Ethiopian Highlands: Its Impact on Downstream Stakeholders Dependent on the Blue Nile*, 6.

CHAPTER 6: CONCLUSION

6.1 Major findings

In this dissertation we investigate the possibility of using Moderate Resolution Imaging Spectroradiometer (MODIS) products for water resources management. We explore its use in measuring sediment concentrations in lakes, in determining lake surface area and in assessing the degree of degradation of the land surface in the Blue Nile Basin. In addition, we use a 10-year sediment data series inferred from MODIS imaginary to calibrate sediment predictions using the SWAT model. MODIS images provide the advantage of increased sensitivity, reduced data volume, near daily availability and easy retrieval. Consistent atmospheric correction is applied to MODIS images. This avoids the uncertainty due to the use of varying atmospheric correction algorithms applied by users.

In general MODIS images could represent the sediment concentration in Lake Tana well (based on the statistical measures) as long as the turbidity was greater than 60NTU. We found that total Dissolved Solids (TSS) and turbidity were linear functions of the NIR band and Secchi depth was exponentially related to the NIR.

Using the calibrated relationship of TSS and NIR in Lake Tana a 10 year historic record of sediment concentration was constructed. SWAT-VSA was used to simulate these concentrations. Since the sediment concentration in the lake was about 100 times lower than in the river 20 km upstream of the lake we concluded that channel erodibility and the sediment transport coefficients were the most significant in modeling the lake sediment concentrations.

Overall Nash–Sutcliff efficiencies were, in the range of 0.3 to 0.4 indicating that more research is needed in using watershed models in simulating the lake sediment concentration.

In exploring MODIS images application for water volume estimation, comparison was made between lake area estimate from MODIS images and that of the existing bathymetric map using lake level measurements as a validation parameter. We found that the MODIS estimates appeared to be more accurate than existing bathymetric survey. Traditional bathymetric maps extrapolate bottom elevations to the inaccessible shores without taking the near shore shelf of sediment deposition into consideration. A method is proposed to refine the near shore bathymetric survey with data obtained from simultaneous measurements of lake area (from MODIS) and lake level.

Applying the energy interaction based vegetation classification approach for quantifying land degradation at basin scale was found to be a promising tool that can be easily updated with additional years of data. Previous methods of determining biomass at river basin scale was traditionally done by applying classification algorithms to satellite images of selected time intervals (often a decade) that essentially is based on statistical inference. This dissertation research showed that energy interaction fundamentals based vegetation classification is more realistic than statistical aggregations.

6.2 Sources of uncertainty

Like any other physical measurements satellite data are not immune from uncertainties. These uncertainties may arise from sensor degradation, change in atmospheric correction algorithm or combinations of these. As the satellites age sensors onboard also gets degraded (Wang et al., 2012). Most of the time sensor degradation effects are eliminated by adjusting the image

production process as new version of a data begins to be released. For example present studies show that the sensor degradation in MODIS had resulted a 0.001 – 0.004 Yr-1 decline in NDVI (Wang et al., 2012). Other uncertainties may originate from the object being imaged. Reflectance characteristic of water for example is very complex that established regression equations may quickly become obsolete. This necessitates planning of a sampling routine for regular updating of the equations.

6.3 Future prospects for using satellite imagery in water resources monitoring

Some of the data collection missions in line for launch include Global Precipitation measurement (GPM[7]), Soil Moisture Active Passive (SMAP[8]), Surface Water Ocean Topography (SWOT[9]), Cold Regions Hydrology High-resolution Observatory ($CoReH_2O$) and Gravity Recovery and Climate Experiment (GRACE II[10]). GPM mission is an international network of satellites that provide global observations of rain and snow. With its capability to measure light rain and falling snow (< 0.5 mm hr-1) in middle and high latitudes GPM provides further improvement over the existing Tropical Rainfall Measuring Mission (TRMM). SMAP will provide global soil moisture measurements which will be used to study processes that link the water, energy and carbon cycles. SWOT mission is designed to cover the world's ocean and freshwater bodies with repeated high resolution elevation measurements giving observation in water volumes in rivers lakes and wetlands. $CoReH_2O$ is intended to improve modeling and prediction of water balance and streamflow in snow and glacier covered basins, water and energy cycles at high latitudes

[7] http://pmm.nasa.gov/GPM
[8] http://smap.jpl.nasa.gov/mission/
[9] http://swot.jpl.nasa.gov/mission/
[10] http://www.csr.utexas.edu/grace/

through high resolution observations of freshwater stored as snow (Rott et al., 2010). GRACE II has become instrumental to model the relative amount of water stored near the surface and underground by detecting changes in Earth's gravity. With these missions the use of remotely sensed data in water resources modeling will ever expand and consequently present shortcomings in spatial, temporal, spectral and radiometric resolutions will also improve. However uncertainties in using image derived data in hydrologic modeling should be addressed in further detail.

References

ROTT, H., YUEH, S. H., CLINE, D. W., DUGUAY, C., ESSERY, R., HAAS, C., HÉLIÈRE, F., KERN, M., MACELLONI, G. & MALNES, E. 2010. Cold regions hydrology high-resolution observatory for snow and cold land processes. *Proceedings of the IEEE,* 98**,** 752-765.

WANG, D., MORTON, D., MASEK, J., WU, A., NAGOL, J., XIONG, X., LEVY, R., VERMOTE, E. & WOLFE, R. 2012. Impact of sensor degradation on the MODIS NDVI time series. Remote Sensing of Environment, 119, 55-61.

APPENDIX A: CHAPTER TWO

Appendix A1:

Table A1- 1: Calibration data sets for Total suspended solids[11]

November 27, 2010				
X	Y	Reflectance (NIR band)	Reflectance (Red band)	TSS (mg/l)
334536	1316787	0.0549	0.0784	70
334561	1317015	0.0357	0.0849	10
335226	1317558	0.1036	0.0811	180
335584	1317525	0.0313	0.0954	10
335995	1317248	0.1016	0.0862	150
336406	1316922	0.0320	0.1006	20
337127	1316783	0.0483	0.0990	50
337762	1316817	0.1130	0.1057	240
338095	1316887	0.0344	0.1042	20
338337	1316846	0.0391	0.1022	30
338462	1316507	0.0391	0.1022	30
338805	1316212	0.0402	0.1001	50
339114	1316332	0.0428	0.0988	60
339599	1316484	0.0444	0.0943	70
340062	1316838	0.0559	0.0988	70
340534	1317310	0.0868	0.1065	135
340739	1317836	0.0361	0.1032	20
341261	1318446	0.0419	0.1029	30
341568	1318966	0.0385	0.1053	20
341851	1319554	0.0477	0.1068	40
341996	1319909	0.0418	0.1070	40
342471	1321109	0.0372	0.1070	20
342639	1321877	0.0336	0.1083	10
342792	1322846	0.0352	0.1083	20
342799	1323557	0.0331	0.1089	10
342795	1324309	0.0318	0.1082	10
342702	1325102	0.0329	0.1071	10
342513	1326048	0.0283	0.1051	10

[11] Only measured values used in the calibration are provided

342476	1326931	0.0532	0.1001	60
343074	1326921	0.0712	0.1041	90
343904	1327079	0.0373	0.1089	20
344508	1327741	0.0360	0.1093	30
345436	1328420	0.0816	0.0810	130
345763	1328889	0.0664	0.0942	100
346170	1329836	0.0405	0.1108	40
346324	1330338	0.0420	0.1132	30
346316	1331065	0.0397	0.1125	30
346321	1330771	0.0397	0.1125	30
346309	1331068	0.0397	0.1125	40
346626	1331894	0.0376	0.1124	30
347278	1332416	0.0379	0.1112	20
347732	1333217	0.0421	0.1134	40
348046	1333851	0.0453	0.1104	50
348325	1334519	0.0686	0.0941	100
348406	1335158	0.0480	0.1160	40
May 13, 2011				
336656	1319735	0.0335	0.151	10
334851	1317479	0.0306	0.1403	10
334597	1316916	0.0328	0.1378	30
341834	1325582	0.0396	0.155	30
338290	1321686	0.0393	0.1508	30
340075	1323579	0.0433	0.1501	30
345055	1329060	0.0485	0.1356	40
345670	1330293	0.0454	0.1376	50
346800	1331547	0.0528	0.1288	70

Table A1- 2: Validation data set for Total suspended solids (collected on November 7, 2011)

X	Y	Reflectance (NIR band)	Measured TSS (mg/l)	Predicted TSS (mg/l)
333323	1310045	0.0312	11	10
334967	1317882	0.0323	14	20
336337	1317934	0.0327	15	20
333819	1309893	0.0330	15	20
338854	1318653	0.033	15	10
334465	1309575	0.0335	17	30
335705	1317983	0.0336	17	30
335231	1309332	0.0337	17	30
336743	1310684	0.0357	22	30
336760	1311043	0.0374	26	40
336627	1311377	0.0374	26	40
336300	1312007	0.0387	29	40
335927	1312517	0.0390	30	50
334576	1317780	0.0391	30	40
338322	1317789	0.0393	30	50

Table A1- 3: Calibration data sets for turbidity

November 27, 2010				
X	Y	Reflectance (NIR band)	Reflectance (Red band)	Turbidity (NTU)
334561	1317015	0.0357	0.0849	73.9
335226	1317558	0.1036	0.0811	307.5
338095	1316887	0.0344	0.1042	68.0
338462	1316507	0.0391	0.1022	81.0
338805	1316212	0.0402	0.1001	83.0
340062	1316838	0.0559	0.0988	97.0
340534	1317310	0.0868	0.1065	274.0
341261	1318446	0.0419	0.1029	88.1
341568	1318966	0.0385	0.1053	74.7
341851	1319554	0.0477	0.1068	98.0
341996	1319909	0.0418	0.1070	85.0
342476	1326931	0.0532	0.1001	104.7
343074	1326921	0.0712	0.1041	194.6
343904	1327079	0.0373	0.1089	61.4
345436	1328420	0.0816	0.0810	172.0
345763	1328889	0.0664	0.0942	176.2
346170	1329836	0.0405	0.1108	84.7
346324	1330338	0.0420	0.1132	88.4
346316	1331065	0.0397	0.1125	69.0
346321	1330771	0.0397	0.1125	65.0
346309	1331068	0.0397	0.1125	84.3
346626	1331894	0.0376	0.1124	64.0
347278	1332416	0.0379	0.1112	61.0
347732	1333217	0.0421	0.1134	73.0
348046	1333851	0.0453	0.1104	71.0
348325	1334519	0.0686	0.0941	119.4
348406	1335158	0.0480	0.1160	79.4
May 13, 2011				
337712	1321032	0.0344	0.1522	67.0
336270	1319358	0.0332	0.1522	67.5
337264	1320423	0.0326	0.1532	67.9
336656	1319735	0.0335	0.1510	69.8
334597	1316916	0.0328	0.1378	74.0
341834	1325582	0.0396	0.1550	79.4

338290	1321686	0.0381	0.1525	80.6
338822	1322264	0.0397	0.1528	81.7
340967	1324634	0.0409	0.1541	84.4
339207	1322669	0.0400	0.1528	87.6
342467	1326670	0.0419	0.1517	88.6
340075	1323579	0.0446	0.1512	93.2
345055	1329060	0.0460	0.1393	96.2
345670	1330293	0.0454	0.1376	98.1
346305	1331291	0.0494	0.1317	106.0
343545	1327333	0.0508	0.1357	119.0
346800	1331547	0.0528	0.1288	120.0
344312	1328096	0.0531	0.1320	122.0

Table A1- 4: Validation data set for turbidity (collected on November 7, 2011)

X	Y	Reflectance (NIR band)	Measured Turbidity (NTU)	Predicted Turbidity (NTU)
331468	1309487	0.0297	45.2	56.4
334990	1314511	0.0299	45.8	58
332765	1309988	0.0300	46.2	57
331785	1309755	0.0302	46.8	59
333323	1310045	0.0312	50.0	63
334967	1317882	0.0323	53.5	67
336337	1317934	0.0327	54.8	64
333819	1309893	0.0330	55.8	64
338854	1318653	0.033	55.8	67
334465	1309575	0.0335	57.4	63
335705	1317983	0.0336	57.7	71
335231	1309332	0.0337	58.0	69.8
336743	1310684	0.0357	64.5	72.6
336627	1311377	0.0374	69.9	76
336760	1311043	0.0374	69.9	73
336300	1312007	0.0387	74.1	77.2
335927	1312517	0.0390	75.0	75
334576	1317780	0.0391	75.4	76
338322	1317789	0.0393	76.0	81

Table A1- 5: Calibration data sets for Secchi depth

November 27, 2010				
X	Y	Reflectance (NIR band)	Reflectance (Red band)	Secchi depth (m)
348046	1333851	0.1479	0.1104	0.08
346626	1331894	0.1036	0.1124	0.1
346316	1331065	0.0712	0.1125	0.12
346321	1330771	0.0816	0.1125	0.12
346309	1331068	0.1016	0.1125	0.12
347732	1333217	0.1130	0.1134	0.12
346324	1330338	0.0686	0.1132	0.14
335120	1314836	0.0868	0.0702	0.14
347278	1332416	0.1036	0.1112	0.14
345436	1328420	0.0549	0.0810	0.17
346170	1329836	0.0664	0.1108	0.17
344985	1327826	0.0532	0.0823	0.18
342513	1326048	0.0444	0.1051	0.19
342245	1326526	0.0453	0.1055	0.19
343904	1327079	0.0477	0.1089	0.19
344131	1327440	0.0480	0.1076	0.19
345763	1328889	0.0559	0.0942	0.19
343074	1326921	0.0465	0.1041	0.2
338462	1316507	0.0372	0.1022	0.21
341851	1319554	0.0397	0.1068	0.21
342234	1320410	0.0402	0.1064	0.21
342639	1321877	0.0418	0.1083	0.21
342795	1324309	0.0421	0.1082	0.21
342476	1326931	0.0460	0.1001	0.21
344508	1327741	0.0483	0.1093	0.21
340534	1317310	0.0385	0.1065	0.22
340062	1316838	0.0379	0.0988	0.24
341261	1318446	0.0391	0.1029	0.24
341568	1318966	0.0397	0.1053	0.24
341996	1319909	0.0397	0.1070	0.24
342792	1322846	0.0419	0.1083	0.24
342702	1325102	0.0428	0.1071	0.24
339599	1316484	0.0376	0.0943	0.25
336406	1316922	0.0344	0.1006	0.27

338095	1316887	0.0360	0.1042	0.27
339114	1316332	0.0376	0.0988	0.27
342471	1321109	0.0405	0.1070	0.27
342799	1323557	0.0420	0.1089	0.27
335995	1317248	0.0342	0.0862	0.29
338337	1316846	0.0361	0.1022	0.29
340739	1317836	0.0391	0.1032	0.29
334536	1316787	0.0318	0.0784	0.3
334561	1317015	0.0320	0.0849	0.3
337762	1316817	0.0357	0.1057	0.3
334839	1316255	0.0313	0.0653	0.31
335226	1317558	0.0331	0.0811	0.31
337127	1316783	0.0352	0.0990	0.31
338805	1316212	0.0373	0.1001	0.31
334889	1317431	0.0329	0.0811	0.32
335584	1317525	0.0336	0.0954	0.32
334717	1315785	0.0283	0.0679	0.34
May 13, 2011				
346800	1331547	0.0528	0.1288	0.145
343545	1327333	0.0508	0.1357	0.160
344312	1328096	0.0531	0.1320	0.160
345670	1330293	0.0454	0.1376	0.170
339207	1322669	0.0400	0.1528	0.175
342467	1326670	0.0419	0.1517	0.175
340075	1323579	0.0446	0.1512	0.180
346305	1331291	0.0494	0.1317	0.180
345055	1329060	0.0460	0.1393	0.190
340967	1324634	0.0409	0.1541	0.200
334597	1316916	0.0328	0.1378	0.205
338290	1321686	0.0381	0.1525	0.205
338822	1322264	0.0397	0.1528	0.205
341834	1325582	0.0396	0.1550	0.215
337264	1320423	0.0326	0.1532	0.225
336270	1319358	0.0332	0.1522	0.240
337712	1321032	0.0344	0.1522	0.245
333896	1313483	0.0314	0.1461	0.285
334157	1314120	0.0312	0.1461	0.290
333062	1311931	0.0331	0.1634	0.320
333576	1312922	0.0313	0.1563	0.335
333277	1312361	0.0309	0.1572	0.340

Table A1- 6: Validation data set for Secchi depth (collected on November 7, 2011)

X	Y	Reflectance (NIR band)	Measured Secchi depth (m)	Predicted Secchi depth (m)
331785	1309755	0.0302	0.26	0.24
332765	1309988	0.0300	0.26	0.27
333323	1310045	0.0312	0.26	0.24
333819	1309893	0.0330	0.25	0.23
334224	1316705	0.0029	0.37	0.35
334364	1317572	0.0058	0.35	0.32
334465	1309575	0.0335	0.25	0.27
334576	1317780	0.0391	0.24	0.27
334725	1315693	0.0040	0.36	0.34
334788	1316112	0.0048	0.36	0.3
334894	1313555	0.0014	0.37	0.34
334967	1317882	0.0323	0.26	0.27
334990	1314511	0.0299	0.26	0.24
335052	1314899	0.0007	0.38	0.35
335178	1313195	0.0005	0.38	0.35
335231	1309332	0.0337	0.25	0.27
335583	1312923	0.0029	0.37	0.35
335705	1317983	0.0336	0.25	0.26
335927	1312517	0.0390	0.24	0.21
336300	1312007	0.0387	0.24	0.21
336337	1317934	0.0327	0.25	0.26
336585	1309267	0.0027	0.37	0.36
336627	1311377	0.0374	0.24	0.21
336743	1310684	0.0357	0.25	0.27
336760	1311043	0.0374	0.24	0.23
337388	1317525	0.0003	0.38	0.34
338322	1317789	0.0393	0.24	0.27
338854	1318653	0.033	0.25	0.27
339162	1320012	0.0023	0.37	0.36

APPENDIX B: CHAPTER THREE

Appendix B1:

Figure B1- 1: Topography (top) and soil topographic index (bottom) maps

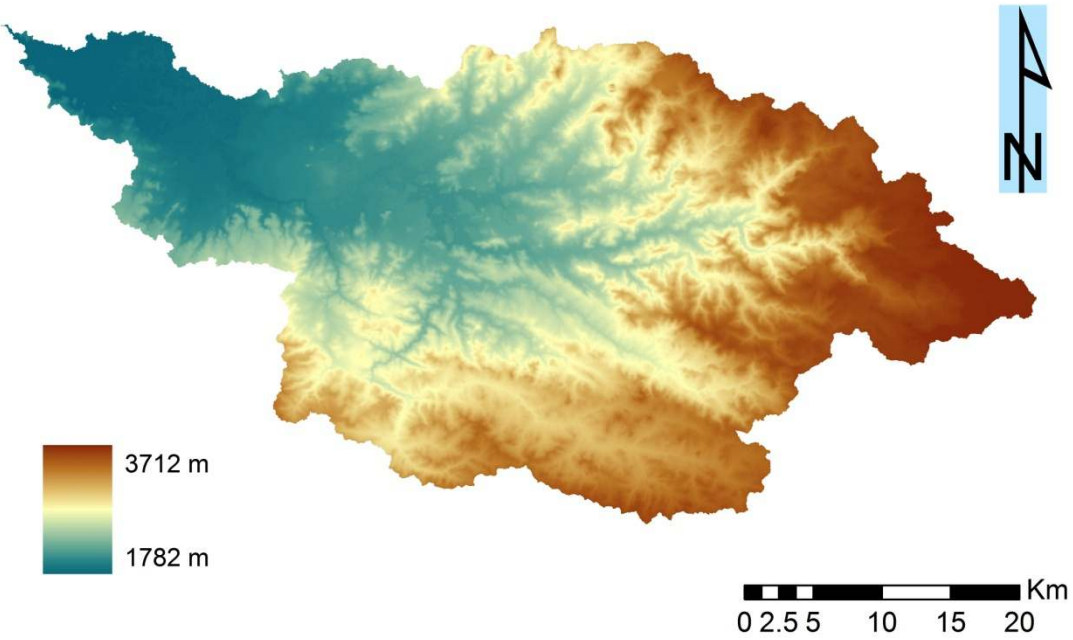

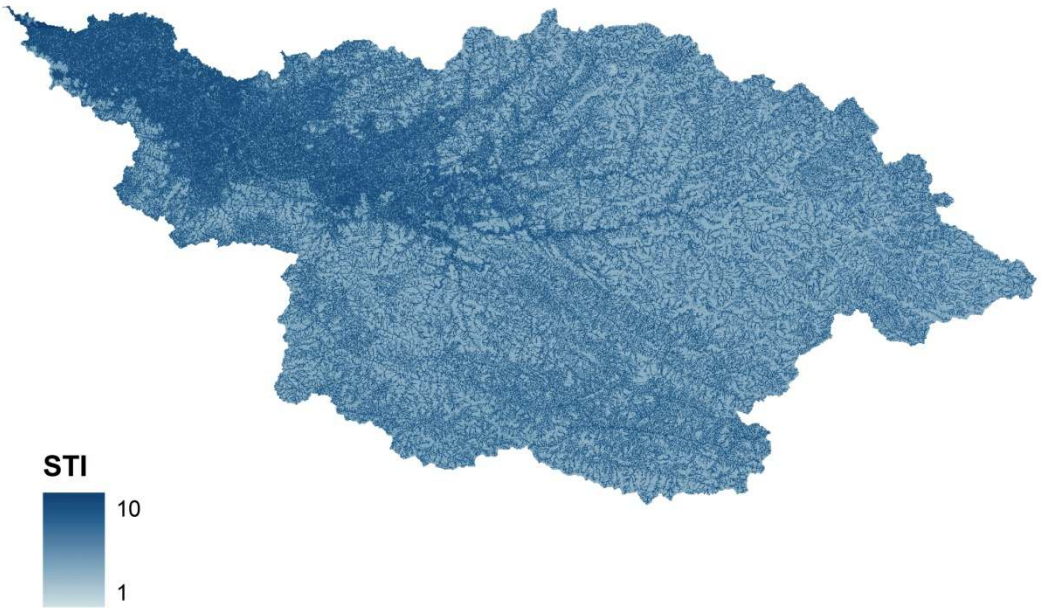

Figure B1- 2: HRUs (top) and land use (bottom)

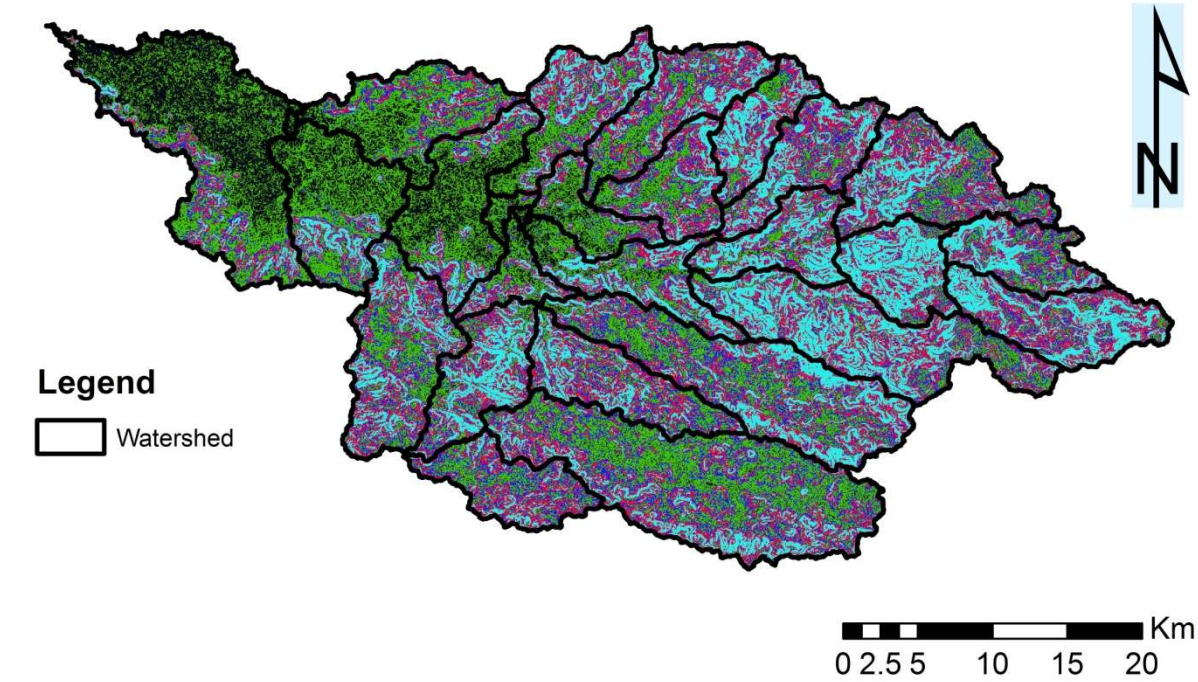

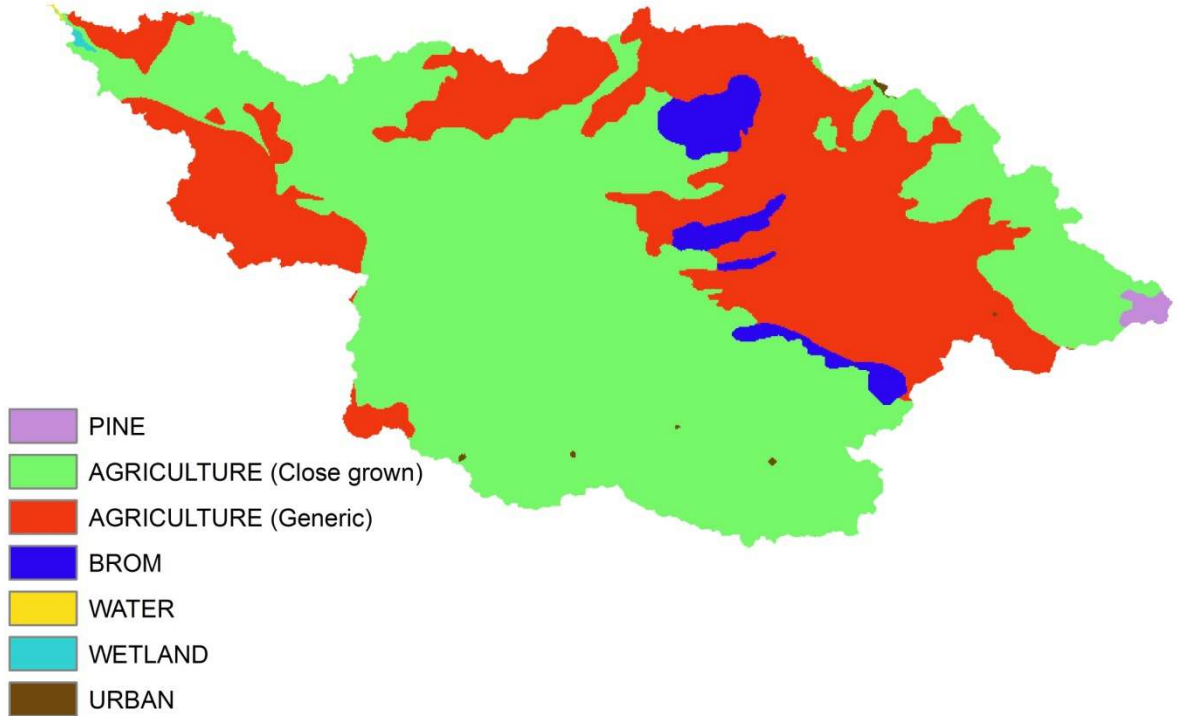

Table B1- 1: TSS time series used in SWAT-VSA model

	Month	Flow (m^3/s)	TSS (mg/l) from MODIS images
Warm−up period	Jan-00	4.38	173.6
	Feb-00	2.74	197.41
	Mar-00	1.89	238.12
	Apr-00	2.66	97.98
	May-00	1.87	112.3
	Jun-00	13.36	107.44
	Jul-00	107.51	204.06
	Aug-00	172.2	207.96
	Sep-00	53.66	178.96
	Oct-00	48.08	88.27
	Nov-00	13.2	55.04
	Dec-00	5.43	45.13
Calibration period	Jan-01	3.26	62.64
	Feb-01	2.02	62.21
	Mar-01	1.8	168.92
	Apr-01	1.38	154.26
	May-01	1.88	152.98
	Jun-01	14.65	143.99
	Jul-01	92.67	300.97
	Aug-01	137.8	244.05
	Sep-01	57.89	195.95
	Oct-01	14.11	151.93
	Nov-01	6.14	146.95
	Dec-01	3.83	101.11
	Jan-02	2.92	122.17
	Feb-02	2.11	83.66
	Mar-02	2.07	215.99
	Apr-02	1.79	190.84
	May-02	1.24	203.63
	Jun-02	23.79	390.03
	Jul-02	91.69	478.87
	Aug-02	155.66	632.06
	Sep-02	80.29	364.23
	Oct-02	12.73	191.90
	Nov-02	7.06	76.07

	Dec-02	5.36	47.89
	Jan-03	3.98	56.14
	Feb-03	3.24	57.11
	Mar-03	3.29	132.81
	Apr-03	2.48	159.65
	May-03	2.35	149.18
	Jun-03	14.48	387.01
	Jul-03	89.95	916.65
	Aug-03	174.63	916.37
	Sep-03	156.33	569.09
	Oct-03	46.86	335.56
	Nov-03	8.29	300.13
	Dec-03	5.3	300.04
	Jan-04	3.81	261.60
	Feb-04	3.24	352.12
	Mar-04	2.66	252.61
	Apr-04	3.09	548.35
	May-04	2.49	496.42
	Jun-04	9.46	775.54
	Jul-04	77.13	607.80
	Aug-04	104.72	1051.45
	Sep-04	52.67	412.95
	Oct-04	20.53	392.65
	Nov-04	8.19	331.00
	Dec-04	5.45	286.51
	Jan-05	4.02	217.60
	Feb-05	3.3	187.48
	Mar-05	3.63	312.42
	Apr-05	2.63	364.98
	May-05	3.45	316.94
	Jun-05	13.93	431.79
	Jul-05	75.3	498.97
	Aug-05	119.49	704.49
	Sep-05	129.77	325.74
	Oct-05	40.01	260.64
	Nov-05	9.04	248.33
	Dec-05	5.88	193.37
	Jan-06	4.28	207.38
	Feb-06	3.49	266.87

	Mar-06	3.32	280.87
	Apr-06	3.28	346.97
	May-06	6.59	437.56
	Jun-06	17.34	444.13
	Jul-06	88.99	532.00
	Aug-06	213.63	259.82
	Sep-06	142.39	247.06
	Oct-06	24.36	246.75
	Nov-06	9.52	234.88
	Dec-06	5.79	258.91
Calibration period	Jan-07	4.05	230.49
	Feb-07	2.84	195.27
	Mar-07	2.48	222.56
	Apr-07	2.2	304.98
	May-07	3.6	493.01
	Jun-07	44.2	440.63
	Jul-07	114.49	386.07
	Aug-07	145.94	285.02
	Sep-07	169.87	292.91
	Oct-07	29.86	247.09
	Nov-07	10.79	139.96
	Dec-07	7.53	147.86
	Jan-08	4.38	164.10
	Feb-08	2.74	236.80
	Mar-08	2.41	292.33
	Apr-08	4.74	411.15
	May-08	6.62	492.72
	Jun-08	39.1	582.58
	Jul-08	158.11	472.24
	Aug-08	229.45	328.16
	Sep-08	106.92	350.37
	Oct-08	13.75	231.19
	Nov-08	13.36	187.56
	Dec-08	7.53	246.61
	Jan-09	4.38	178.61
	Feb-09	2.84	233.09
	Mar-09	2.48	237.95
	Apr-09	2.2	252.17
	May-09	3.21	377.48

	Jun-09	4.4	406.49
	Jul-09	108.32	339.61
	Aug-09	204.92	473.76
	Sep-09	87.44	439.72
	Oct-09	23.63	250.56
	Nov-09	13.8	220.66
	Dec-09	7.53	239.02

Table B1- 2: Output of sensitivity analysis in SWAT

Parameter	Rank	Mean
Ch_N2	1	4.130
Spcon	2	3.720
Cn2	3	2.780
Alpha_Bf	4	1.700
Spexp	5	0.949
Usle_P	6	0.425
Esco	7	0.393
Ch_K2	8	0.324
Surlag	9	0.226
Sol_Awc	11	0.133
Sol_K	13	0.098
Gwqmn	14	0.087
Canmx	15	0.074
Gw_Delay	18	0.042
Revapmn	19	0.022
Epco	20	0.018
Gw_Revap	21	0.015
Sol_Alb	22	0.013
Ch_Cov	33	0.000
Ch_Erod	33	0.000

Table B1- 3: SWAT calibration parameters (Arnold et al., 2007)

Parameter	**Explanation**
Flow	
CN2	Moisture condition II curve number
ALPHA_BF	Base flow recession constant
GW_DELAY	Delay time for aquifer recharge
GWQMN	Threshold water level in shallow aquifer for base flow
GW_REVAP	Groundwater re-evaporation coefficient
ESCO	Soil evaporation compensation coefficient
EPCO	Plant uptake compensation factor
CH_N2	Manning's n for main channel
CH_K2	Effective hydraulic conductivity of channel (mm/hr)
SOL_AWC	Available water capacity (mm)
SOL_K	Saturated hydraulic conductivity (mm/hr)
SOL_ALB	Moist soil albedo
CANMX	Maximum canopy storage
REVAPMN	Threshold water level in shallow aquifer for base flow (mm)
SURLAG	Surface runoff lag coefficient
USLE_C	Minimum value for the cover and management factor for the land cover
Sediment	
SPCON	Coefficient in sediment transport coefficient
SPEXP	Exponent in sediment transport equation
CH_COV	Channel cover factor
USLE_P	USLE support practice factor
CH_EROD	Channel erodibility factor (cm/hr/Pa)

APPENDIX C: CHAPTER FOUR

Appendix C1:

Table C1- 1: Comparison of lake area estimates using MODIS NDVI (250m) and Storage characteristic curve

Date	Lake water Level (MoWE)	Lake area from MODIS NDVI (250m)	Lake area from Storage Characteristics curve
10-Sep-00	1787.52	3025	3086
16-Sep-00	1787.58	3037	3091
17-Sep-01	1787.46	3036	3082
20-Sep-01	1787.46	3015	3082
21-Sep-01	1787.50	3010	3085
22-Sep-01	1787.47	3032	3083
22-Sep-02	1786.41	3004	3001
24-Sep-02	1786.42	2962	3002
10-Jun-03	1784.32	2946	2822
12-Jun-03	1784.40	2944	2830
26-Sep-03	1786.62	2982	3017
28-Sep-03	1786.64	3003	3019
9-Jun-04	1784.89	2973	2873
4-Oct-04	1786.50	3003	3008
7-Oct-05	1786.54	3011	3011
10-Oct-05	1786.53	2995	3010
15-Jun-06	1784.88	2921	2872
16-Jun-06	1784.87	2950	2872

Table C1- 2: Comparison of lake area estimates using MODIS NDVI (500m) and Storage characteristic curve

Date	Lake water Level (MoWE)	Lake area from MODIS NDVI (500m)	Lake area from Storage Characteristics curve
10-Sep-00	1787.52	3004	3087
16-Sep-00	1787.58	3016	3091
17-Sep-01	1787.46	3024	3082
20-Sep-01	1787.46	2983	3082
21-Sep-01	1787.50	2986	3085
22-Sep-01	1787.47	3008	3083
22-Sep-02	1786.41	2973	3001
24-Sep-02	1786.42	2924	3002
10-Jun-03	1784.32	2940	2822
12-Jun-03	1784.40	2940	2830
26-Sep-03	1786.62	2942	3017
28-Sep-03	1786.64	2981	3019
9-Jun-04	1784.89	2956	2873
4-Oct-04	1786.50	2981	3008
7-Oct-05	1786.54	2986	3011
10-Oct-05	1786.53	2966	3010
15-Jun-06	1784.88	2897	2873
16-Jun-06	1784.87	2928	2872

Table C1- 3: Comparison of lake area estimates using MODIS ENDWI (250m) and Storage characteristic curve

Date	Lake water Level (MoWE)	Lake area from MODIS ENDWI (250m)	Lake area from Storage Characteristics curve
10-Sep-00	1787.52	3025	3087
16-Sep-00	1787.58	3037	3091
17-Sep-01	1787.46	3036	3082
20-Sep-01	1787.46	3015	3082
21-Sep-01	1787.50	3010	3085
22-Sep-01	1787.47	3032	3083
22-Sep-02	1786.41	3010	3001
24-Sep-02	1786.42	2962	3002
10-Jun-03	1784.32	2946	2822
12-Jun-03	1784.40	2944	2830
26-Sep-03	1786.62	2982	3017
28-Sep-03	1786.64	3003	3019
9-Jun-04	1784.89	2962	2873
4-Oct-04	1786.50	3002	3008
7-Oct-05	1786.54	3011	3011
10-Oct-05	1786.53	2995	3010
15-Jun-06	1784.88	2921	2873
16-Jun-06	1784.87	2950	2872

Table C1- 4: Comparison of lake area estimates using MODIS ENDWI (500m) and Storage characteristic curve

Date	Lake water Level (MoWE)	Lake area from MODIS ENDWI (500m)	Lake area from Storage Characteristics curve
10-Sep-00	1787.52	3004	3087
16-Sep-00	1787.58	3016	3091
17-Sep-01	1787.46	3024	3082
20-Sep-01	1787.46	2983	3082
21-Sep-01	1787.50	2986	3085
22-Sep-01	1787.47	3010	3083
22-Sep-02	1786.41	2978	3001
24-Sep-02	1786.42	2931	3002
10-Jun-03	1784.32	2940	2822
12-Jun-03	1784.40	2940	2830
26-Sep-03	1786.62	2980	3017
28-Sep-03	1786.64	2980	3019
9-Jun-04	1784.89	2956	2873
4-Oct-04	1786.50	2980	3008
7-Oct-05	1786.54	2986	3011
10-Oct-05	1786.53	2966	3010
15-Jun-06	1784.88	2897	2873
16-Jun-06	1784.87	2928	2872

APPENDIX D: CHAPTER FIVE

Appendix D1:

Figure D1- 1: Biomass recovery on year by year basis

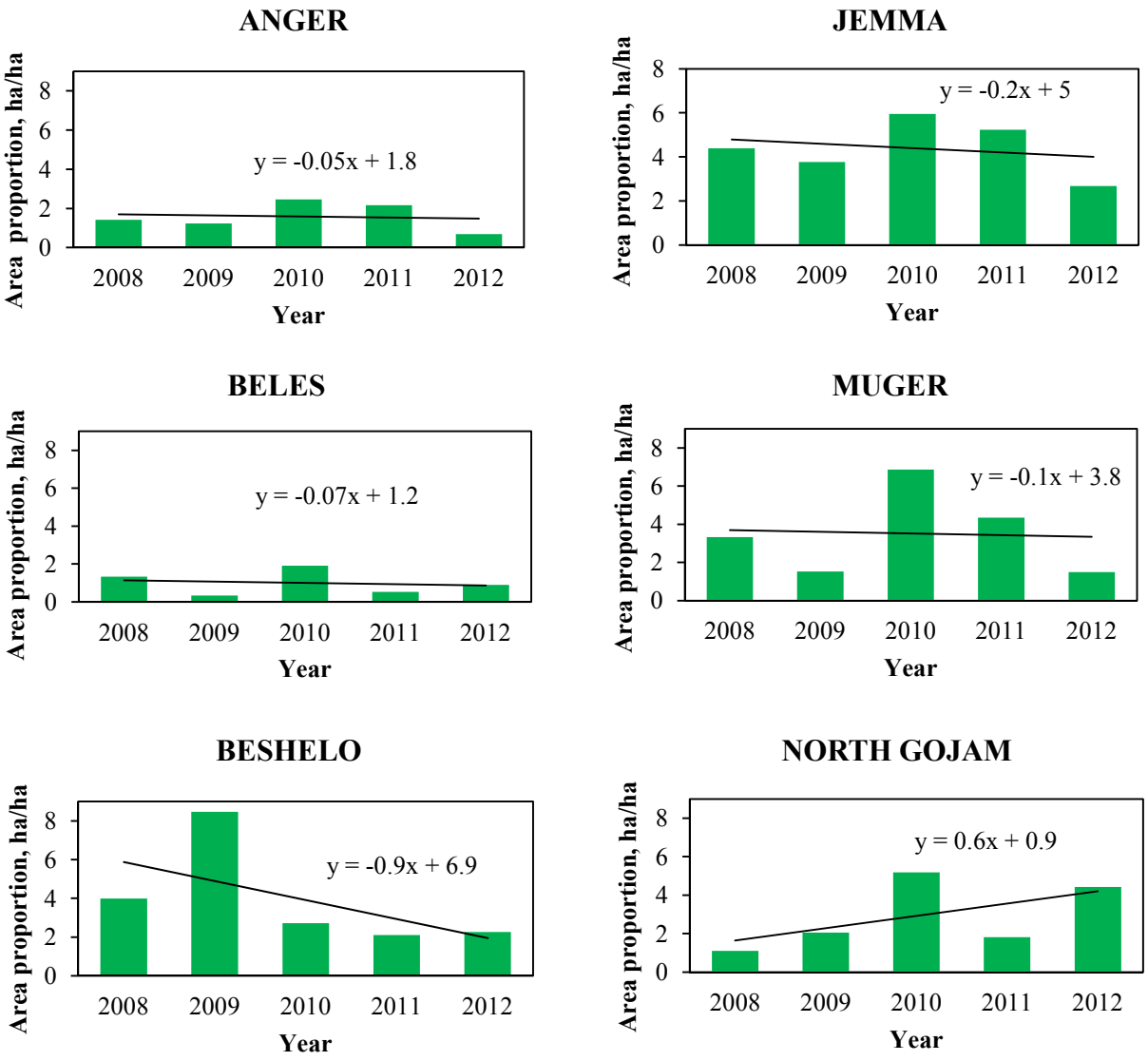

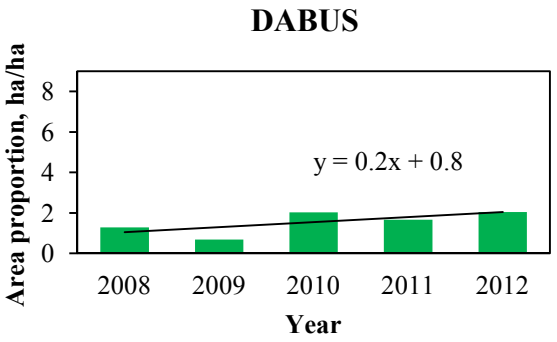
DABUS
Area proportion, ha/ha
y = 0.2x + 0.8
0
2
4
6
8
2008
2009
2010
2011
2012
Year

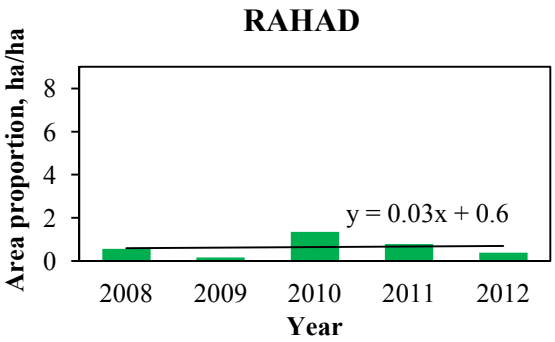
RAHAD
Area proportion, ha/ha
y = 0.03x + 0.6
0
2
4
6
8
2008
2009
2010
2011
2012
Year

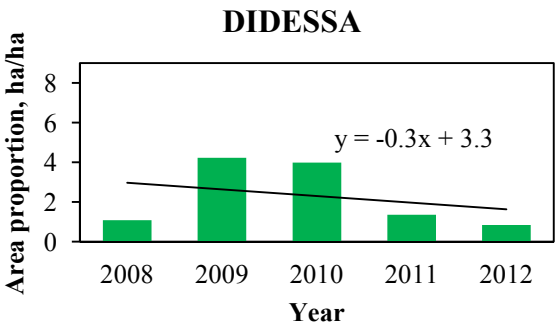
DIDESSA
Area proportion, ha/ha
y = -0.3x + 3.3
0
2
4
6
8
2008
2009
2010
2011
2012
Year

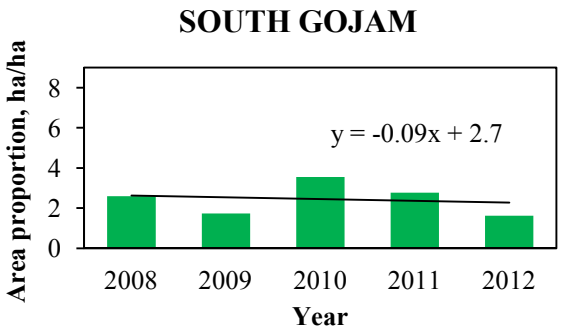
SOUTH GOJAM
Area proportion, ha/ha
y = -0.09x + 2.7
0
2
4
6
8
2008
2009
2010
2011
2012
Year

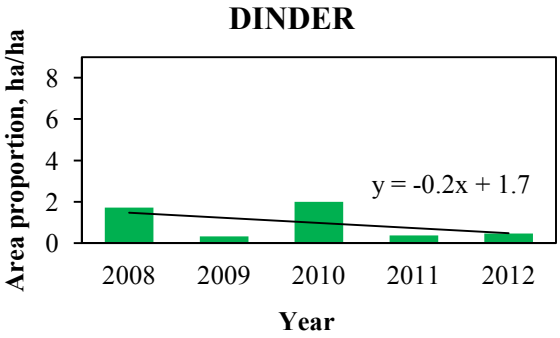
DINDER
Area proportion, ha/ha
y = -0.2x + 1.7
0
2
4
6
8
2008
2009
2010
2011
2012
Year

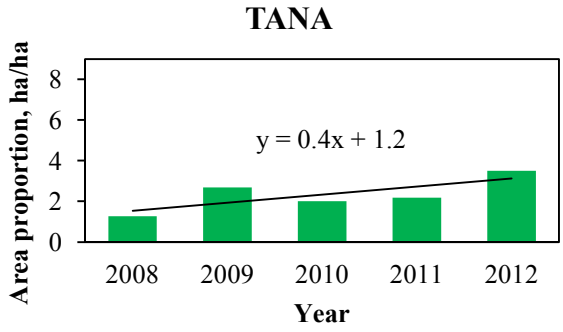
TANA
Area proportion, ha/ha
y = 0.4x + 1.2
0
2
4
6
8
2008
2009
2010
2011
2012
Year

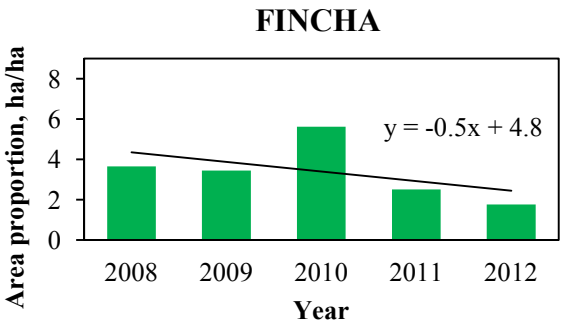
FINCHA
Area proportion, ha/ha
y = -0.5x + 4.8
0
2
4
6
8
2008
2009
2010
2011
2012
Year

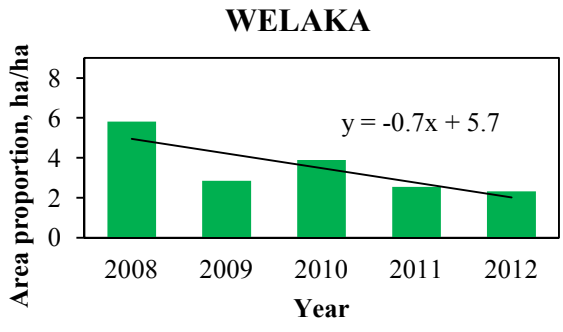
WELAKA
Area proportion, ha/ha
y = -0.7x + 5.7
0
2
4
6
8
2008
2009
2010
2011
2012
Year

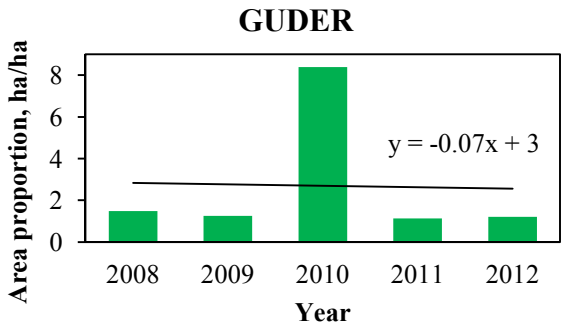
GUDER
Area proportion, ha/ha
8
6
4
2
0
y = -0.07x + 3
2008
2009
2010
2011
2012
Year

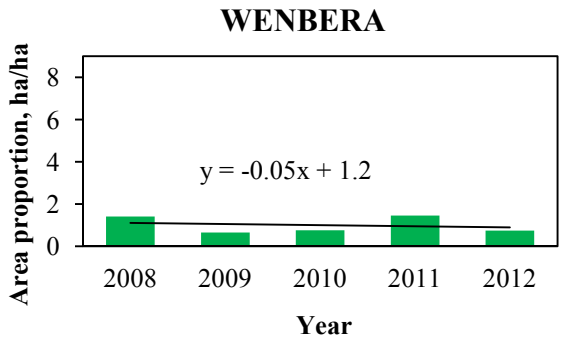
WENBERA
Area proportion, ha/ha
8
6
4
2
0
y = -0.05x + 1.2
2008
2009
2010
2011
2012
Year

Figure D1- 2: Total area recovered as proportion of sub basin area for five years (2008 – 2012)

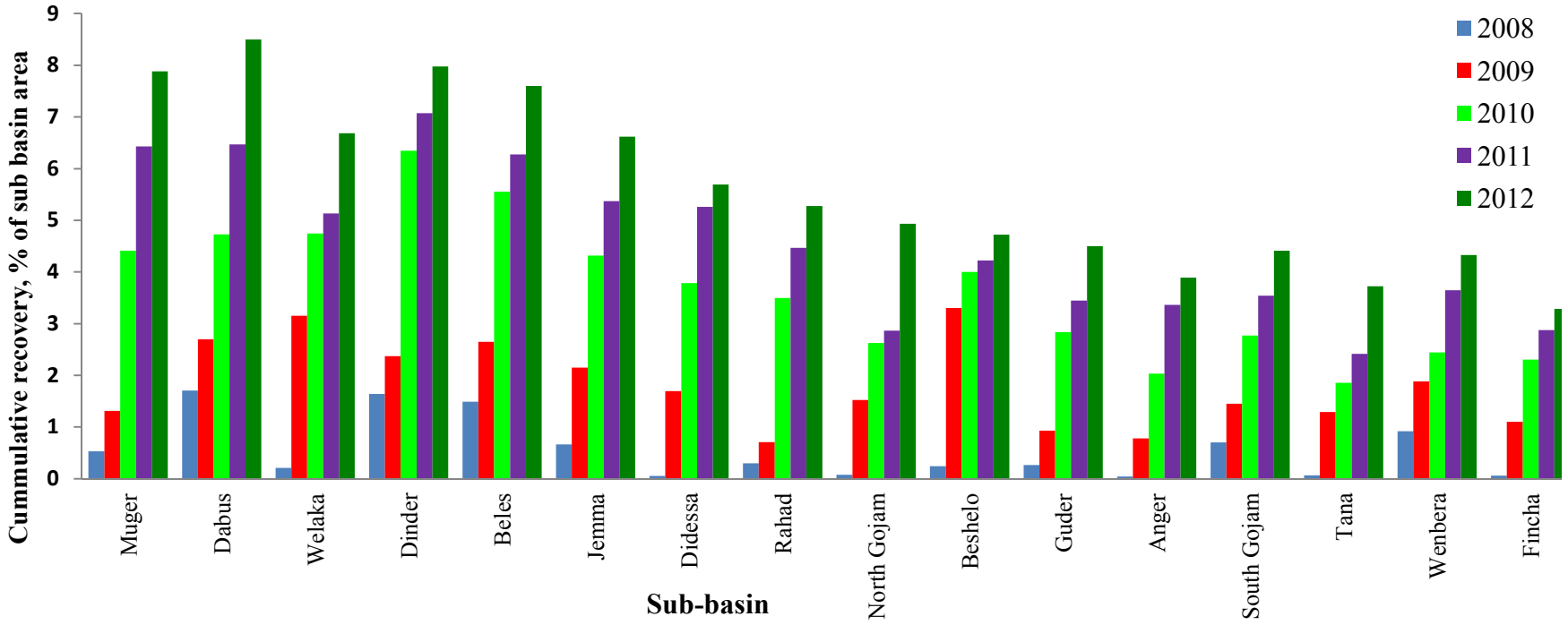

Figure D1- 3: Comparison of recovered area proportion to the immediate previous year

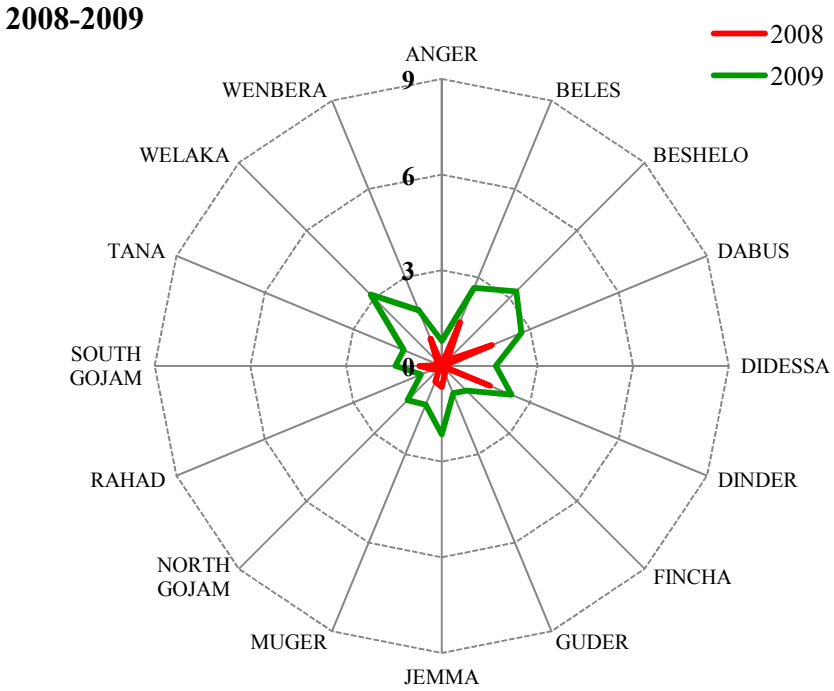

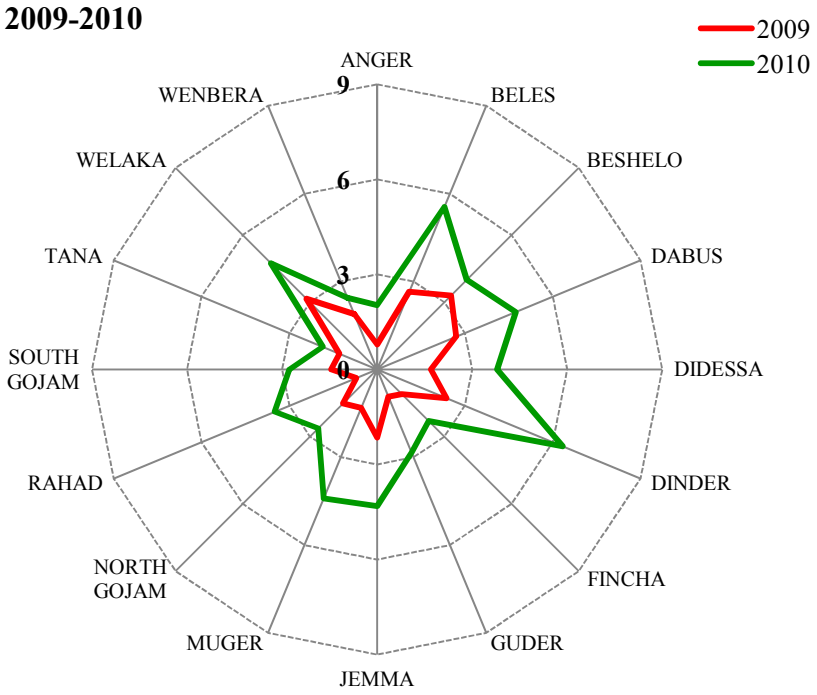

2010-2011

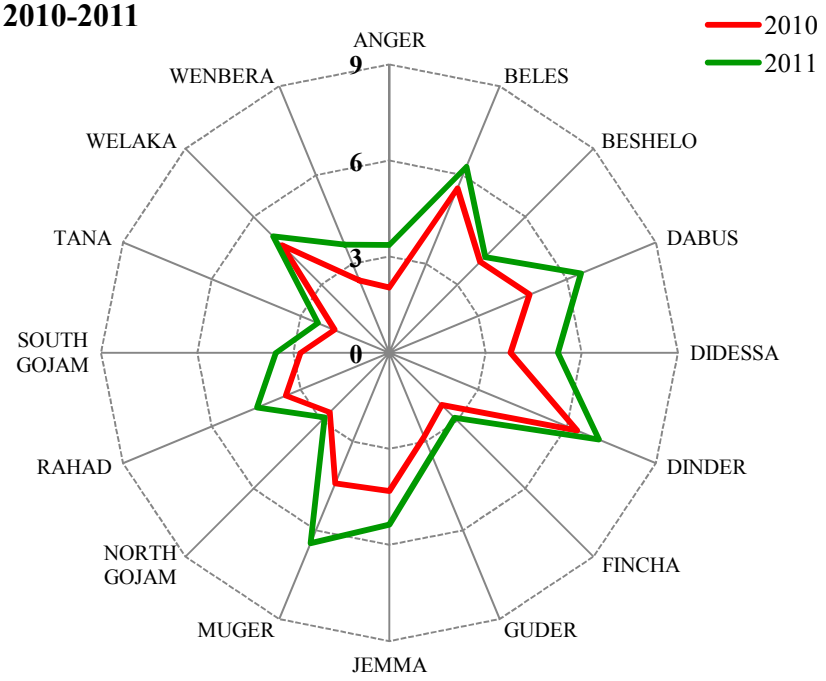

2011-2012

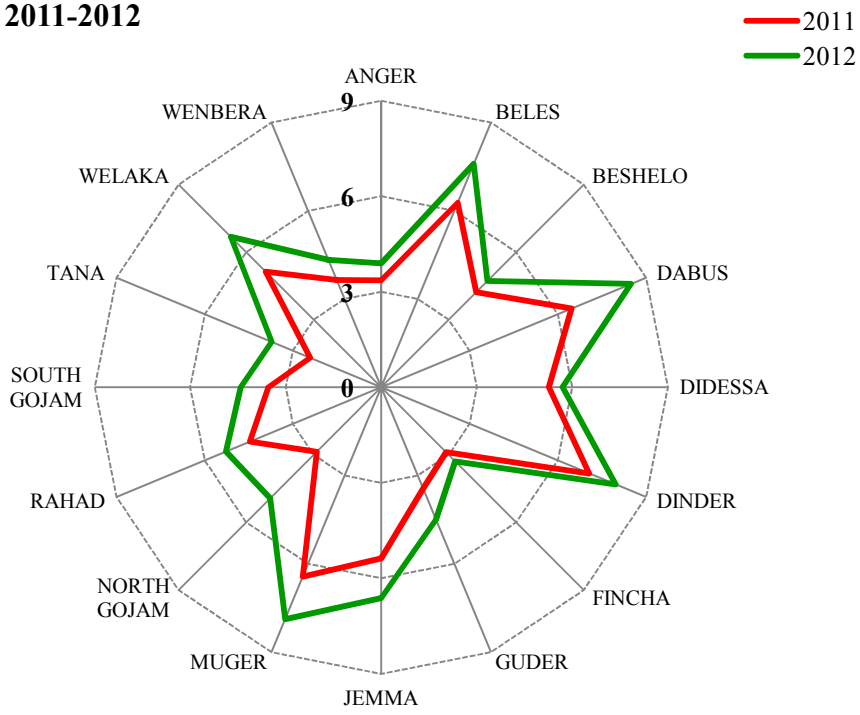

Table D1- 1: Biome stratified mean-maximum Enhanced Vegetation Index (EVI) and mean-maximum land surface temperature (LST) (2003–2012)

	2003		2004		2005		2006		2007		2008		2009		2010		2011		2012	
Land cover	EVI	LST	EVI	LST	EVI	LST	EVI	LST	EVI	LST	EVI	LST	EVI	LST	EVI	LST	EVI	LST	EVI	LST
ENF	0.57	51	0.58	51	0.57	50	0.56	49	0.56	50	0.57	50	0.50	51	0.56	49	0.52	49	0.53	50
EBF	0.63	40	0.62	40	0.61	41	0.59	40	0.61	39	0.61	40	0.59	39	0.60	40	0.57	43	0.56	41
DNF	0.49	53	0.63	49	0.48	49	0.52	48	0.45	47	0.45	49	0.42	46	0.48	51	0.48	49	0.58	49
MF	0.59	50	0.57	50	0.57	49	0.55	49	0.56	49	0.56	50	0.54	49	0.54	49	0.53	50	0.53	49
CS	0.46	52	0.41	53	0.43	51	0.40	51	0.44	51	0.42	52	0.36	52	0.40	51	0.37	52	0.39	52
OS	0.35	51	0.34	52	0.33	51	0.33	51	0.34	50	0.33	53	0.32	51	0.32	50	0.31	54	0.32	52
WSAV	0.61	46	0.59	46	0.58	45	0.56	45	0.60	44	0.57	46	0.56	44	0.58	44	0.55	56	0.53	46
SAV	0.51	49	0.45	50	0.45	48	0.44	49	0.49	47	0.45	50	0.43	48	0.47	47	0.43	52	0.43	50
G	0.47	51	0.42	51	0.42	50	0.41	51	0.43	49	0.42	52	0.39	49	0.41	49	0.39	51	0.40	51
PWET	0.62	50	0.59	50	0.59	50	0.57	49	0.61	48	0.58	48	0.56	49	0.57	50	0.55	49	0.55	50
C	0.51	48	0.46	48	0.49	48	0.47	48	0.47	47	0.49	51	0.42	47	0.48	47	0.44	61	0.42	50
URB	0.34	52	0.31	52	0.31	51	0.30	52	0.32	51	0.31	52	0.31	51	0.30	50	0.29	54	0.29	52
CNATVEG	0.54	46	0.53	46	0.53	46	0.51	45	0.51	44	0.52	46	0.51	45	0.49	44	0.49	48	0.47	47
BAR	0.40	55	0.40	56	0.40	54	0.38	55	0.39	55	0.39	55	0.36	54	0.39	55	0.38	57	0.37	55

Table D1- 2: Biome stratified standard deviation for maximum Enhanced Vegetation Index (EVI) and maximum land surface temperature (LST) (2003–2012)

	2003		2004		2005		2006		2007		2008		2009		2010		2011		2012	
Land cover	EVI	LST	EVI	LST	EVI	LST	EVI	LST	EVI	LST	EVI	LST	EVI	LST	EVI	LST	EVI	LST	EVI	LST
ENF	0.14	10	0.13	9	0.14	10	0.14	10	0.14	10	0.14	9	0.11	10	0.14	11	0.13	11	0.14	9
EBF	0.11	10	0.11	10	0.11	9	0.10	9	0.11	10	0.11	10	0.10	10	0.11	10	0.10	17	0.11	9
DNF	0.04	9	0.11	9	0.05	11	0.16	10	0.08	11	0.11	8	0.15	10	0.09	9	0.12	5	0.05	10
MF	0.13	8	0.12	8	0.13	8	0.12	8	0.12	8	0.13	7	0.12	8	0.12	8	0.12	11	0.12	7
CS	0.15	8	0.17	8	0.15	7	0.15	8	0.15	8	0.15	7	0.17	8	0.15	8	0.15	11	0.15	8
OS	0.16	9	0.16	8	0.16	8	0.15	9	0.15	9	0.16	8	0.15	8	0.15	9	0.15	23	0.15	8
WSAV	0.17	10	0.15	10	0.15	9	0.15	10	0.17	10	0.15	10	0.15	10	0.16	10	0.15	25	0.16	9
SAV	0.20	11	0.20	10	0.20	9	0.20	10	0.21	10	0.20	10	0.20	10	0.21	11	0.20	28	0.20	9
G	0.18	10	0.19	9	0.19	8	0.18	10	0.18	10	0.19	9	0.18	9	0.19	11	0.18	25	0.18	9
PWET	0.12	6	0.11	6	0.11	6	0.11	6	0.13	6	0.11	6	0.12	6	0.12	7	0.11	6	0.12	6
C	0.17	10	0.18	9	0.18	9	0.17	10	0.18	10	0.17	9	0.18	9	0.17	11	0.18	28	0.18	9
URB	0.16	8	0.18	8	0.17	7	0.16	9	0.16	8	0.17	7	0.17	7	0.15	9	0.16	14	0.15	7
CNATVEG	0.10	7	0.10	7	0.10	6	0.09	7	0.10	7	0.10	6	0.09	7	0.11	8	0.10	12	0.10	6
BAR	0.21	6	0.22	6	0.21	6	0.21	7	0.21	7	0.21	6	0.19	6	0.21	7	0.20	13	0.20	6

Table D1- 3: ISLSCP II MODIS IGBP[12] Land covers data nomenclature

Symbol	Land cover
ENF	Evergreen Needle forest
EBF	Evergreen Broadleaf forest
DNF	Deciduous Needle forest
MF	Mixed Forest
CS	Closed Shrub
OS	Open Shrub land
WSAV	Woody Savannas
SAV	Savannas
G	Grasslands
PWET	Permanent Wetlands
C	Croplands
URB	Urban
CNATVEG	Crop/Natural Vegetation Mosaic
BAR	Barren

[12] **I**nternational **S**atellite **L**and – **S**urface **C**limatology **P**roject, **I**nitiative II **M**ODIS **I**nternational **G**eosphere – **B**iosphere **P**rogram

Table D1- 4: Proportion of sub basin area undergone minus one and plus one standard deviation disturbance from the long term mean DI

NAME	2004		2005		2006		2007		2008		2009		2010		2011		2012	
	-1 STDV	+1 STDV	-1 STDV	+1 STDV	-1 STDV	+1 STDV	-1 STDV	+1 STDV	-1 STDV	+1 STDV	-1 STDV	+1 STDV	-1 STDV	+1 STDV	-1 STDV	+1 STDV	-1 STDV	+1 STDV
ANGER	2.61	0.00	5.48	0.00	0.56	0.00	9.71	0.00	1.42	0.00	1.24	0.00	2.45	0.00	2.16	0.00	0.69	0.00
BELES	1.14	0.00	0.60	0.00	0.40	0.00	3.58	0.00	1.32	0.00	0.34	0.00	1.90	0.00	0.52	0.00	0.89	0.03
BESHELO	2.70	0.01	1.05	0.00	2.35	0.00	15.74	0.00	3.99	0.00	8.47	0.00	2.72	0.00	2.11	0.00	2.27	0.00
DABUS	1.50	0.01	1.77	0.00	1.10	0.00	4.66	0.00	1.29	0.00	0.68	0.00	2.03	0.00	1.67	0.00	2.04	0.00
DIDESSA	3.30	0.00	3.95	0.00	2.01	0.00	11.63	0.00	1.08	0.00	4.22	0.00	3.98	0.00	1.35	0.00	0.85	0.00
DINDER	1.80	0.00	0.75	0.00	0.51	0.00	3.93	0.00	1.73	0.00	0.33	0.00	2.00	0.00	0.37	0.00	0.47	0.00
FINCHA	9.92	0.02	12.33	0.00	5.47	0.00	12.47	0.00	3.65	0.00	3.45	0.00	5.61	0.00	2.51	0.02	1.76	0.02
GUDER	9.59	0.00	7.10	0.00	2.16	0.00	7.00	0.00	1.49	0.00	1.25	0.00	8.39	0.00	1.13	0.00	1.21	0.17
JEMMA	6.29	0.01	2.11	0.00	3.15	0.00	9.86	0.00	4.39	0.00	3.77	0.00	5.95	0.00	5.23	0.03	2.68	0.05
MUGER	2.26	0.01	2.54	0.00	1.23	0.00	5.72	0.00	3.33	0.00	1.53	0.00	6.87	0.00	4.35	0.00	1.49	0.11
NORTH GOJJAM	10.68	0.01	1.69	0.00	3.09	0.00	4.31	0.00	1.10	0.00	2.05	0.00	5.18	0.00	1.80	0.00	4.43	0.01
RAHAD	1.17	0.00	0.45	0.01	0.42	0.00	1.91	0.00	0.56	0.00	0.17	0.00	1.35	0.00	0.79	0.00	0.38	0.00
SOUTH GOJJAM	5.26	0.00	4.16	0.00	1.89	0.00	4.62	0.00	2.59	0.00	1.73	0.00	3.54	0.00	2.77	0.00	1.62	0.09
TANA	7.25	0.01	2.16	0.00	2.52	0.00	1.48	0.00	1.26	0.00	2.69	0.00	2.01	0.01	2.19	0.04	3.50	0.03
WELAKA	7.39	0.04	2.02	0.00	2.00	0.00	14.01	0.00	5.82	0.00	2.84	0.00	3.89	0.00	2.55	0.00	2.31	0.04
WENBERA	3.14	0.00	3.74	0.00	0.73	0.00	5.63	0.00	1.41	0.00	0.66	0.00	0.75	0.00	1.45	0.00	0.75	0.00

Table D1- 5: Amhara Region MERET Project watersheds

No	Region		Amhara						
	Zone	Woreda	Watershed sites		Area (Ha)	Year of intervention started (E.C)	Rehabilitated land year to Date(Ha)	Coverage in %Year to Date	Remark
			#	Name of CBWS					
		Enebsie		Guansa	435	1999	346	80	
				Teja baje	461	1999	411	89	
				Feresmeda	305	1999	264.25	87	
				Adefwoha	662	1999	631	95	
			4	**Total**	**1863**		**1652**	89	as of 2011
		Goncha		Woybla	532	2002	505	95	
				Wochit wuha	556	1999	313.59	56	
				Betabate	486	1999	176.635	36	
				Tiwa	632	1999	492.87	78	
				Berbere	1023	1999	758.75	74	
				Jensemariam	830	1999	509.4	61	
				Kechinwonz	344	1999	267.15	78	
1	E/Gojjam		7	**Total**	**4403**		**3023**	69	as of 2011
		Adiarkay		Ambaber	302	1999		0	
				Gualbuya	350	1999		0	
				Mai-Teklit	512	2007		0	
				Damota	365	1999		0	
				Dagarob	381	1999		0	
			5	**Total**	**1910**		**1442**	75	as of 2011
		East Belessa		Molesh	250	1999	189	76	
				Azmarsh	300	1999	182.25	61	
				Amba	250	1999	121.5	49	
			3	**Total**	**800**		**492.75**	62	as of 2011
		West Belessa		Lamgered	270	2006	175.5	65	
				Zaya	417	2006	279.39	67	
				Jandeb	343	2006	219.52	64	
			3	**Total**	**1030**		**674**	65	as of 2011
2	N/Gondar	Janamora		Deresigie	824	1999	613.8	75	as of 2010

				Denkoloko	1125	1999	456.96	41	
				Enchet kab	278	1999	165.5	59	
				Sabra	600	1999	256.56	43	
				Serebar	1125	1999	403.6	36	
			6	Abo	1500	1999	682.76	46	
				Total	**5453**		**2579.18**	47	
		Menzmama		Awa Kola	379	1999	284.75	75	
				Dasa Hana	474	1999	260.7	55	
				Fila	326	1999	218.42	67	
3	N/Shoa		3	**Total**	**1179**		**764**	65	as of 2011
		Lasta		Darewa	726	1999	578.75	80	
				Debre Loza	987	1999	579.63	59	
				Bilbala	705	1999	525.75	75	
				Genete Mariam	409	1999	218.4	53	
				Irfa	996	1999	711.8	71	
				Kumemesk	531	1999	292.92	55	
	N/wolo		6	**Total**	**4353**		**2907**	67	as of 2011
		Delanta		Chercharit	620	2000	475.09	77	
				Terrie	574	2000	415.8	72	
				Chebreko	244	2000	190.5	78	
				Deber	302	2000	265	88	
	S/Wollo		4	**Total**	**1739**		**1346.39**	77	as of 2011
		Gidan		Tigremender	904	1999	416.76	46	
				Agewyie	587	1999	227.25	39	
				Zagolzafe	594	1999	188.07	32	
				Betehara	400	2000	234.9	59	
				Chebermesk	540	1999	139.83	26	
			5	**Total**	**3025**		**1206.81**	40	as of 2011
		Kobo		Tekulesh	289	1999	197	68	
				Shehoch	967	1999	638	66	
				Gedeba	493	1999	238	48	
			3	**Total**	**1749**		**1073**	61	as of 2011
		Meket		Warkaye	1187	1999	619.43	52	
				Addis Amba	795	1999	723.45	91	
4	N/wolo			Dabza	767	1999	621.27	86	as of 2011

				Tirtrit	1015	1999	659.75	65	
				Denkena	572	1999	357.87	63	
			6	Zibe	1545	1999	505.4	33	
				Total	**5881**		**3155.4**	54	
		Bati		Kamie	396	1999		0	
				Gariro	396	1999		0	
				Salmane	508	1999		0	
				Jeljedi	304	1999		0	
5	Oromiya		4	**Total**	**1604**		**613.6375**	38	as of 2010
		Ebinat		Deregeha	1110	2002		0	
				Akuha	830	2002		0	
				Abina	596	2002		0	
				Serawdie	730	2002		0	
			4	**Total**	**3266**		**2230**	68	as of 2010
		Simada		Dereke wonze	577.2	1999	458.2	79	
				Gorer	371.5	2006	317.25	85	
				Geta mado	828.4	1999	361.35	44	
6	S/Gondar		3	**Total**	**1777.1**		**1137**	64	as of 2011
		Ambasel		Tisa-totito	681	1999	556.09	82	
				Limo-aromba	706	1999	568.95	81	
				Robit-dehadit	1068	1999	846.81	79	
				Minchu-minchu	587	1999	491.07	84	
				Yebar-saledila	434	1999	329	76	
				Kolet-guba	412	1999	322	78	
				Dino-dino	512	1999	401	78	
				Golbo-woleti	692	1999	544	79	
				Chefe-gamara	935	1999	761	81	
			9	**Total**	**6027**		**4820**	80	as of 2011
		Kalu		Borkenashana	1092	2000	966.42	89	
				Addis alem	780	2000	641.16	82	
				Bistima/Adamie	411	2000	355.515	87	
				Worseye	780	2000	670.8	86	
				Aref Lebie	425	2000	354.875	84	
				Dirma	346	2000	275.07	80	
7	S/Wollo		7	chekortie	490	2000	436.1	89	as of 2011

				Total	**4324**		**3700**	86	
		Kutaber		Dire	630	1999	393	62	
				Abaselama	406	1999	293	72	
				Kundi	427	1999	214	50	
				Yekumba	403	1999	198.5	49	
				Tebela	535	1999	213.75	40	
			5	**Total**	**2401**		**1312.25**	55	as of 2011
		Mekedela		Meyana	389	2001	204	52	
				Mekena	3733	2001	2896.75	78	
				Molla defer	731	2001	633	87	
				Yesiga	2128	2001	1446.38	68	
				Tiwat tay	673	2005	382.53	57	
				Abatklie	547	2003	498.5	91	
			6	**Total**	**8200**		**6061.16**	74	as of 2011
		Tenta		Tigosh	903	2000	727.91	81	
				Biruhtesfa	798	2000	648.57	81	
				Meguat	800	2000	680.00	85	
				Meslaye	1303	2000	908.26	70	
				Dewot	1075	2000	827.75	77	
				Tedat	1263	2000	921.63	73	
			7	**Total**	**6141**		**4714**	77	as of 2011
		Worebabo		Chali	566	1999	430.15	76	
				Kuno Wokilo	490	1999	409.4	83	
				Guha chali	694	1999	638.25	92	
				Bokeksa chali	581	1999	493.85	85	
				Adamie meia	582	1999	462.69	80	
				Gendebash wokilo	481	1999	355.74	74	
				Gubusa miea	745	1999	525.1	71	
				Fito mille	758	1999	515.4	68	
				Gedero wokilo	499	1999	399	80	
			9	**Total**	**5395**		**4230**	78	as of 2011
		Sekota		Wateb	950	1999	882	93	
				Dibakuan	1130	2007	675.4	60	
				Berbero	437	2003	261.66	60	
8	WagHemera		3	**Total**	**2517**		**1819**	72	as of 2011

		Ziquala		Abitaba	238	1999	168.98	71	
				Bisku	292	1999	175.08	60	
				Alidery	320	1999	192	60	
			3	**Total**	**850**		**536**	63	as of 2011
	Total	**23**	**115**		**75888**		**51489**	**68**	